Electron microscopies for magnetism

Bénédicte Warot-Fonrose
CEMES
Toulouse, France

Introduction on electron microscopes

SPLEEM

SEMPA

Lorentz microscopy

Electron holography

Scanning Electron Microscope

- Principle
- Modes
- Resolution and sample

Low Energy Electron Microscope

Transmission Electron Microscope

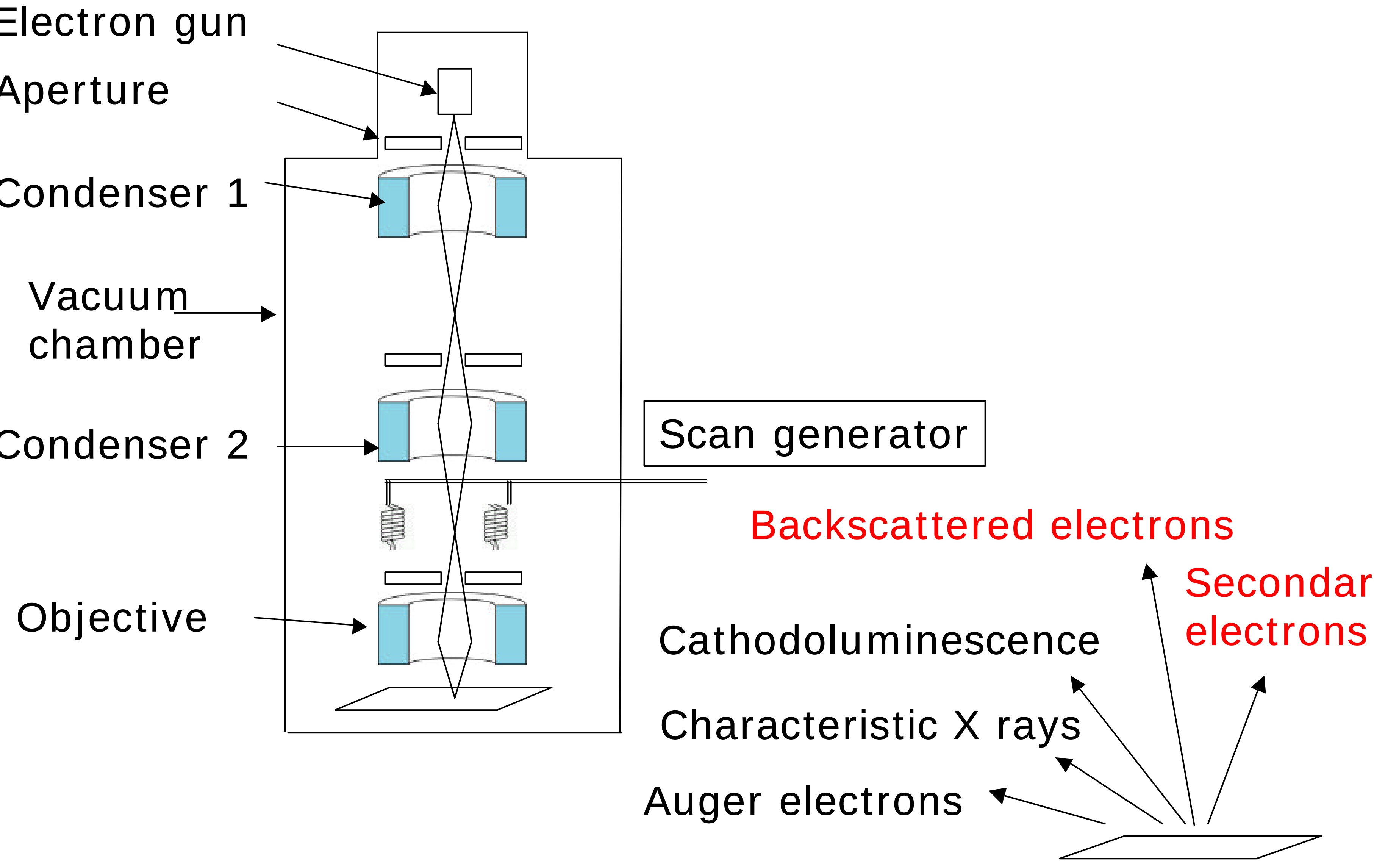

Electron gun
Aperture
Condenser 1
Vacuum chamber
Condenser 2
Objective
Scan generator
Backscattered electrons
Secondary electrons
Cathodoluminescence
Characteristic X rays
Auger electrons

Low energy (few tenths of eV)

- Surface topographical image
- Can be manipulated by Faraday cage
- Production of SE is primarily independent of atomic number (however, since backscattered electrons do produce SE, heavier elements tend to create more SE)
- Not much information on the atomic composition of the sample

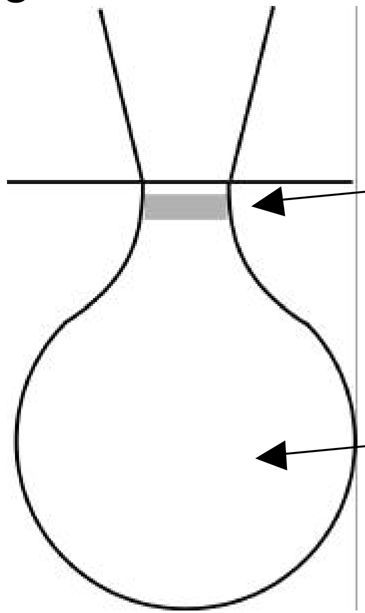

Secondary electron generated and able to escape (depends on the escape depth)

Secondary electron generated and unable to escap

Depth image

- Large width of escape depth
- High energy (>50eV)
- Heavy elements produce more backscattered electrons
- Provides information on the atomic composition of the sample

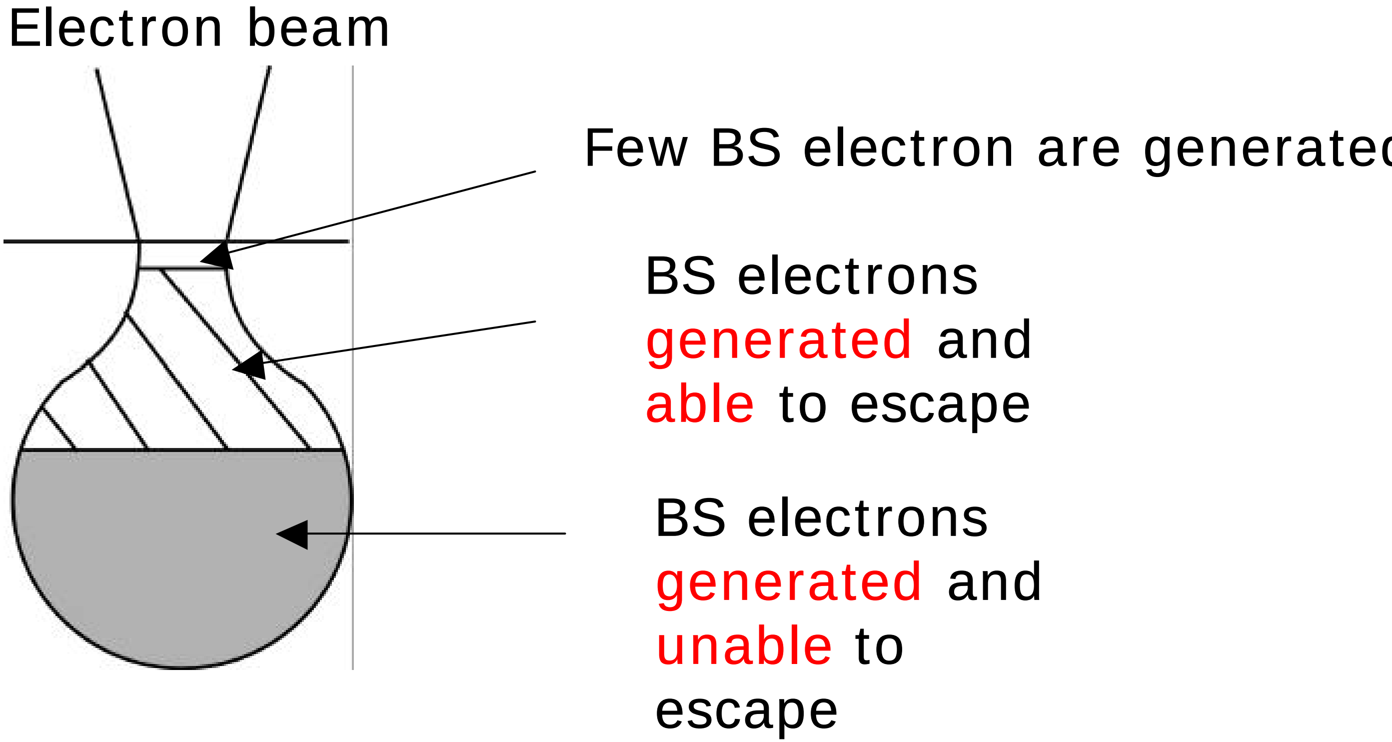

EBSD : Electron Back Scattered Diffraction

Secondary e⁻

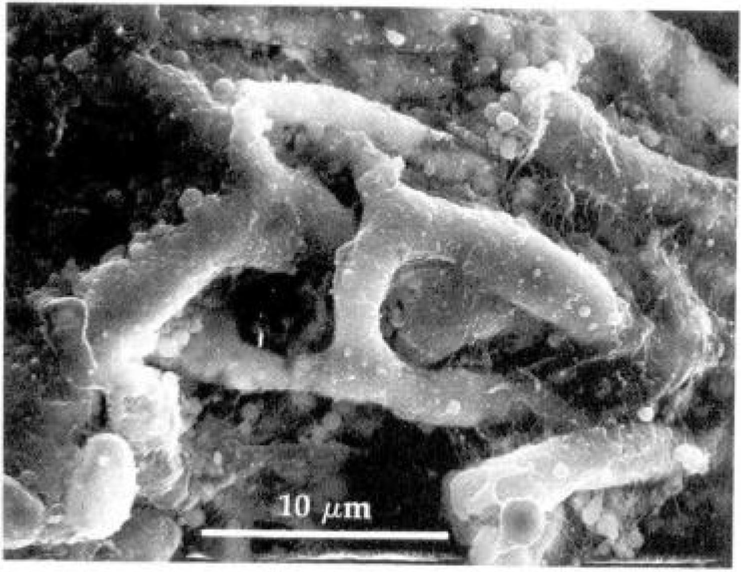

Backscattered e⁻

Fungal hyphae with Ag preferentially deposited at polysaccharides

sample topography

sample composition

www.courses.vcu.edu/PHYS661/pdf/06TechMicroscopy041.ppt

Resolution

- Primarily determined by spot size
- Small spot size gives high resolution
- Spot size increases with working distance

~ few nanometers

Sample preparation

- Tedious for biological specimen (drying, ...)
- Carbon coating to make materials conductive

Scanning Electron Microscope

Low Energy Electron Microscope

- Principle
- Modes
- Resolution and sample

Transmission Electron Microscope

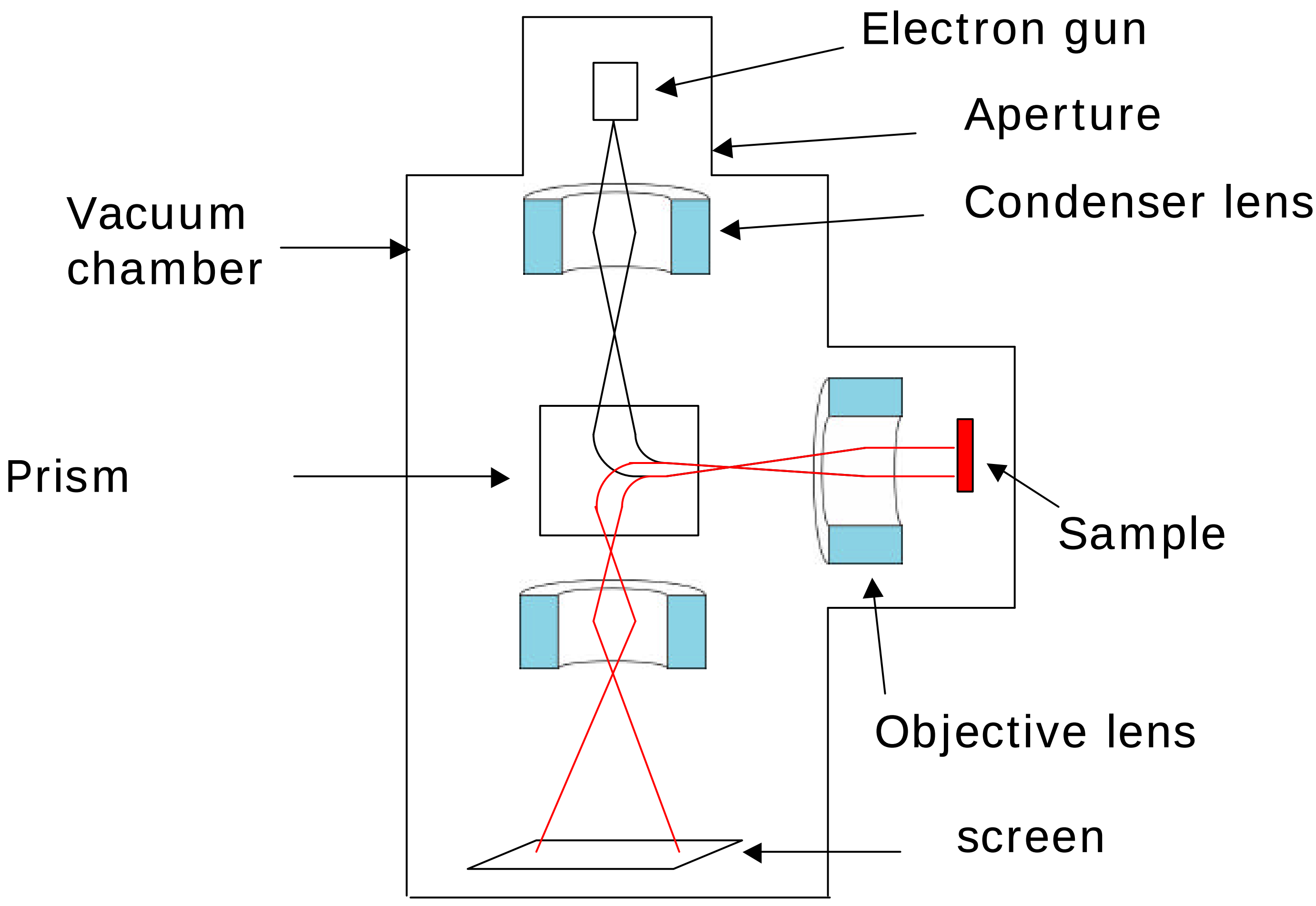
Electron gun
Aperture
Condenser lens
Vacuum chamber
Prism
Sample
Objective lens
screen

- Electron Energy is 0eV
  - Electrons Return Before they Hit the Sample
- Contrast created by outer Potential
  - Workfunction
- Image appears Blurred

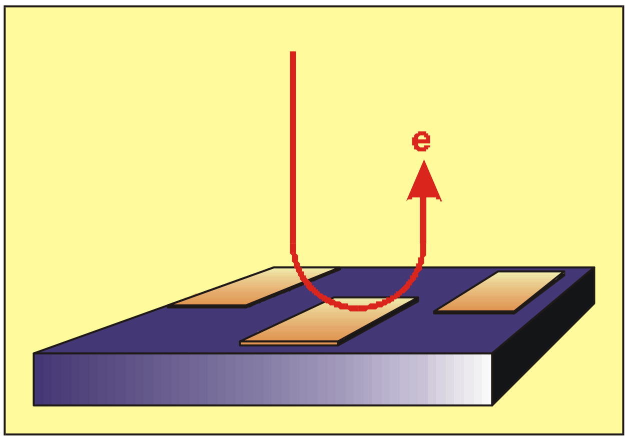

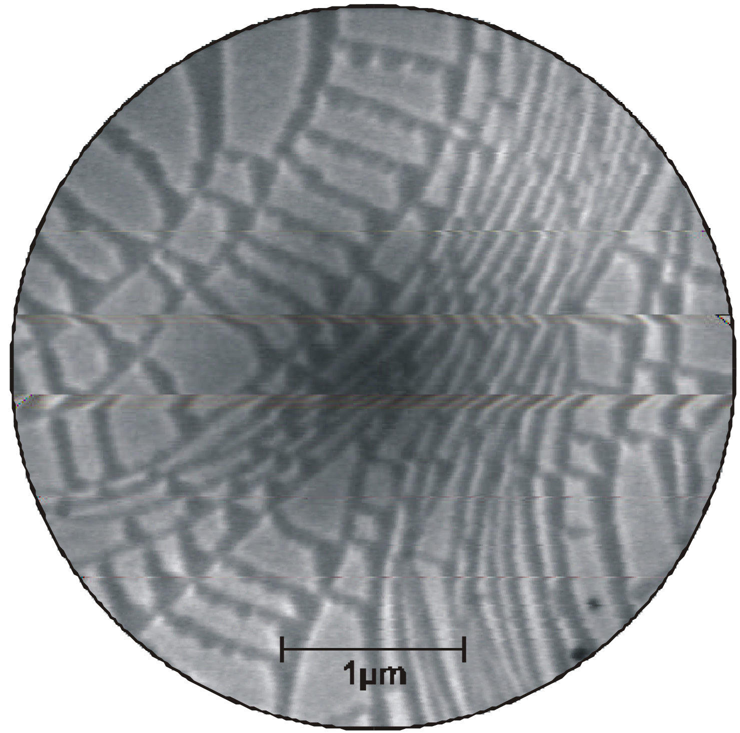

From F. Meyer zu Heringdorf's LEEM-Basics , http://www.leem-user.com/

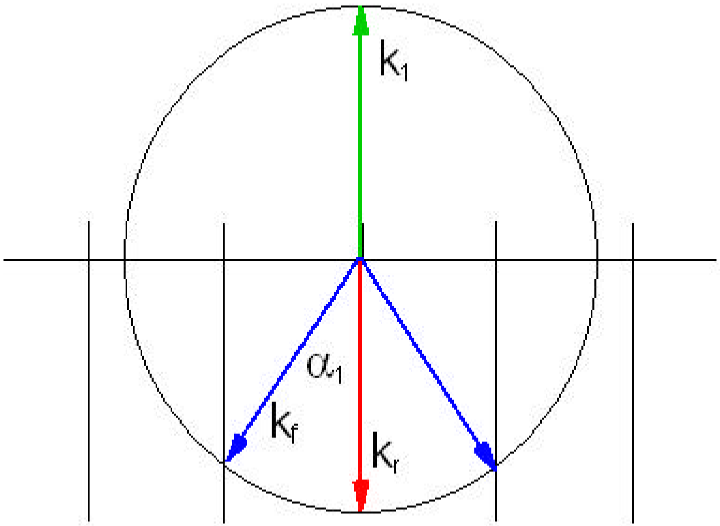

Bright field image:
incident beam normal to surface
reflected (0,0) beam normal to surface
select (0,0) with contrast aperture

From R. Tromp's LEEM-Basics, http://www.leem-user.com/

Dark Field Imaging

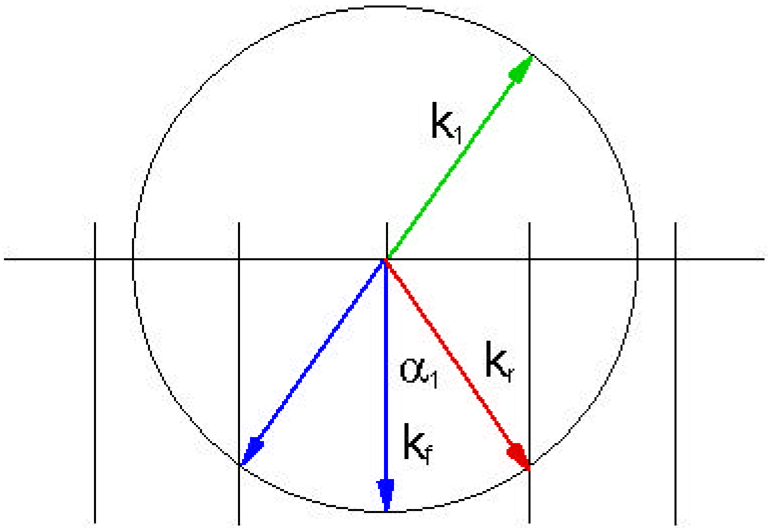

Dark field image:
incident beam inclined to surface
reflected (h,k) beam normal to surface
select (h,k) with contrast aperture

From R. Tromp's LEEM-Basics, http://www.leem-user.com/

Resolution
Limited by the diffraction at the contrast aperture, the spherical and chromatic aberrations of the objective lens
Lateral 5-10nm
Depth subÅ

Samples
Mainly semi-conductive samples
No special preparation required

Scanning Electron Microscope

Low Energy Electron Microscope

Transmission Electron Microscope

- Principle
- Modes
- Resolution and sample

TEM Principle

Transmission Electron Microscope

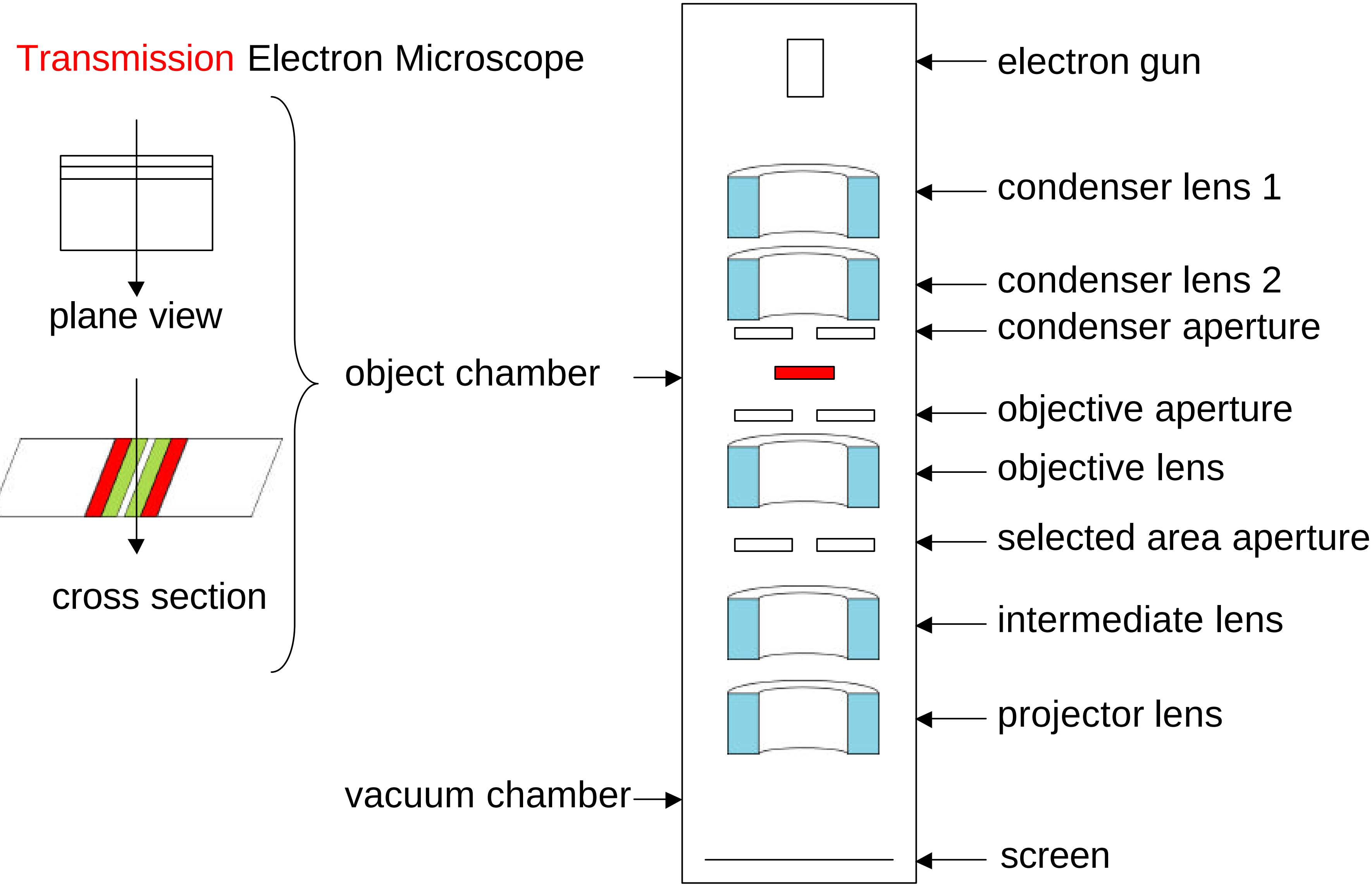

Bright field mode

Dark field mode

High resolution mode

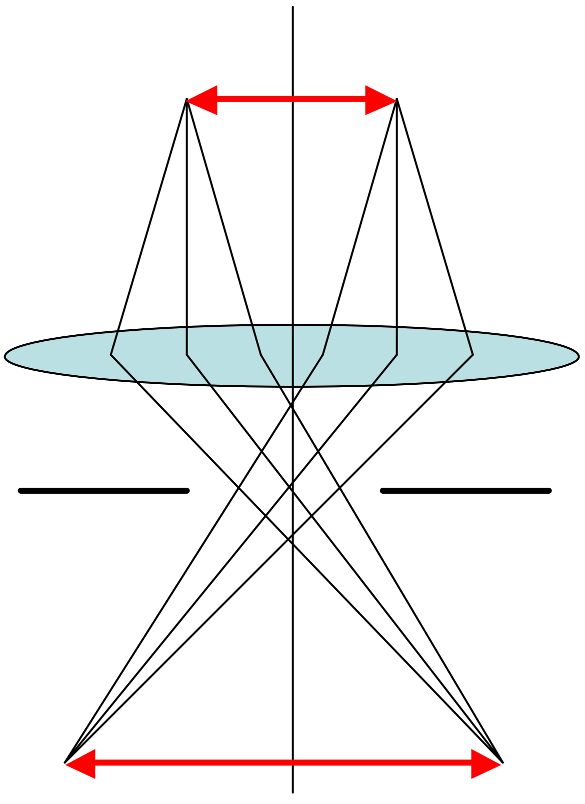

Link between magnetism and structure :

- Crystallographic structure of the elements (bcc, hcp, fcc) – metastable phase
- Interface quality (roughness)
- Grain size and morphology of polycristalline materials
- Surface topography
- Strain in layers (magnetoelastic energy)
- Chemical distribution of the elements

Epitaxial Co/NiO/MgO
M along the NiO[110] axis, structure?

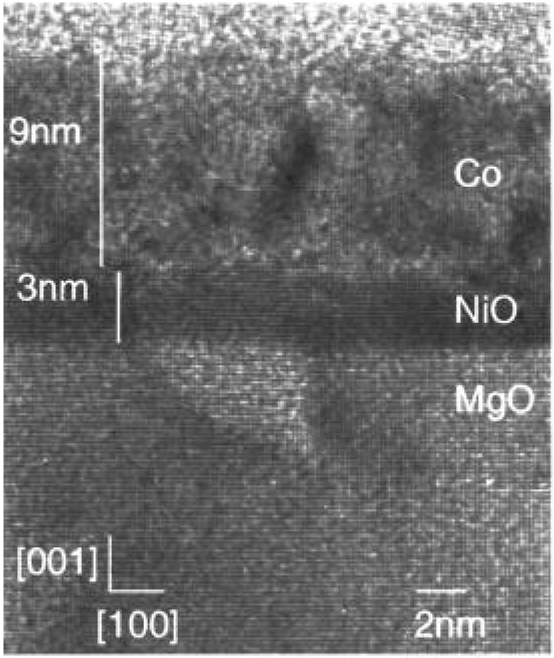

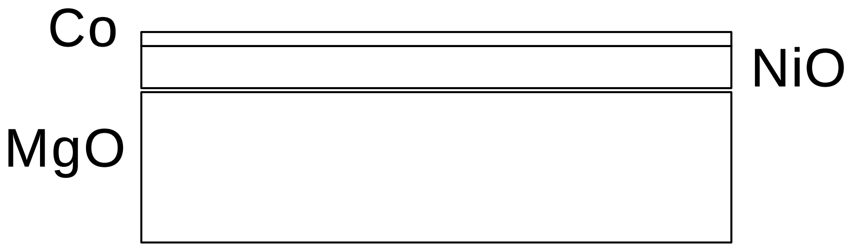

Structure of the cobalt layer?

hcp (easy axis along [0001] c axis)
fcc (easy axis along the [111] axis)

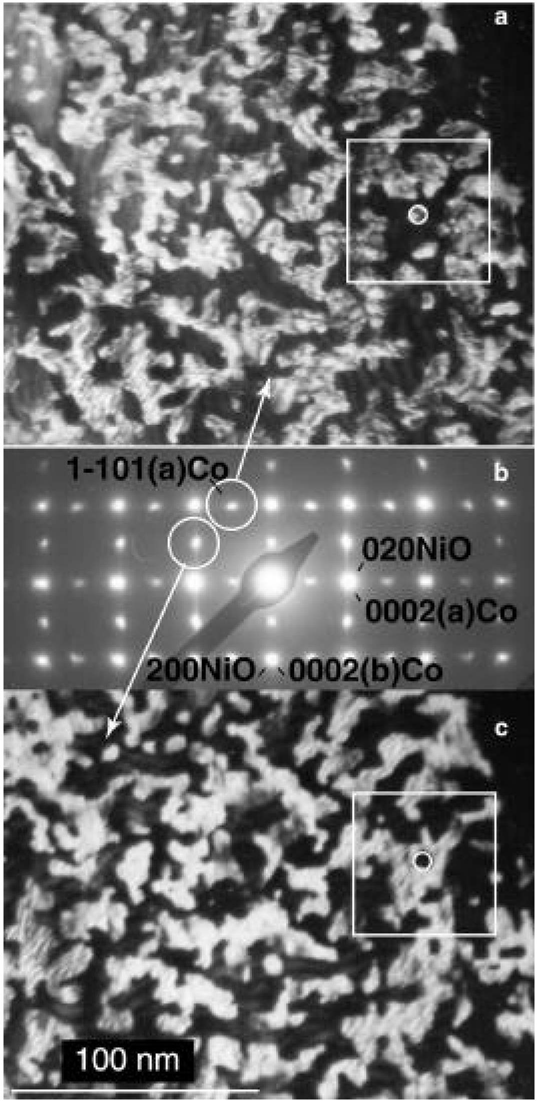

hexagonal structure with 2 variants:
Co[0002]($11\bar{2}0$) // NiO[200](001) or
Co[0002]($11\bar{2}0$) // NiO[020](001)

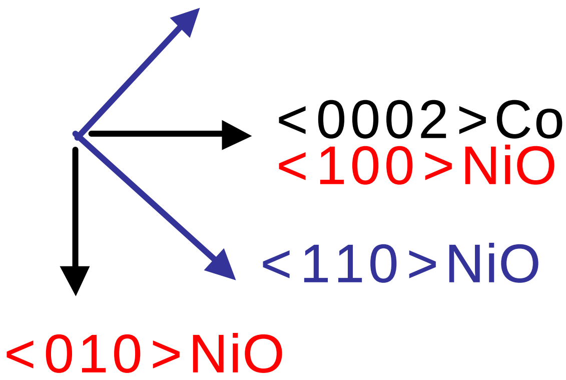

c axis : easy axis
c // [100]NiO or
c//[010]NiO
M // <110>

B. Warot et al., J. Appl. Phys. 2001 **89** 5414-5420

Example : Fe_3O_4

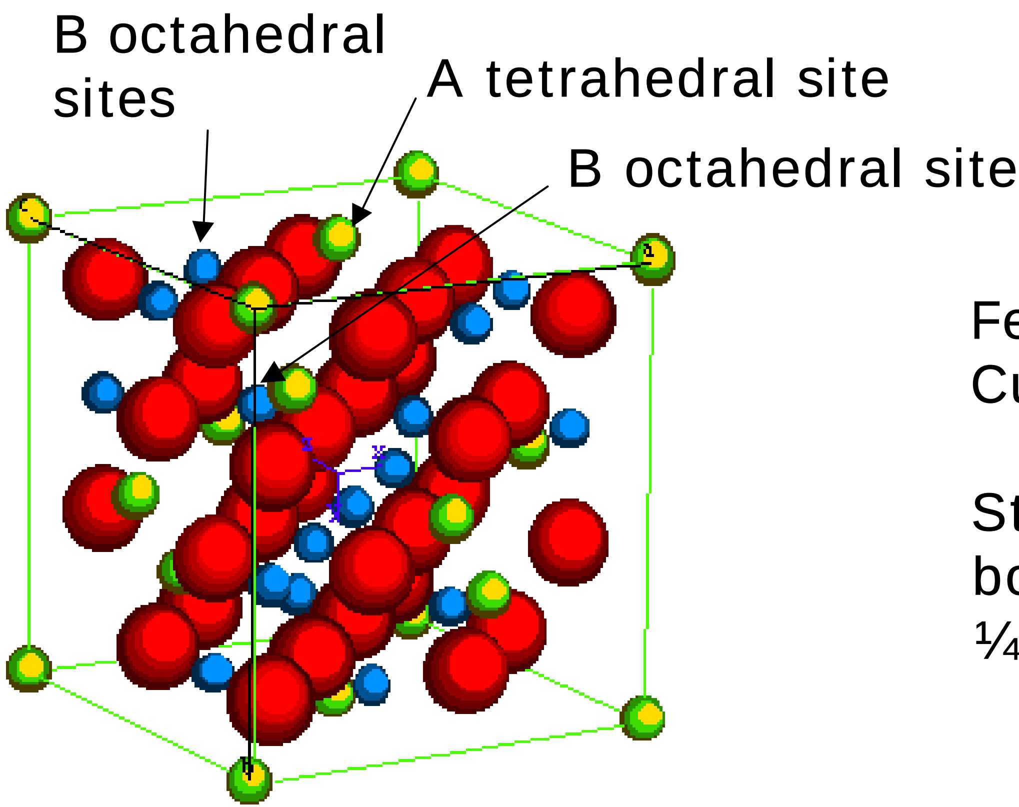

- B sites: Fe^{3+}, Fe^{2+}
- A sites: Fe^{3+}
- O^{2-}

Ferrimagnetic
Cubic inverse spinel structure

Structural defect : antiphase boundary
¼<110> shift of the stack

Fe_3O_4 /NiO/MgO

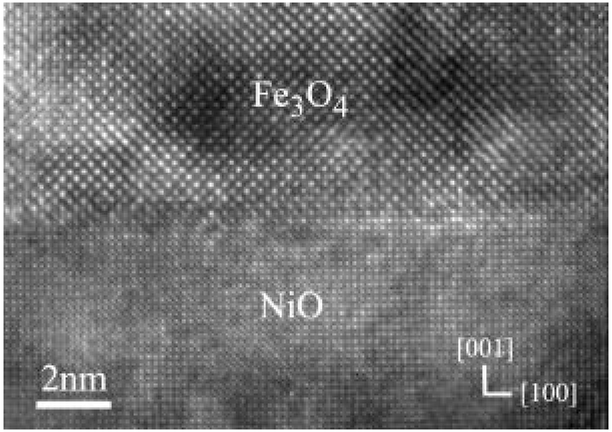

NiO/Fe_3O_4 /Al_2O_3

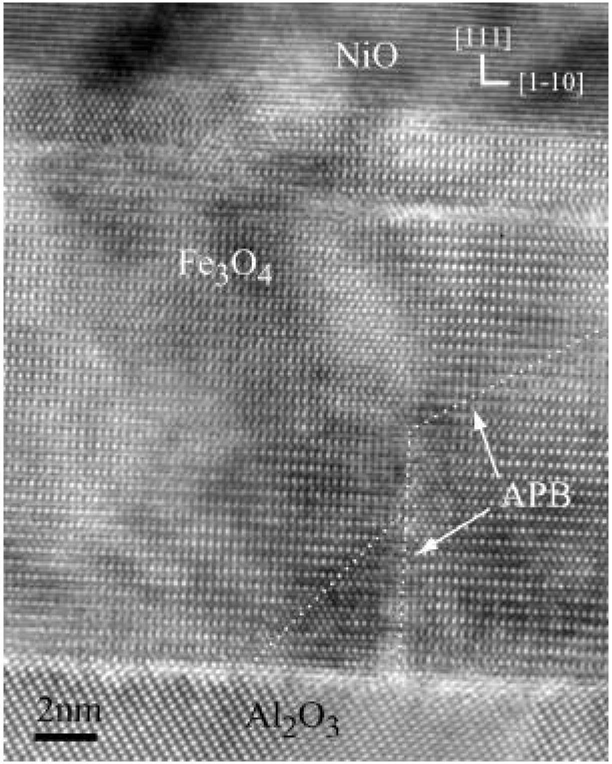

epitaxial growth
interface quality
observation of defects (APBs in Fe_3O_4)

C. Gatel et al., J. Mag. Mag. Mat. 2004 **272–276** e823–e824

Electron energy loss spectroscopy – EELS

Energy loss due to inelastic interactions between the incoming electron beam and the target electron
Loss characteristic of one element

Local probe (beam diameter size)

Quantitative chemical analysis

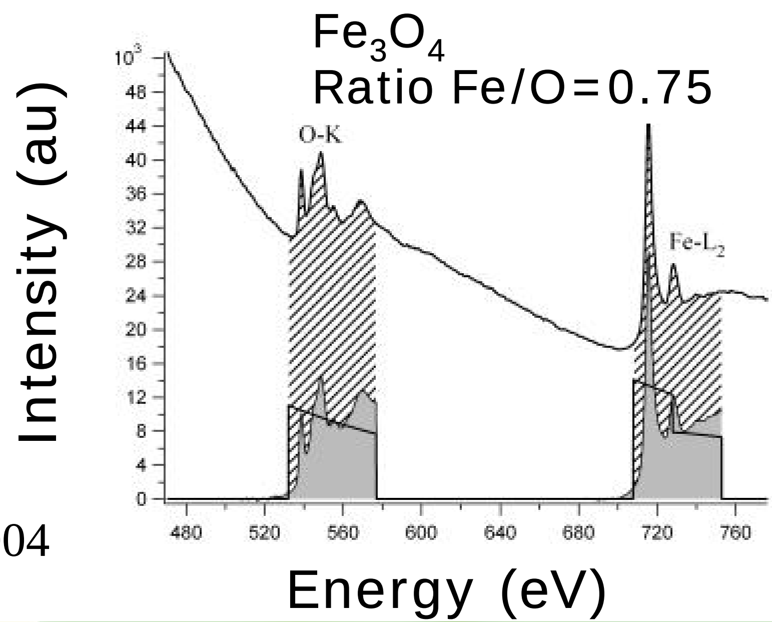

C.Gatel, PhD thesis, Toulouse, 2004

Composition profile in a Scanning TEM : a spectrum is recorded at each spot position

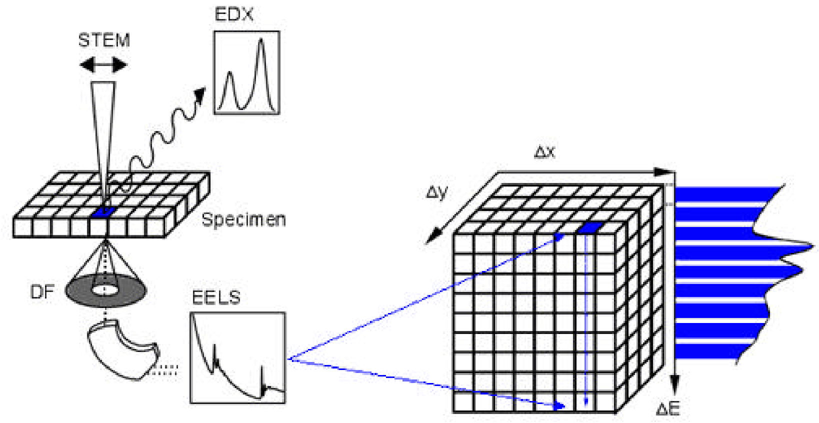

Composition maps using Electron Spectroscopic Imaging or Energy Filtered TEM: an image is recorded for each energy slit

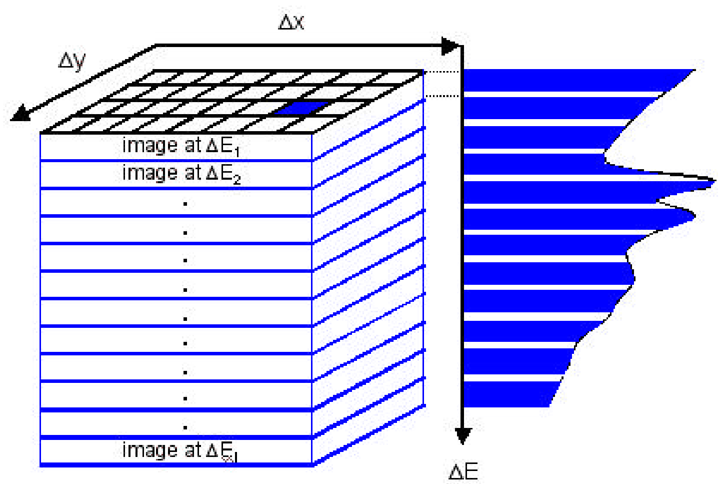

TEM

Chemical analysis

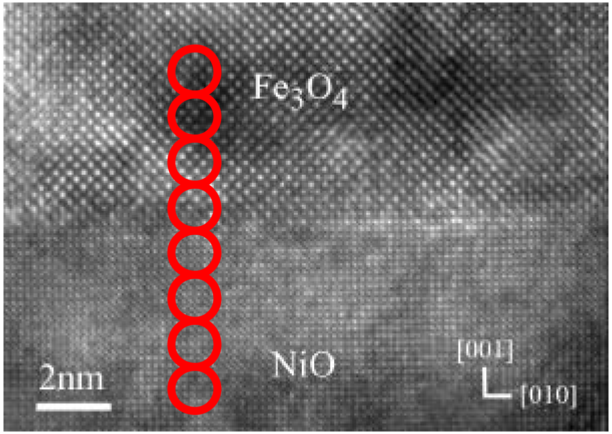

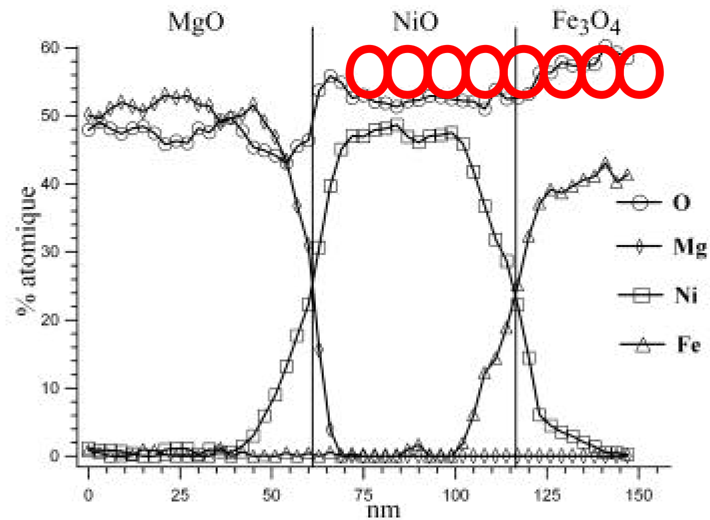

Composition profile

C.Gatel, PhD thesis, Toulouse, 2004

Composition map
Oxygen

Cr
Co
Cr

MgO

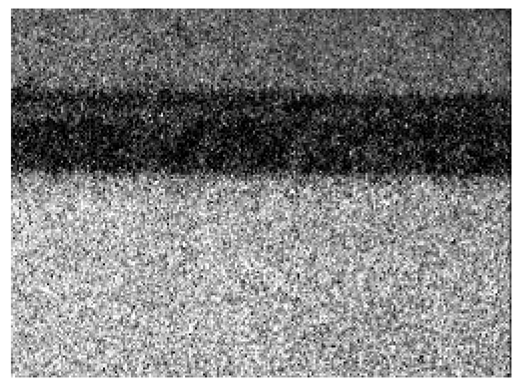

glue

10nm

Resolution

- Determined by the wavelenght of the incident electron
- Limited by lens aberration (spherical, chromatic)

Few Å

Sample preparation : electron transparent sample (from 10nm to 300nm thick)

Mechanical polishing
Chemical polishing
FIB system

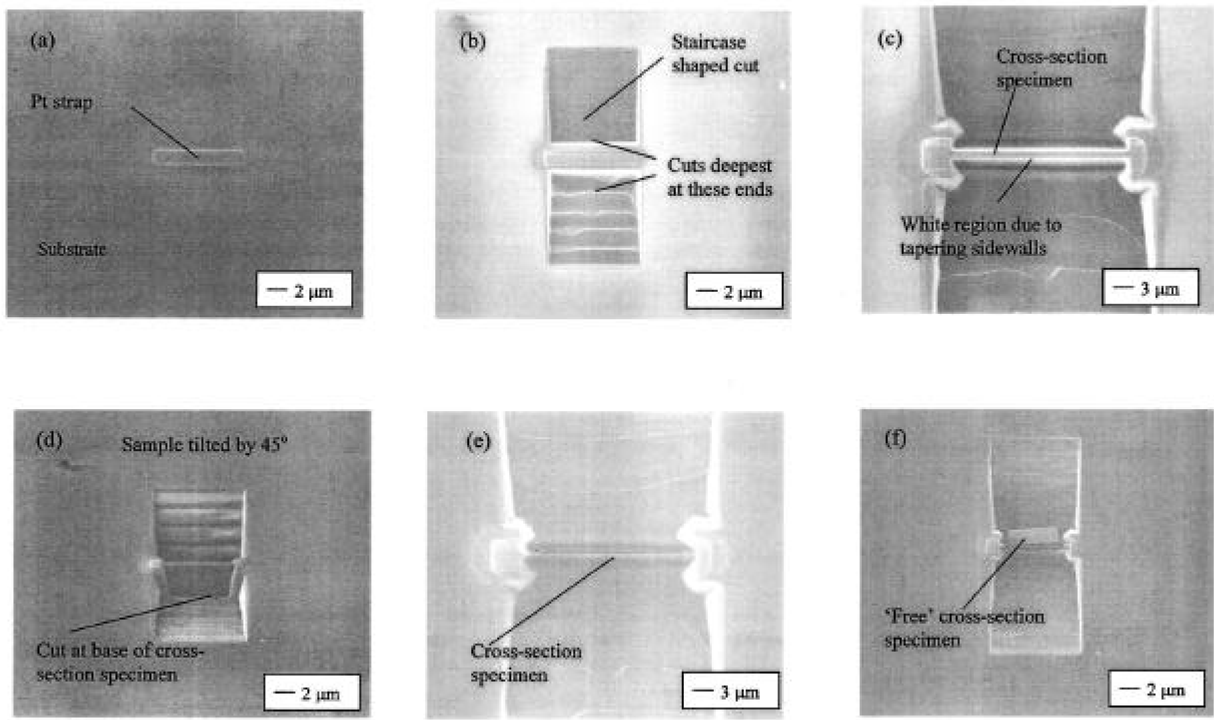

. M. Langford et al., J. Vac. Sci. Technol. A 2001 **19(5)** 2186-2193

Introduction on electron microscopes

SEMPA : Scanning Electron Microscopy with Polarization Analysis

SPLEEM

Lorentz microscopy

Electron holography

- Theoretical principle
- Experimental set-up
- Examples

SEMPA measures the spin polarization of the secondary electrons that exit from a magnetic sample as the finely focused (unpolarized) beam of the scanning electron microscope rasters over the sample.

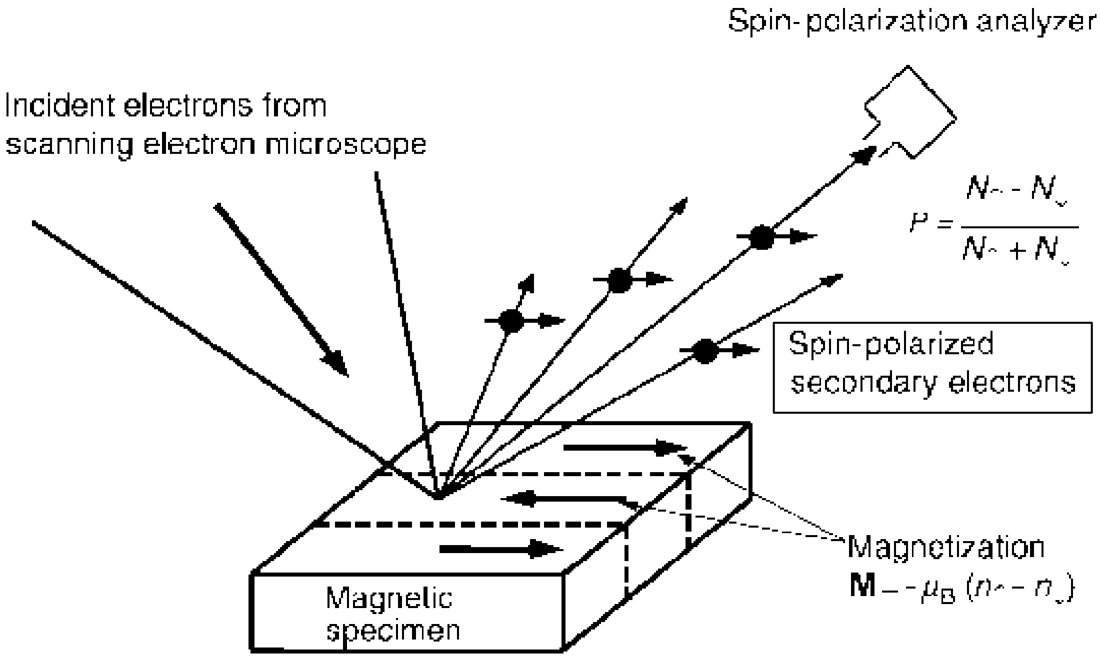

Interaction : Incident electron beam-specimen

Result from an incident electron passing "near" an atom in the specimen, near enough to impart some of its energy to a lower energy electron

Emission: Secondary electrons

Secondary electrons are predominantly produced by the interactions between energetic beam electrons and weakly bonded conduction-band electrons in metals

If the sample is ferromagnetic : the emitted electrons are spin-polarized (difference of occupancy of the up and down bands)

SEMPA measures the spin polarization of the secondary electrons that exit from a magnetic sample as the finely focused (unpolarized) beam of the scanning electron microscope rasters over the sample.

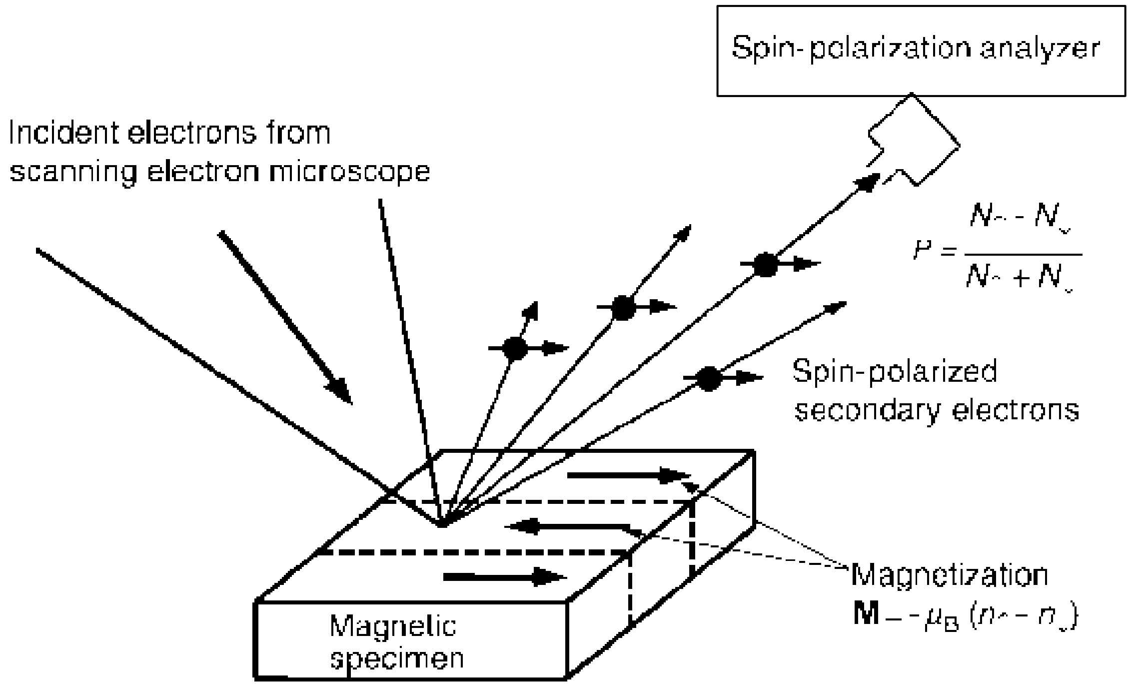

Physical principle : use of the spin-orbit interaction as a means of transforming a spin asymmetry into a spatial asymmetry.

Example
Mott detector : the electrons are accelerated to high energies (typically 50 to 100 keV) and scattered by a high-atomic-number target.
This scattering is spin-dependent because of the spin-orbit interaction.

Therefore, electrons with spin up and spin down with respect to the scattering plane are preferentially scattered into different directions.

SEMPA measures the spin polarization of the secondary electrons that exit from a magnetic sample as the finely focused (unpolarized) beam of the scanning electron microscope rasters over the sample.

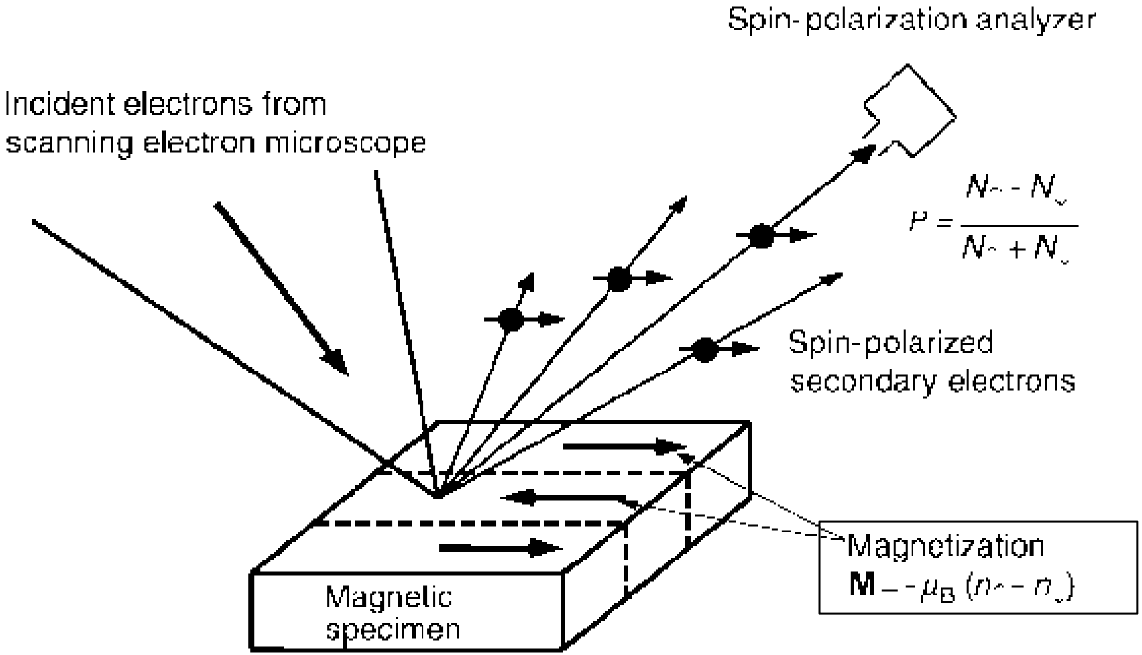

The spin of the secondary electrons points preferentially in the opposite direction of the magnetisation vector : $M=-\mu_B(n_+-n_-)$ as the electron spin magnetic moment and the electron spin are opposite

the "spin" magnetic moment

$$\vec{m}_s = \frac{q}{2m_e}\sum \vec{L}_i = -\frac{e}{2m_e}\vec{S}$$

the "spin" angular momentum

Theoretical principle

Measure of the topography ($n_+ + n_-$) and the magnetisation at the same time ($n_+ - n_-$)

Surface technique : secondary electrons are emitted from 1 nm

Measure without applying a field (deviation of the electron beam)

Theoretical principle

Experimental set-up

Examples

Non polarized incident beam

Work at low incident energies:
High I
High P : the spin of the 2dary electron is dependent on the 2dary electron energy. The P at low energy is 2 or 3 times higher than expected due to preferential inelastic scattering of spin down electrons which leads to a higher escape probability for spin up electrons

BUT

Large beam diameter
Beam more susceptible to deflections and distortions

Typical work tension 10kV

Mott detector

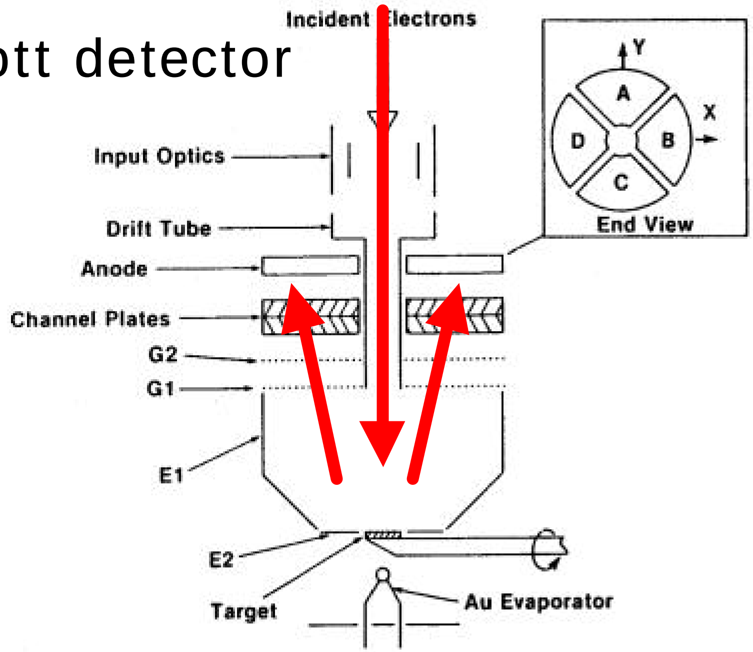

Schematic drawing of a low energy diffuse scattering spin polarization analyzer.
Based on the scattering of 150eV electrons from an evaporated Au target.

The anode is divided into quadrants so that the polarization components along both x and y may be measured simultaneously

$$P_x = \frac{1}{S}\frac{N_A - N_C}{N_A + N_C}$$

$$P_y = \frac{1}{S}\frac{N_B - N_D}{N_B + N_D}$$

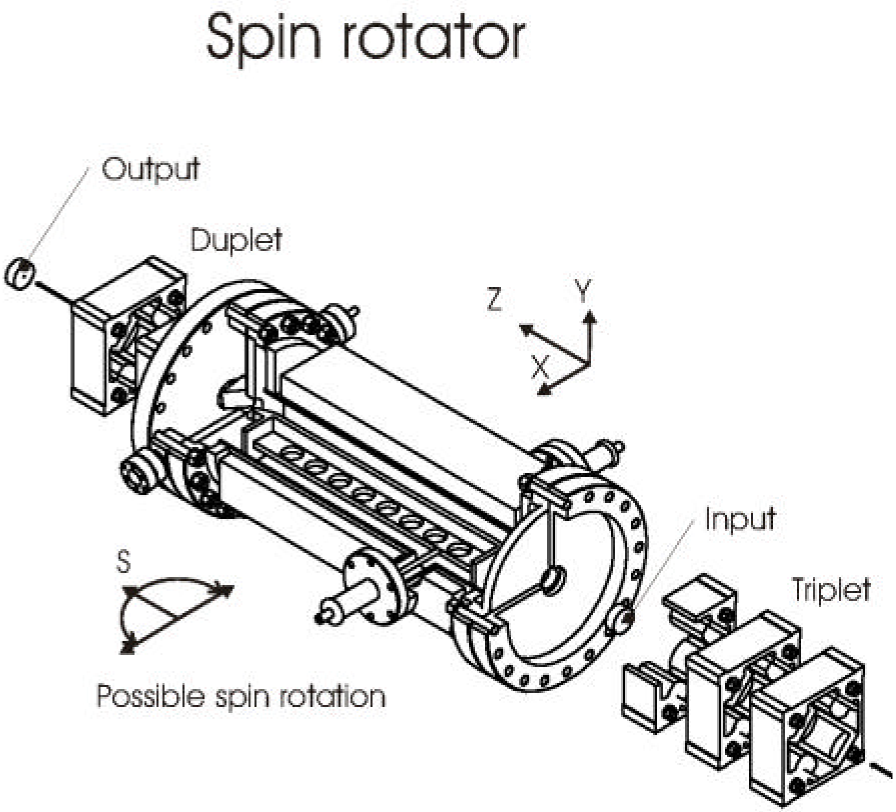

A Wien filter is a suitable spin rotator. An electric field rotates the spin, while a crossed magnetic field balances the Lorentz force.

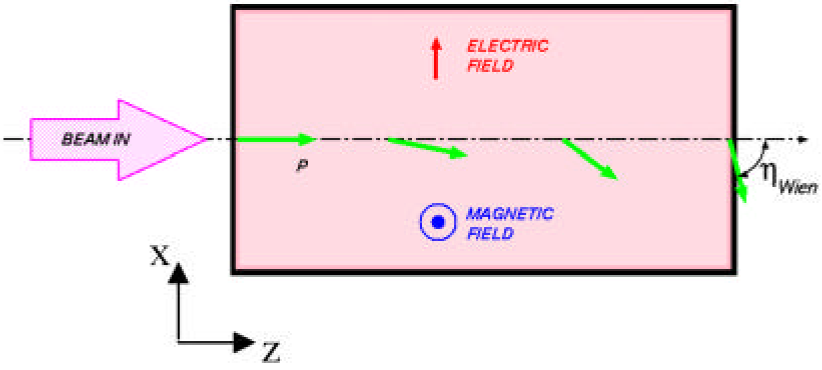

Spatial **resolution** : determined largely by the electron beam diameter of the SEM.

Beam current ↘ as beam diameter ↘

Compromise between resolution (beam diameter) and acquisition time
Limited by :

- sample drift
- deterioration of the sample surface
- operator patience

beam current of 1 nA acquisition in about 1 h
resolution limits 50 nm for LaB6 and 10 nm for field emission SEM electron gun cathodes.

Samples : conductive (carbon coating)

Theoretical principle

Experimental set-up

Examples

First experiments : Koike et al. – 1987

K.Koike, H.Matsuyama, H.Todokoro, K.Hayakzwa,
Scanning microscopy 1987 **1** 31

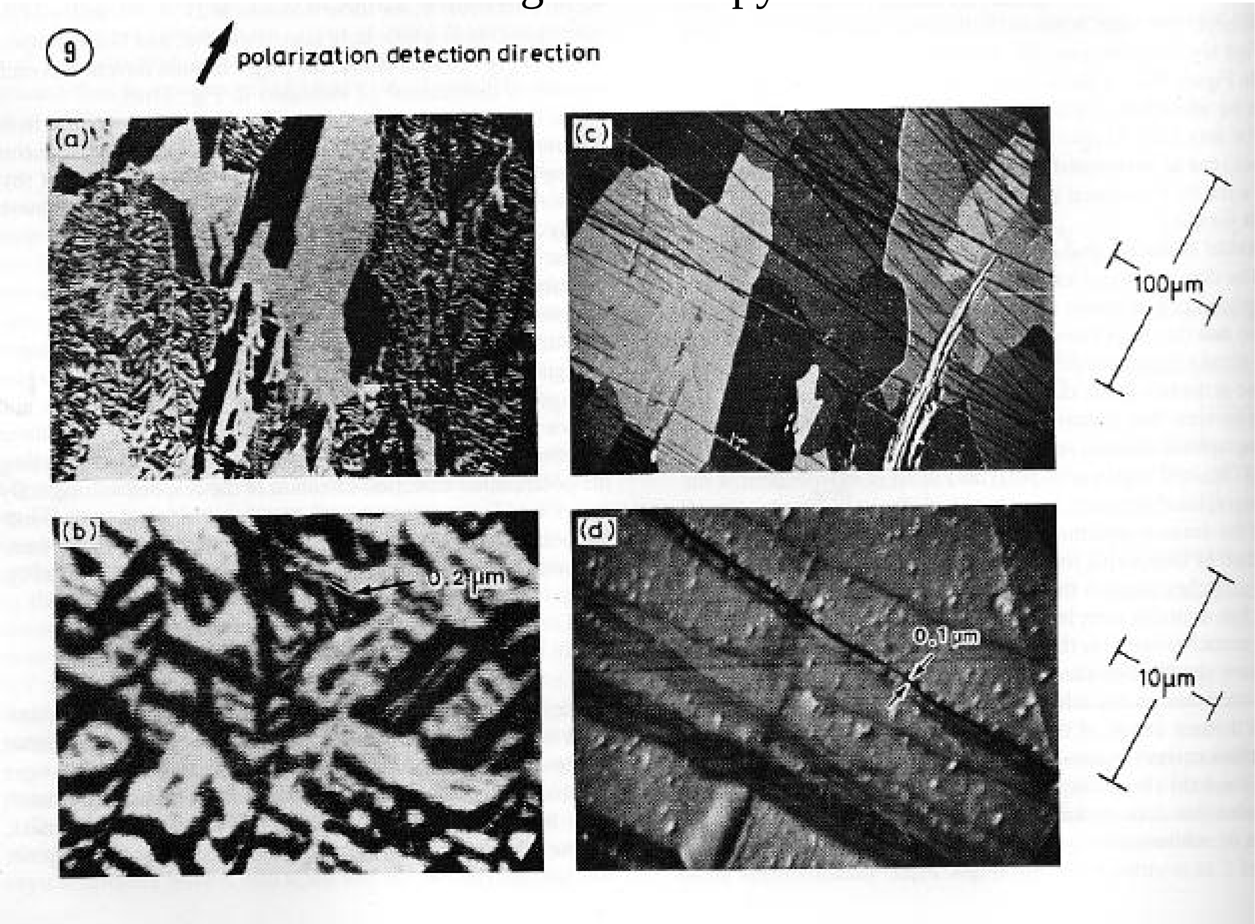

Domain images $n_+ - n_-$ Absorption current images $n_+ + n_-$

Scanning electron microscopy with polarization analysis (SEMPA)

M. R. Scheinfein, J. Unguris, M. H. Kelley, D. T. Pierce, and R. J. Celotta

Rev. Sci. Instrum. 1990 **61** 2501

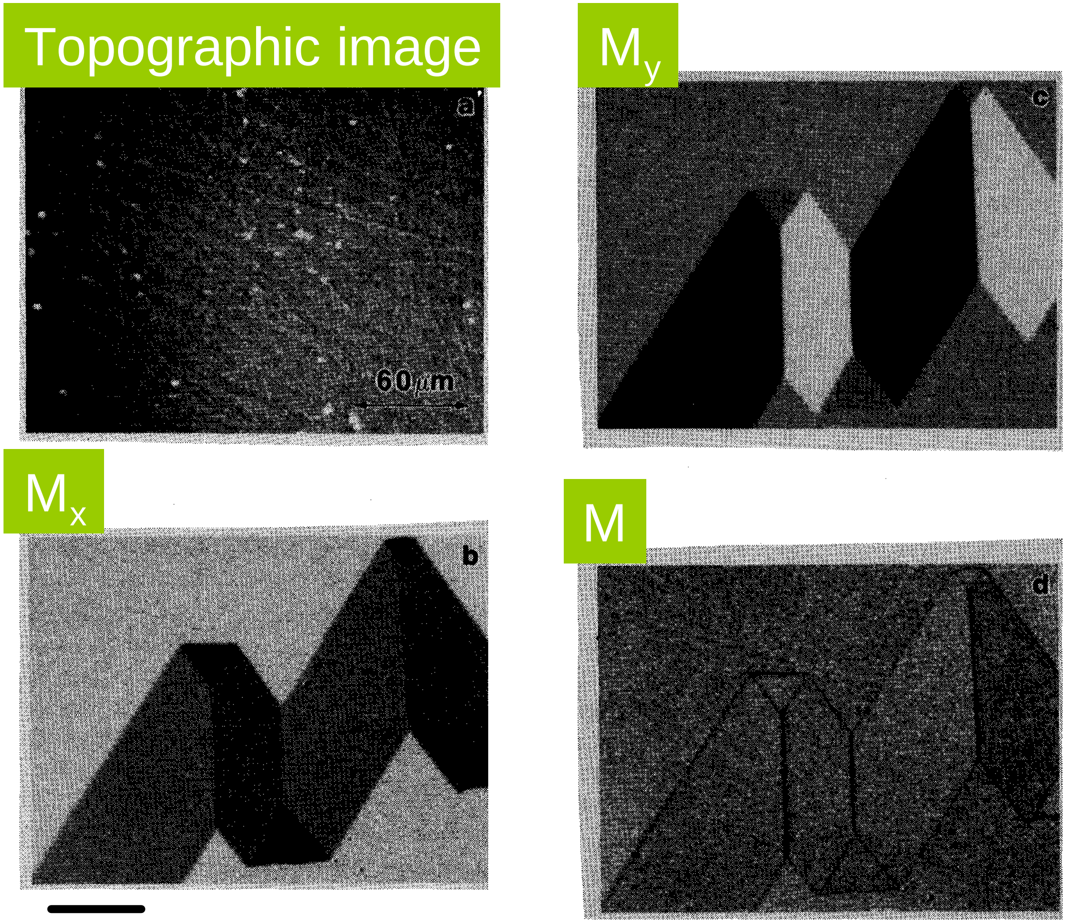

50µm

FeSi(100)

white

black white

black

Probe diameter ~ 50nm

Observation of Antiparallel Magnetic Order in Weakly Coupled Co/Cu Multilayers

J. A. Borchers, J. A. Dura, J. Unguris, D. Tulchinsky, M. H. Kelley, and C. F. Majkrzak
National Institute of Standards and Technology, Gaithersburg, Maryland 20899

S. Y. Hsu, R. Loloee, W. P. Pratt, Jr., and J. Bass
Department of Physics and Astronomy, Michigan State University, East Lansing, Michigan 48824

Phys. Rev. Lett. 1999 **82** 2796

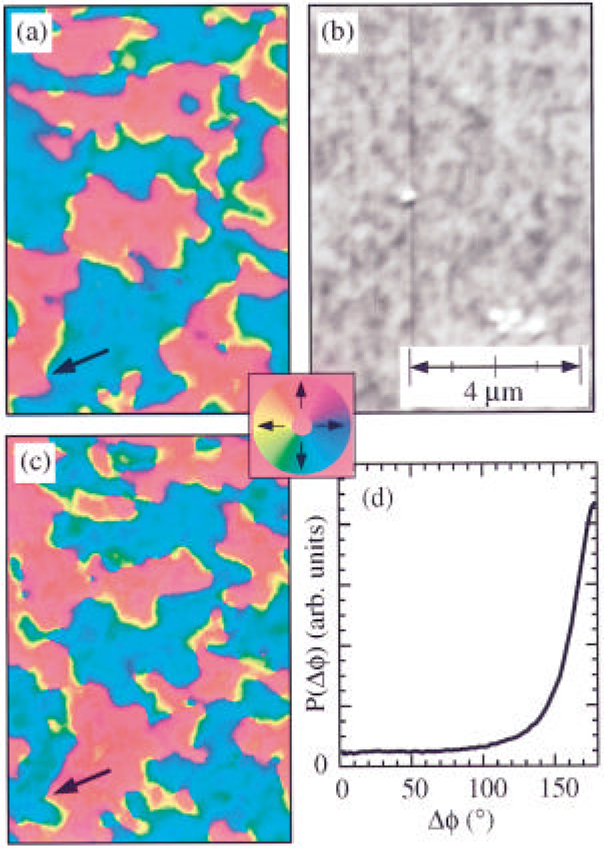

$[Co(6nm)/Cu(6nm)]_{20}$ multilayer

FIG. 3(color). SEMPA images of the topmost Co layer magnetization (a) and topography (b) and second Co layer magnetization (c) in the $[Co(6\ nm)|Cu(6\ nm)]_{20}$ sample. The magnetization direction is mapped into color as indicated by the color wheel in the center. A histogram of the difference in the magnetization direction between the two layers, $\Delta\phi$, is shown in (d).

Antiferromagnetic coupling between two adjacent Co layers due to the Cu spacer

In situ ion sputtering using 2 keV Ar^+ ions was used to clean and depth profile the sample.

SEMPA

Perpendicular magnetisation of a Co/Au(111) sample

M.Speckmann, H.P.Oepen, H.Ibach, Phys. Rev. Lett. 1995 **75** 2035

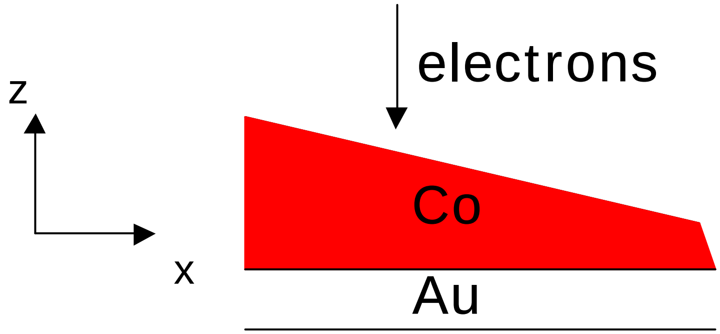

Wedge shaped Co layer

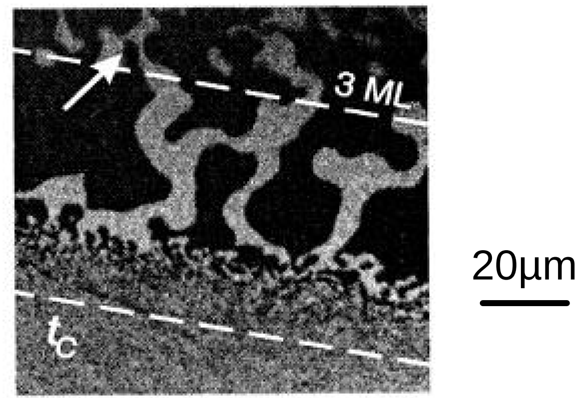

Out-of-plane mag : white
In-plane mag : black

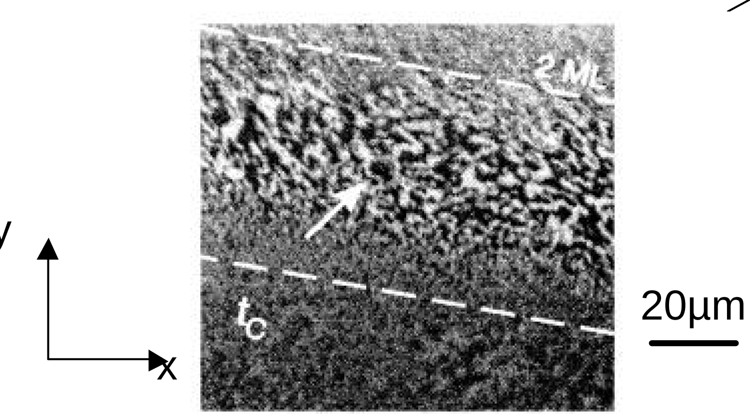

After annealing
240°C 10 min

Domain
enlargement
Increase of t_c

Examples Zigzag elements

Zigzag-shaped magnetic sensors

F. C. S. da Silva
National Institute of Standards and Technology, Boulder, Colorado 80305

W. C. Uhlig
National Institute of Standards and Technology, Gaithersburg, Maryland 20899

A. B. Kos, S. Schima, and J. Aumentado
National Institute of Standards and Technology, Boulder, Colorado 80305

J. Unguris
National Institute of Standards and Technology, Gaithersburg, Maryland 20899

D. P. Pappas[a)]
National Institute of Standards and Technology, Boulder, Colorado 80305

Appl. Phys. Lett. 2004 **85** 6022

Aim : design of an element in which a bias is maintained between the current and the magnetisation

Zigzag element
Ta(5nm)/**NiFe**(30nm)/Ta(5nm)

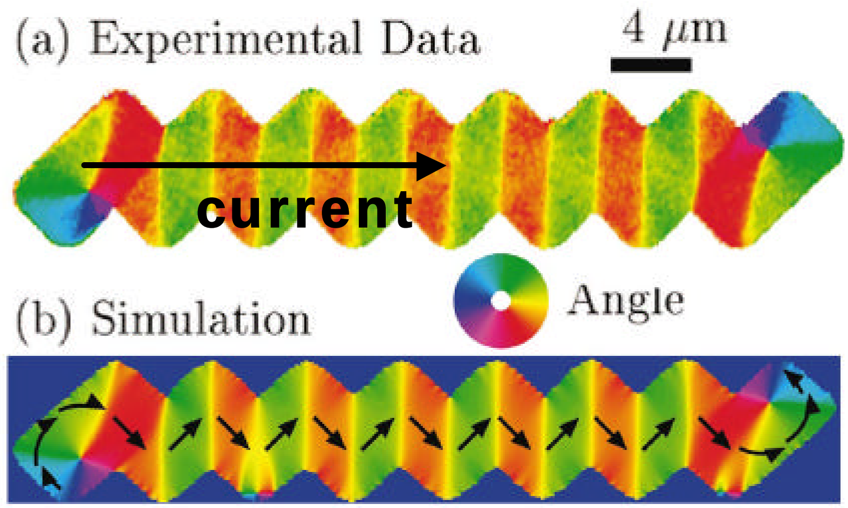

FIG. 2. (Color) (a) Experimental SEMPA image of the eight-block zigzag structure. (b) Simulation performed on the same geometry using OOMMF. The magnetization direction maps onto the angle color map ring.

SEMPA

Two magnetic states:

- the flux-closure vortex state
- the ‘onion’ state, accessible reversibly from saturation and characterized by the presence of two opposite head-to-head walls.

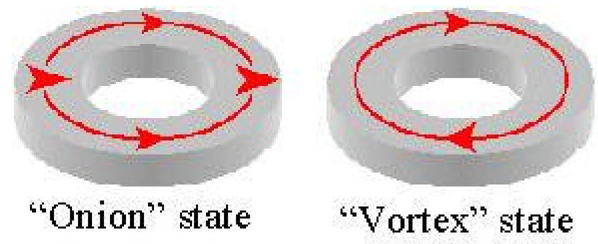

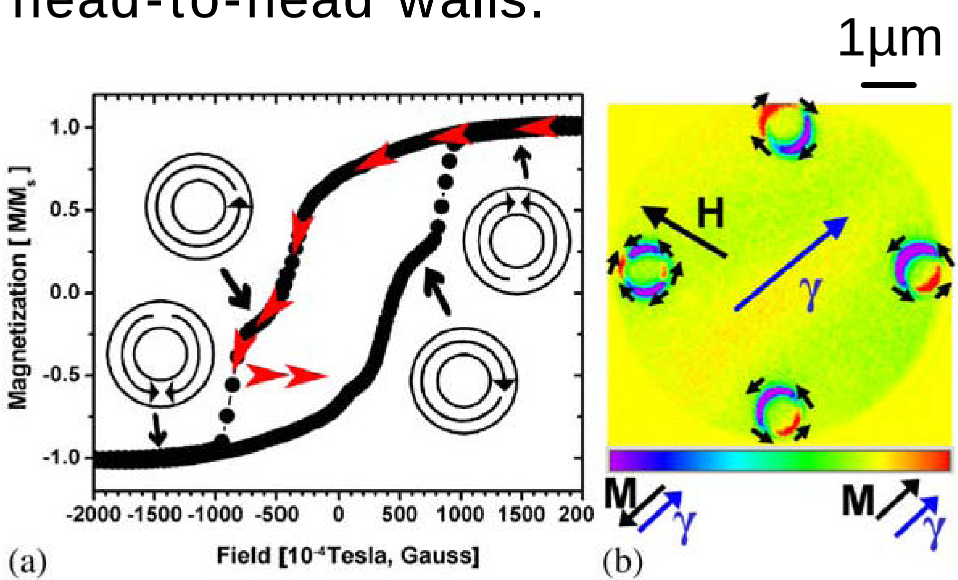

Fig. 1. (a) Hysteresis loop measured on an array of rings (outer diameter $D = 1200$ nm, inner diameter $d = 900$ nm and thickness $t = 15$ nm polycrystalline Co). The magnetization configurations of the onion and the vortex states are shown schematically. Red arrows indicate the field path used to obtain the rings in the states imaged with PEEM in (b). (b) PEEM image of four polycrystalline Co rings. The top ring is in the clockwise vortex state, the bottom and right rings are in the counter-clockwise vortex state and the left ring is in the onion state pointing along the direction of the applied field H. The field of view is ≈10 μm across and the blue arrow points in the direction of the photon beam. The colour scale indicates the direction of the magnetization with reference to the direction of the incoming photon beam (magnetization parallel to the incoming photon beam (red) to anti-parallel (purple)). For colour, please see on-line version.

Spin configurations and classification of switching processes in ferromagnetic rings down to sub-100 nm dimensions

M. Klaui, C.A.F. Vaz, T.L. Monchesky, J. Unguris, E. Bauer, S. Cherifi, S. Heun, A. Locatelli, L.J. Heyderman, Z. Cui, J.A.C. Bland, J. Mag. Magn. Mat. 2004 **272-276** 1631

500nm

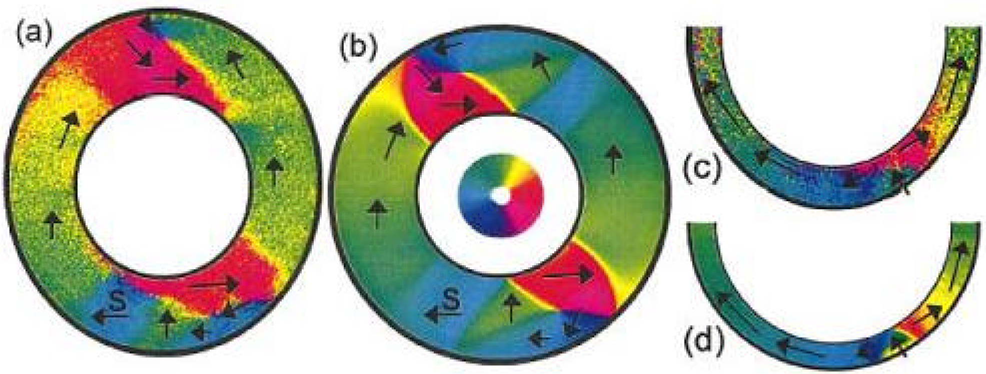

Onion state in a wide (inner diameter=900nm) and in a narrow (inner diameter=1200nm) epitaxial 34-nm fcc Co ring, outer diameters 1.7 µm.
SEMPA images of the wide (a) and the narrow (c) ring.
Corresponding micromagnetic simulations (OOMF) of the wide (b) and the narrow (d) ring, showing the vortex- and transverse-type domain walls.

NIST Gaithersburg (USA)
http://physics.nist.gov/Divisions/Div841/Gp3/Facilities/sempa.html

ETH Zürich (Switzerland)
http://www.solid.phys.ethz.ch/pescia/sempa.htm

University of Hamburg (Germany)
http://www.physnet.uni-hamburg.de/iap/group_g/index.htm

University of Seoul (South Korea)
http://csns.snu.ac.kr/lab/systems/sempa/

University of California, Irvine (USA)
http://www.physics.uci.edu/NEW/cmexpt.shtml

Introduction on electron microscopes

SEMPA

SPLEEM : Spin Polarized Low Energy Electron Microscopy

Lorentz microscopy

Electron holography

Theoretical principle

Experimental set-up

Examples

Exchange interaction between the incident electrons with spin $\mathbf{s}_j$ and the target electrons with spin $\mathbf{s}_i$

$$Vex = \sum_{ij} J(\mathbf{r}_i - \mathbf{r}_j)\mathbf{s}_i \bullet \mathbf{s}_j$$

J being the exchange coupling strength

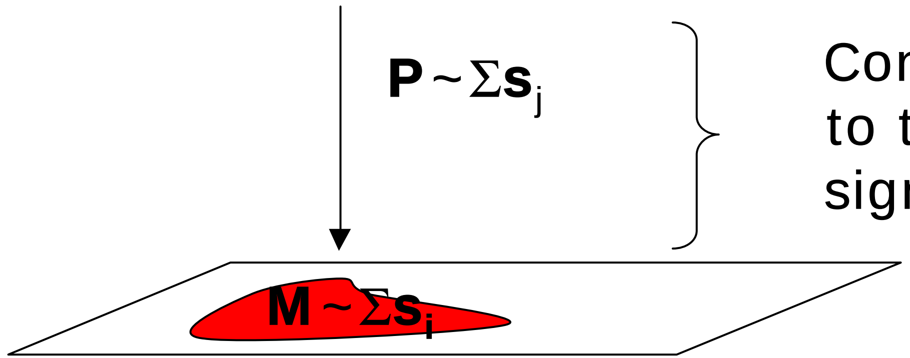

Contribution ~**P.M** to the scattered signal

E. Bauer, Rep. Prog. Phys. 1994 **57** 895

In crystalline materials, the contrast can also be understood in terms of spin-dependent band structure

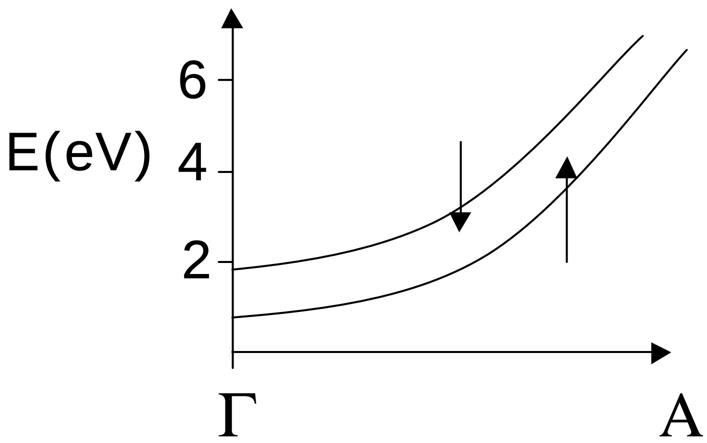

$E_{beam} < 1eV$
reflection because no energy state is available

$1eV < E_{beam} < 2eV$
low reflectivity for spin up and large for spin down

$E_{beam} > 2eV$
difference in reflectivity due to the difference in the densities of states (up and down)

Combination of two effects explaining the contrast:

- The exchange interaction
- The different inelastic mean free paths of electrons with spin parallel and antiparallel to the spin of the electrons in the ferromagnet

Best magnetic contrast for low electron energy, typically 10eV

Most of the contrast is determined by the microstructure

Theoretical principle

Experimental set-up

Examples

Experimental set-up

Requirements

- Spin Polarized incident beam with high intensity

- Possibility to rotate the polarisation of the incident beam to optimize the orientation between P and M : acquisition with antiparallel P directions

- No magnetic lenses in the system
  Electrostatic condenser and objective lenses

- Rapid and flexible image accumulation and processing so that the difference (up-down) can be obtained rapidly
  Suitable acquisition system

T.Duden et al., Jour. Elec. Micr.. 1998 **47** 379

GaAs band-gap photoexcitation

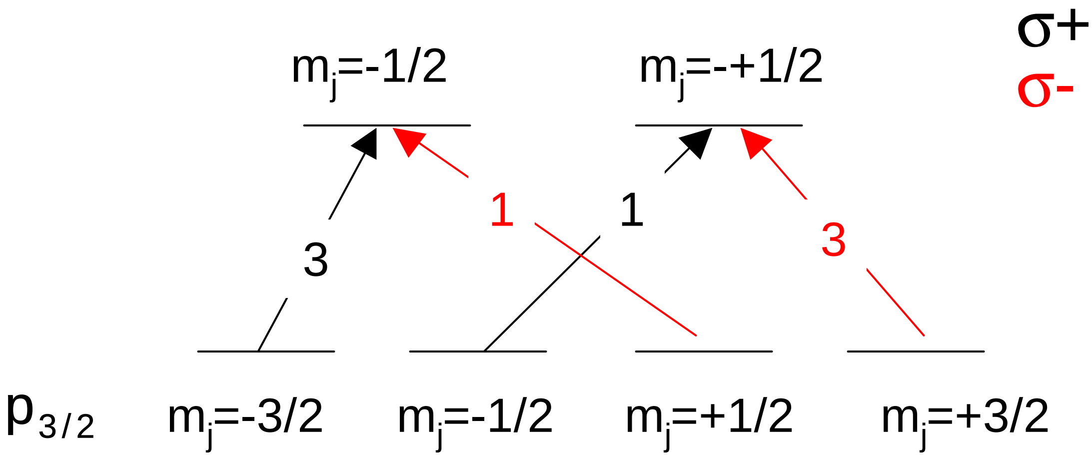

Polarisation $$P = \frac{N_+ - N_-}{N_+ + N_-}$$

	σ+	σ-
N_+/N_-	0.25	0.75
P	-0.5	0.5

Spin polarized beam

http://nvl.nist.gov/pub/nistpubs/sp958-lide/203-208.pdf

Reduction of the vacuum level of the GaAs (4eV) by a surface treatment using CsO

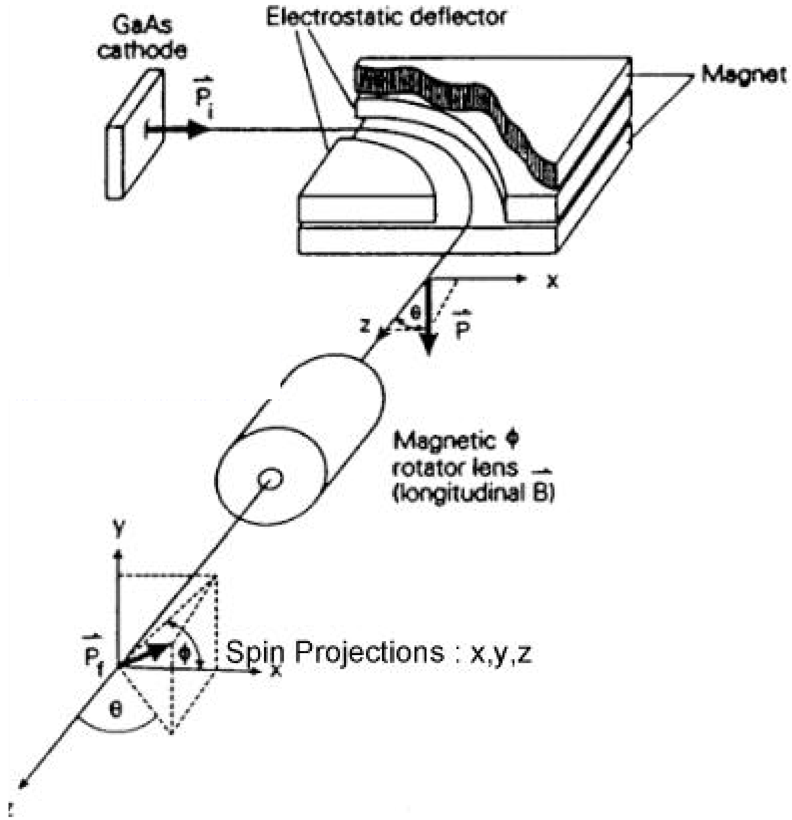

Spatial **resolution** : 20 nm

Samples : ferromagnetic or ferrimagnetic
conductive

Theoretical principle

Experimental set-up

Examples

Example

atomically flat ultrathin (110)-oriented Fe films on a W(110) surfac

LEEM

SPLEEM

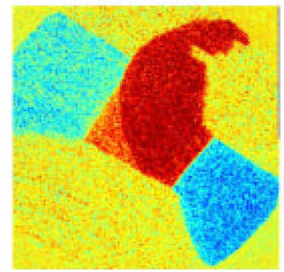

5µm

blue and red colours ⟺ regions with opposite magnetization
intensity ⟺ magnitude of the asymmetry.

R. Zdy et al., Applied Surface Science 249 (2005) 38–44

SPLEEM

University of Arizona, USA

http://phy.asu.edu/homepages/bauer/spleem.htm

University of California, Berkeley, USA

http://ncem.lbl.gov/frames/spleem.htm

http://www.leem-user.com/

Introduction on electron microscopes

SEMPA

SPLEEM

Lorentz microscopy

Electron holography

Theoretical principle

Experimental set-up

Examples

Electron moving through a region of space with an electrostatic field and a magnetic field B experiences the Lorentz force F_L : $\mathbf{F}_L = -e(\mathbf{E}+\mathbf{v}\wedge\mathbf{B})$

If $E=\mathbf{0}$, F_L acts normal to the travel direction of the electron, a deflection will occur.Only the in-plane magnetic $B_\perp$ induction will contribute to the deflection

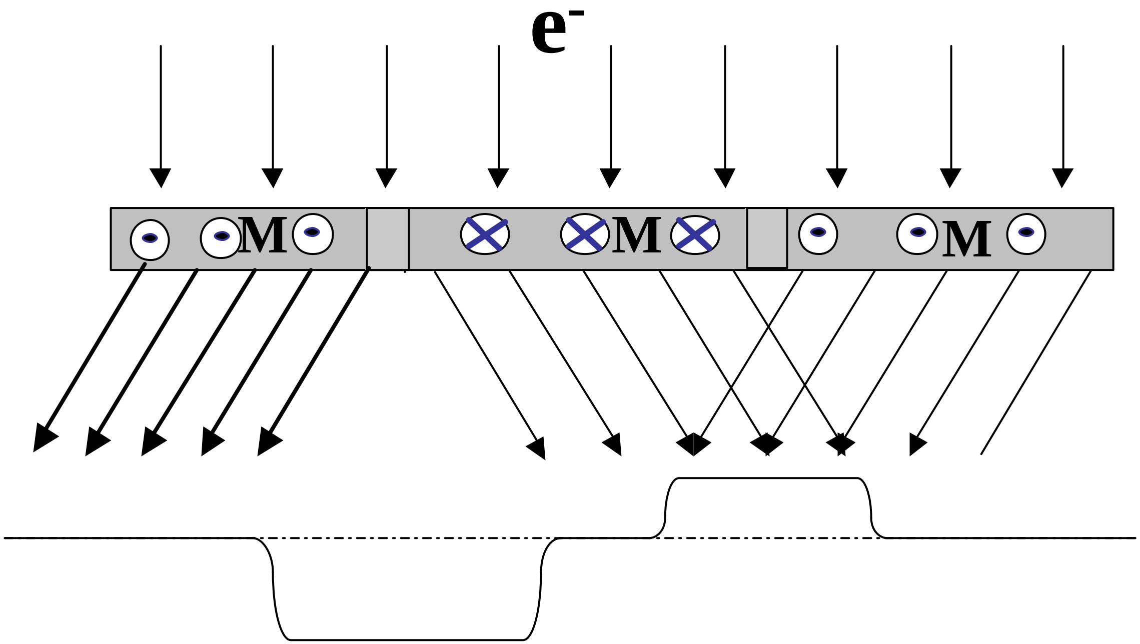

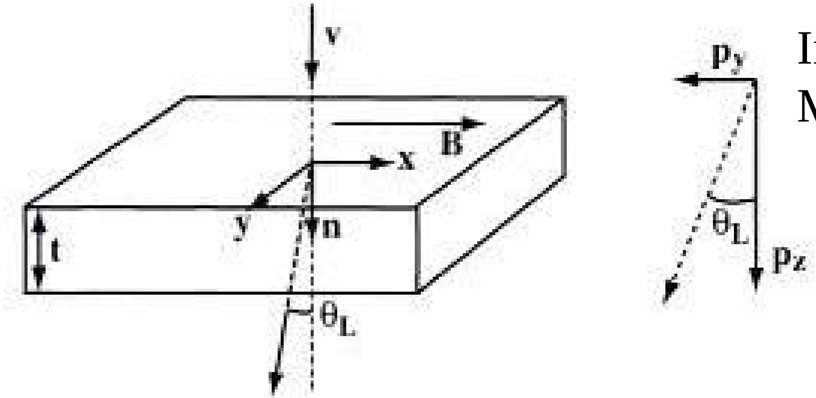

Introduction to conventional electron microscopy
M. De Graef, 2003, Cambridge University Press

Schematic of a magnetic thin foil and the resulting deflection of an incident electron beam

$$p_y = \int_0^t F_L \, dt \qquad \text{with } F_L = e v_z B_\perp \qquad p_y = e \int_0^t B_\perp \, dz = e B_\perp t$$

$C_L(E)$ depends on the acceleration voltage of the microscope

$$q_L = \frac{p_y}{p_z} = \frac{e B_\perp t}{m v} = C_L(E) B_\perp t$$

θ_L depends on $B_\perp$ and t

θ_L ~ tens of μrad

θ_B (electron diffraction angles) ~ tens of mrad

Theoretical principle

Experimental set-up

Examples

Experimental set-up

Modes

Fresnel mode :
domain walls and
magnetisation ripples

Foucault mode :
domains

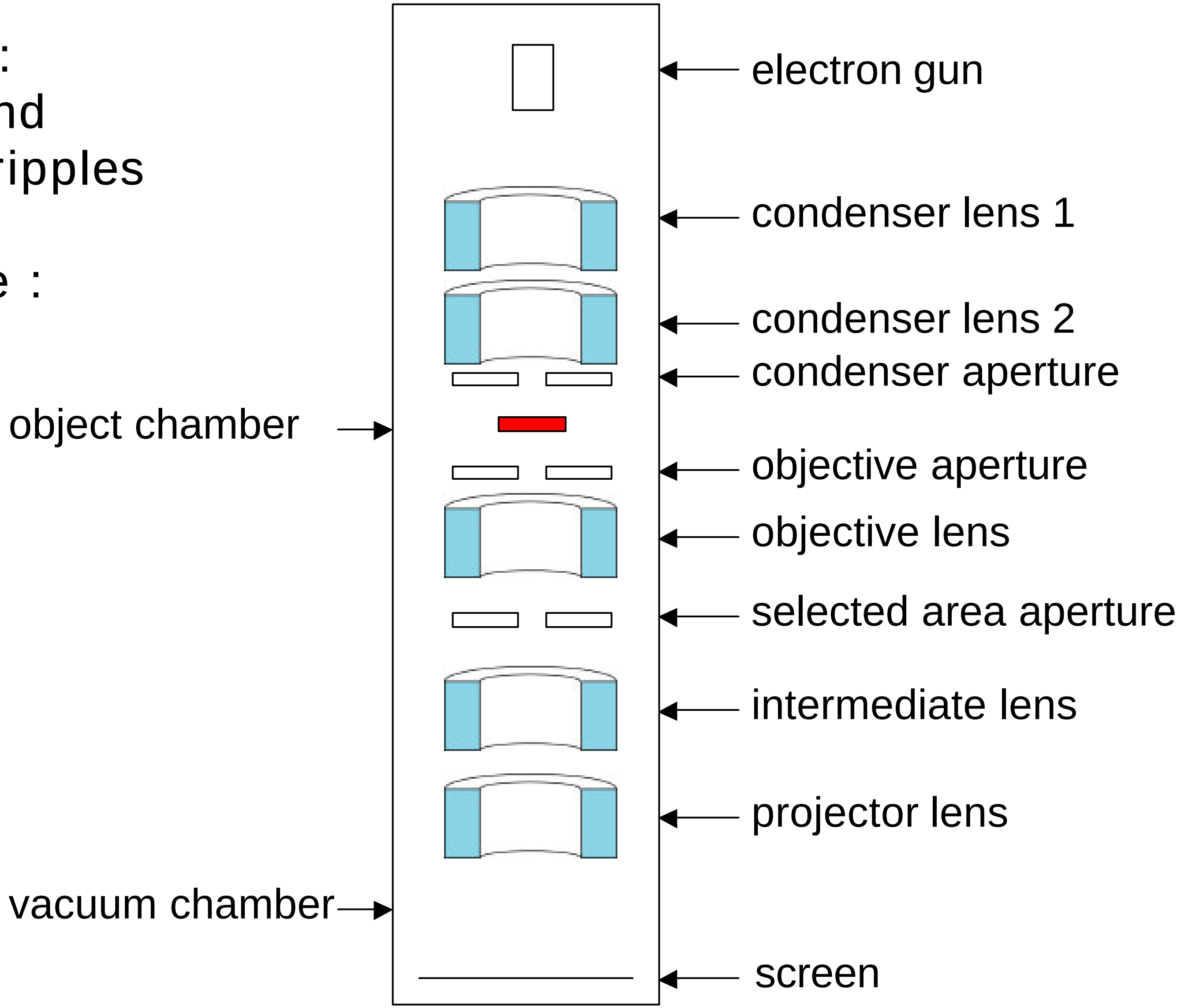

Lorentz microscopy

Experimental set-up

Fresnel mode

Dr. Josef Zweck University of Regensburg

Domain wall imaging

Co nanodots

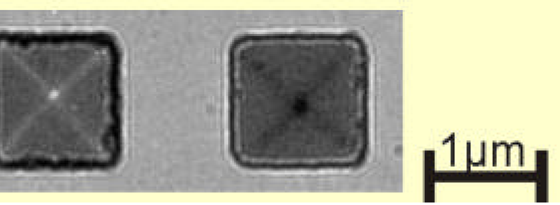

Underfocus Δf = -83 mm

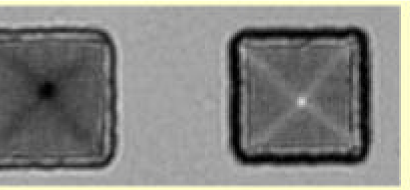

Overfocus Δf = 108 mm

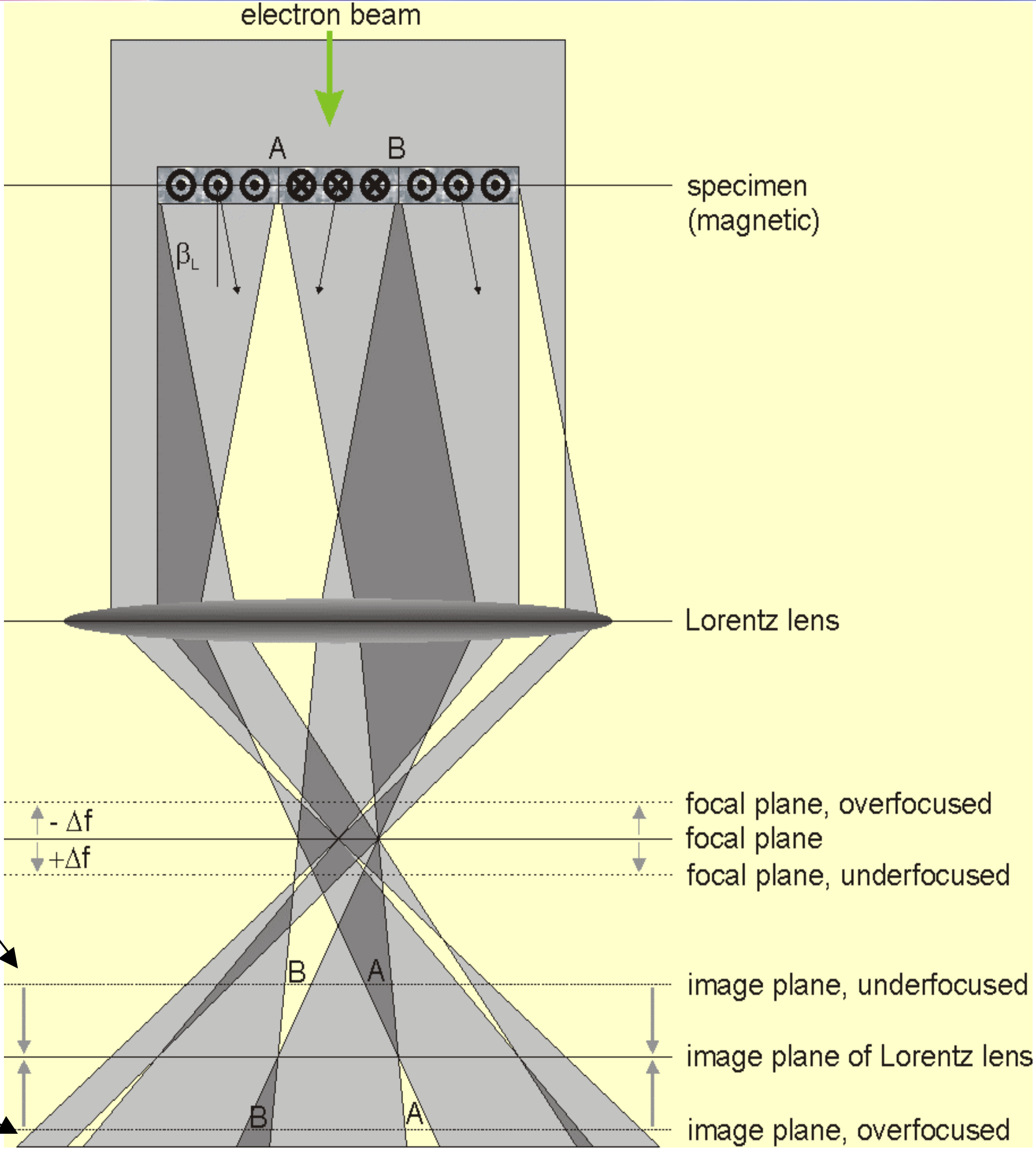

Lorentz microscopy

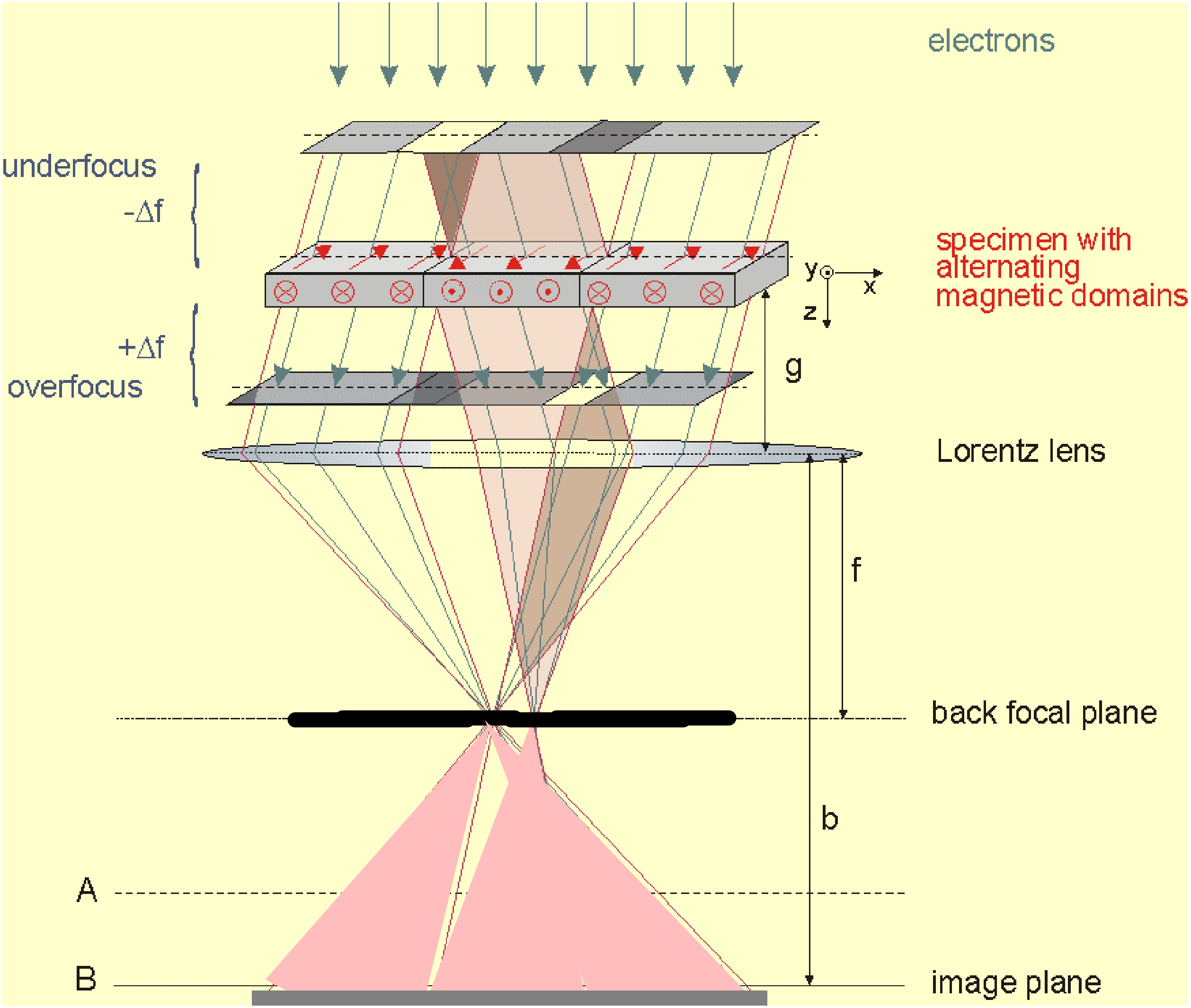
electrons
underfocus
-Δf
specimen with
alternating
magnetic domains
y
x
z
+Δf
overfocus
g
Lorentz lens
f
back focal plane
b
A
B
image plane

Experimental set-up

Foucault mode

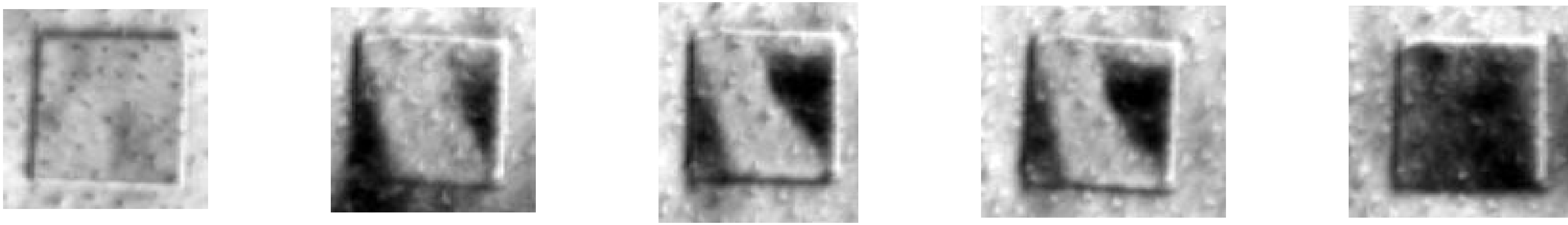

0 Oe | 19 Oe | 38 Oe | 45 Oe | 51 Oe

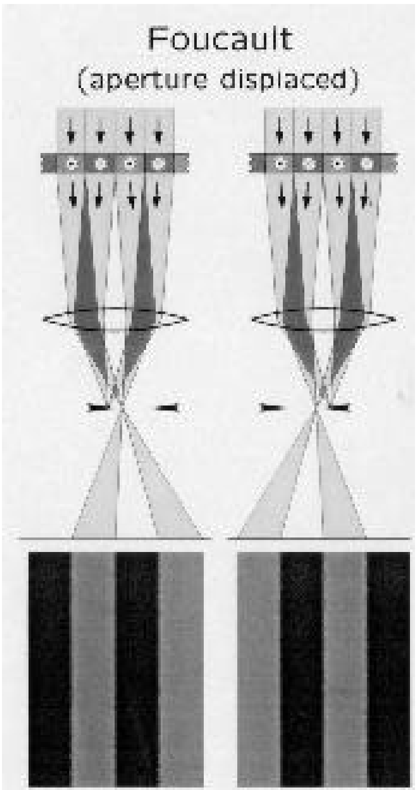

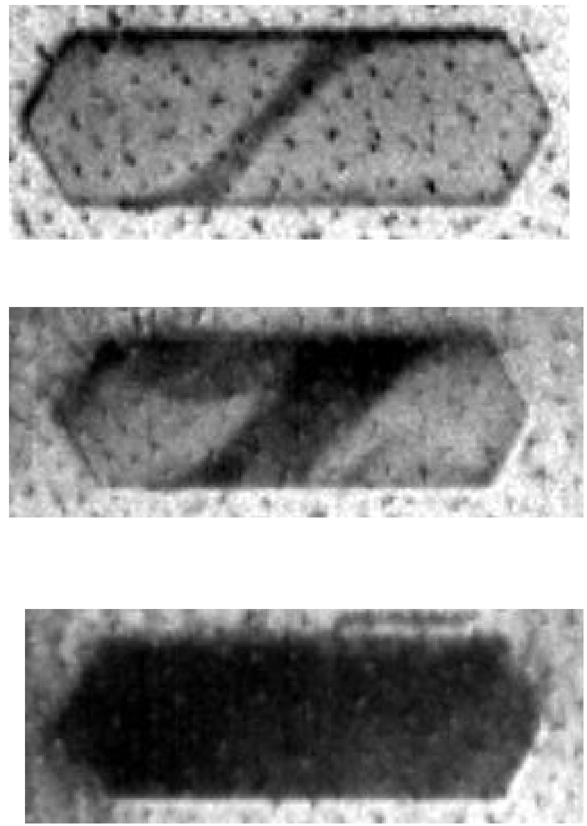

0 Oe

-10 Oe

-40 Oe

Lorentz microscopy

Problem : objective lens magnetic field : 2T

How to get rid of this field?

- Turn of the objective lens -> no magnification
- **Lorentz lens**

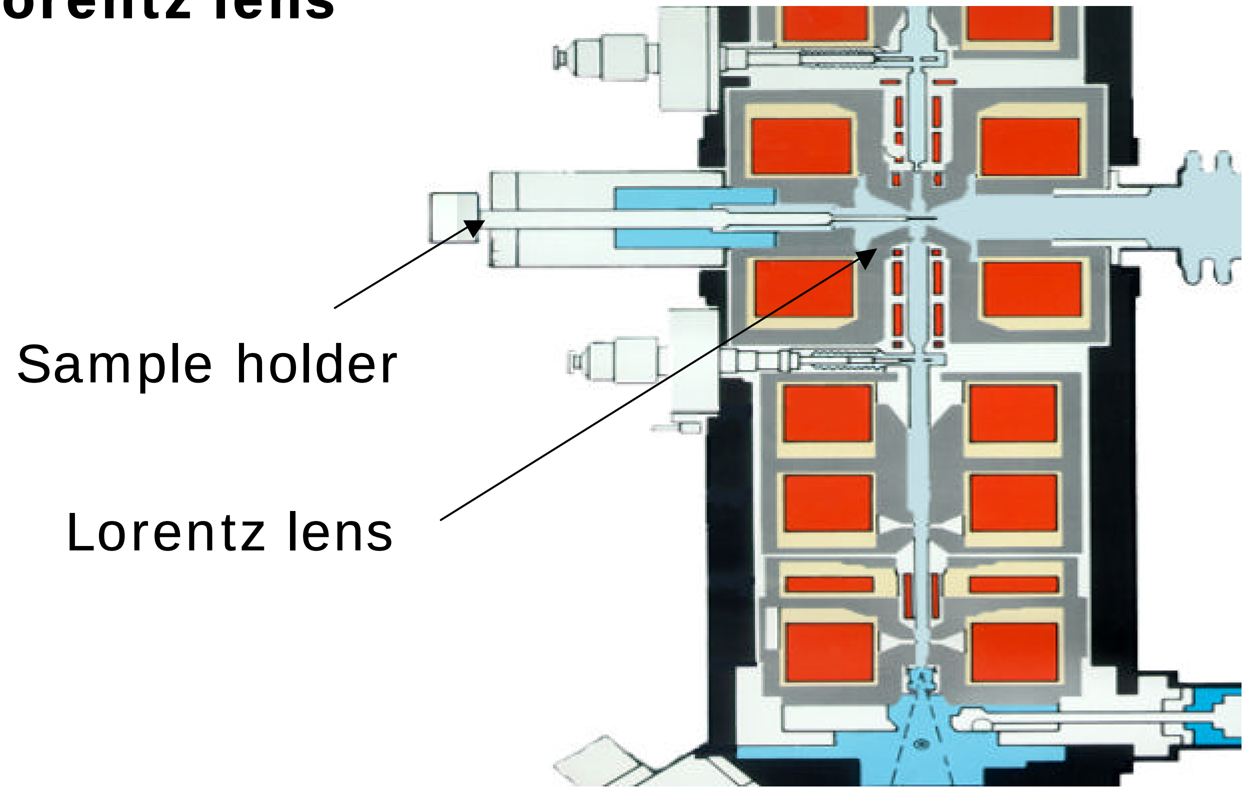

Lorentz TEM useful to observe the domain evolution under an applied field

Applying a field :

- **Use the objective lens low excitation, rotate the sample holder in the fixed vertical field : the in-plane field depends on the tilt angle**
- Build a dedicated sample holder with coils to apply a field

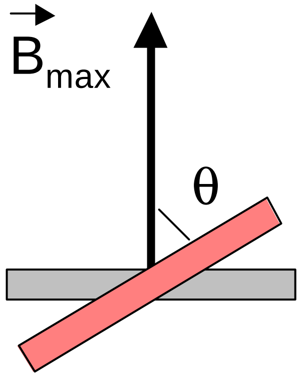

$B = B_{max} \cos\theta$

$B=0$

θ

Tilt angle

B_{max} set to a low value by adjusting the current in the objective lens

- Use the objective lens low excitation, rotate the sample holder in the fixed vertical field : the in-plane field depends on the tilt angle
- **Build a dedicated sample holder with coils to apply a field**

Uhlig at al. Ultramicroscopy. 2003 **94** (3-4) 193-6

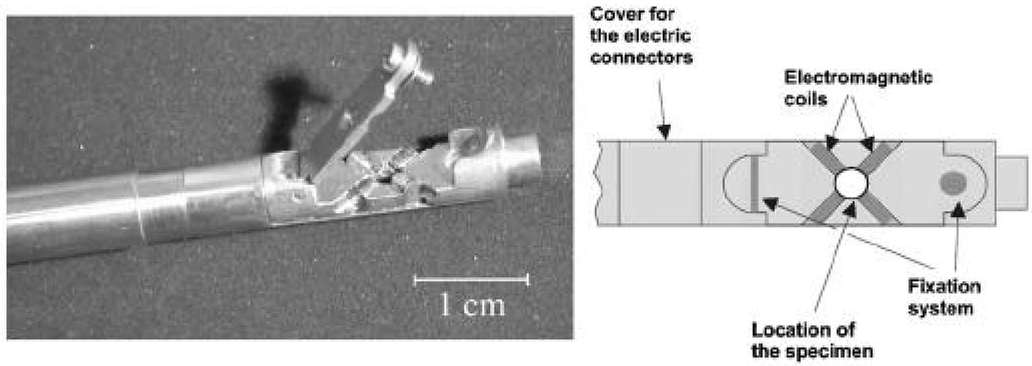

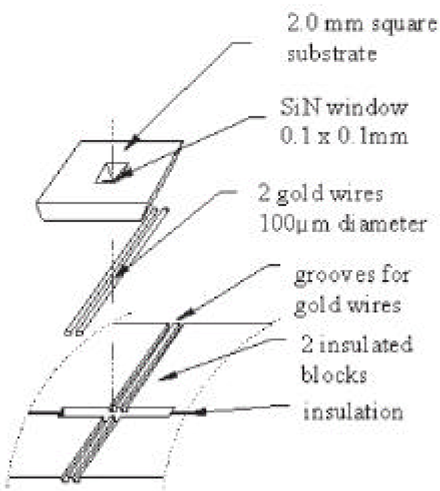

Figure 1. Schematic of the new magnetizing stage.

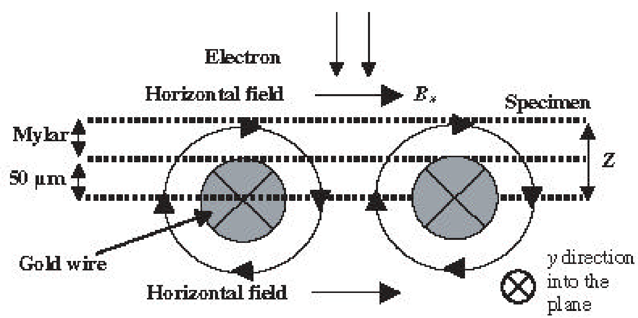

C K Lim *et al* J. Phys. D: Appl. Phys. 2003 **36** 3099-3102

Samples

- •Plane view
- •On transparent windows (example : Si3N4) polycrystalline samples
- •Sample deposition dedicated to Lorentz experiments

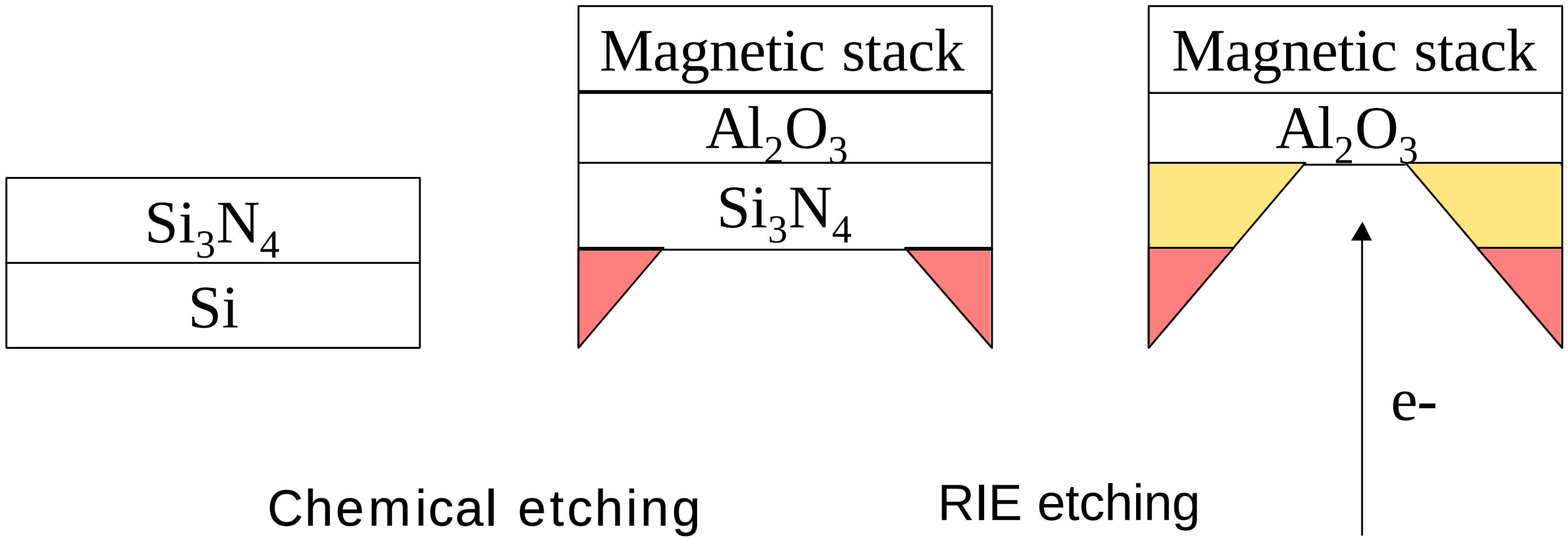

Chemical etching
Si_3N_4 etch top layer

RIE etching

Resolution 20nm

Theoretical principle

Experimental set-up

Examples

Determination of the magnetization axis

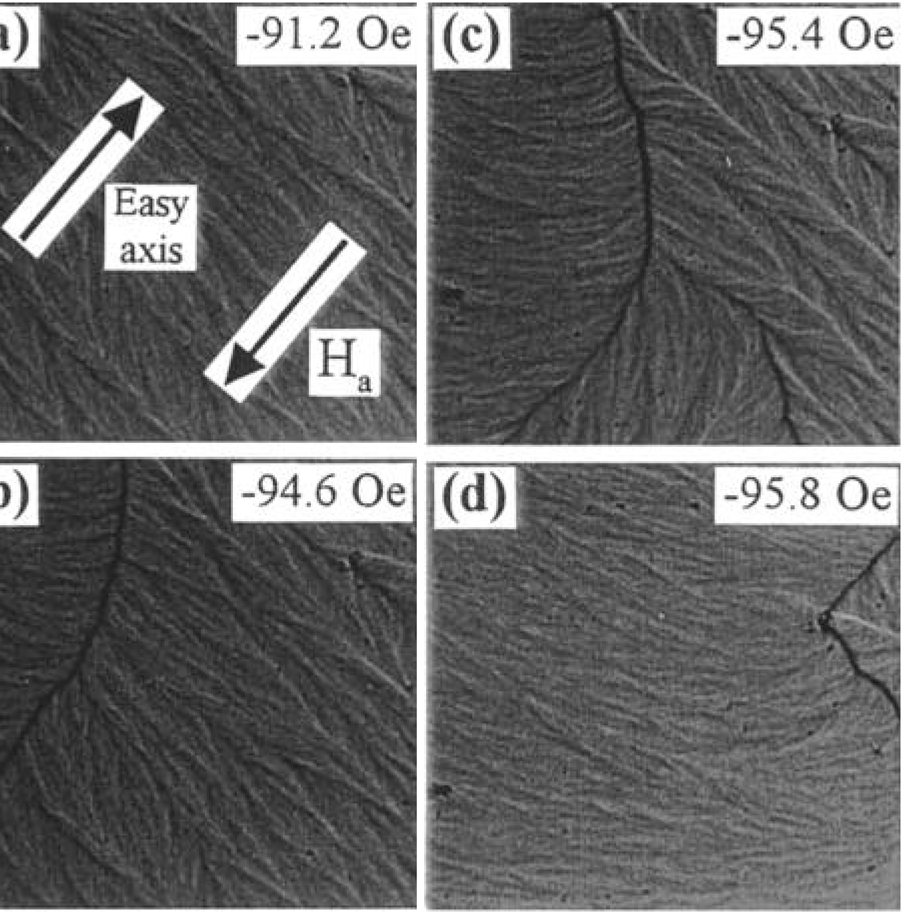

Magnetisation ripple visible in Fresnel images of polycrystalline specimens as a result of small fluctuations in the magnetisation direction.

Series of Fresnel images showing the magnetization loop of NiFe/FeMn exchange coupled layers.
Applied field direction and values together with easy-axis direction are indicated.

X.Portier et al. J. Appl. Phys., 2000 **87** 6412

Kirk et al., Appl. Phys. Lett. 1999 **75** 3683

Co elements

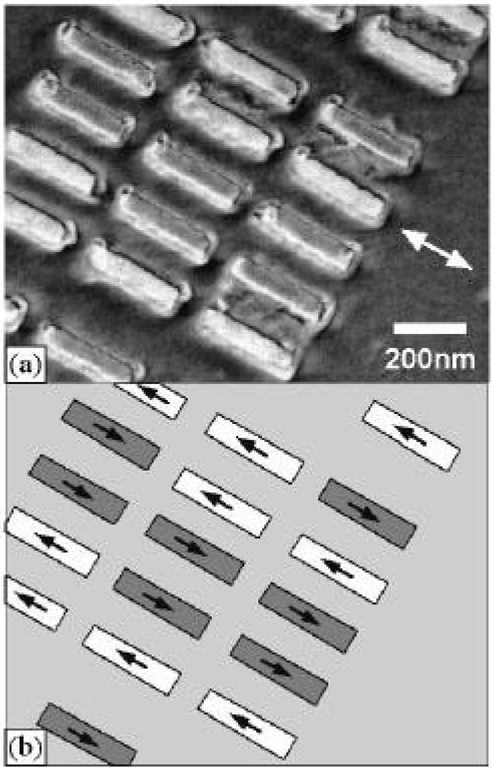

FIG. 2. Array of Co elements $300\times 80\ nm^2$, with elements in opposite magnetization states as indicated by light and dark shading. (a) Foucault image with magnetic induction mapped parallel to the double-headed arrow, and (b) schematic diagram showing magnetization directions.

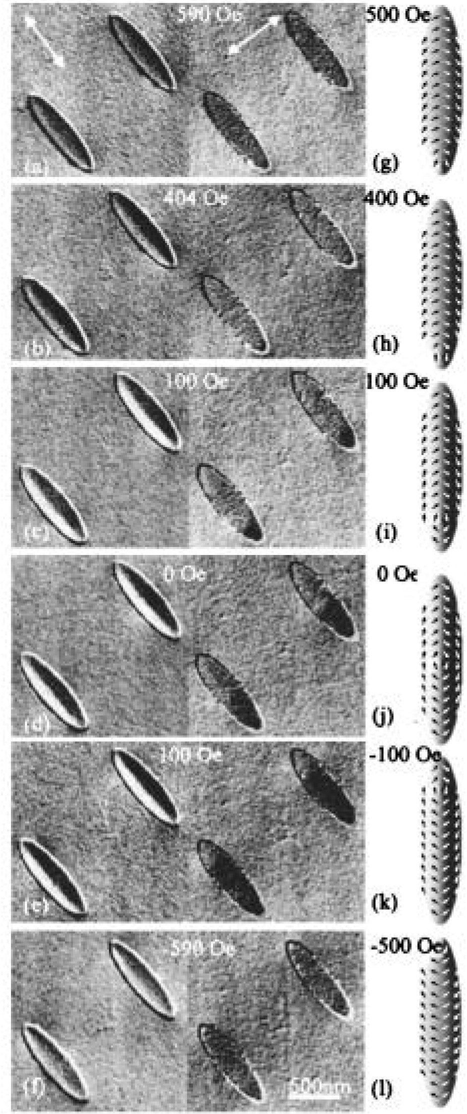

NiFe elements

DPC analysis

Liu et al.,
J. Appl. Phys
2004 **96** 5173

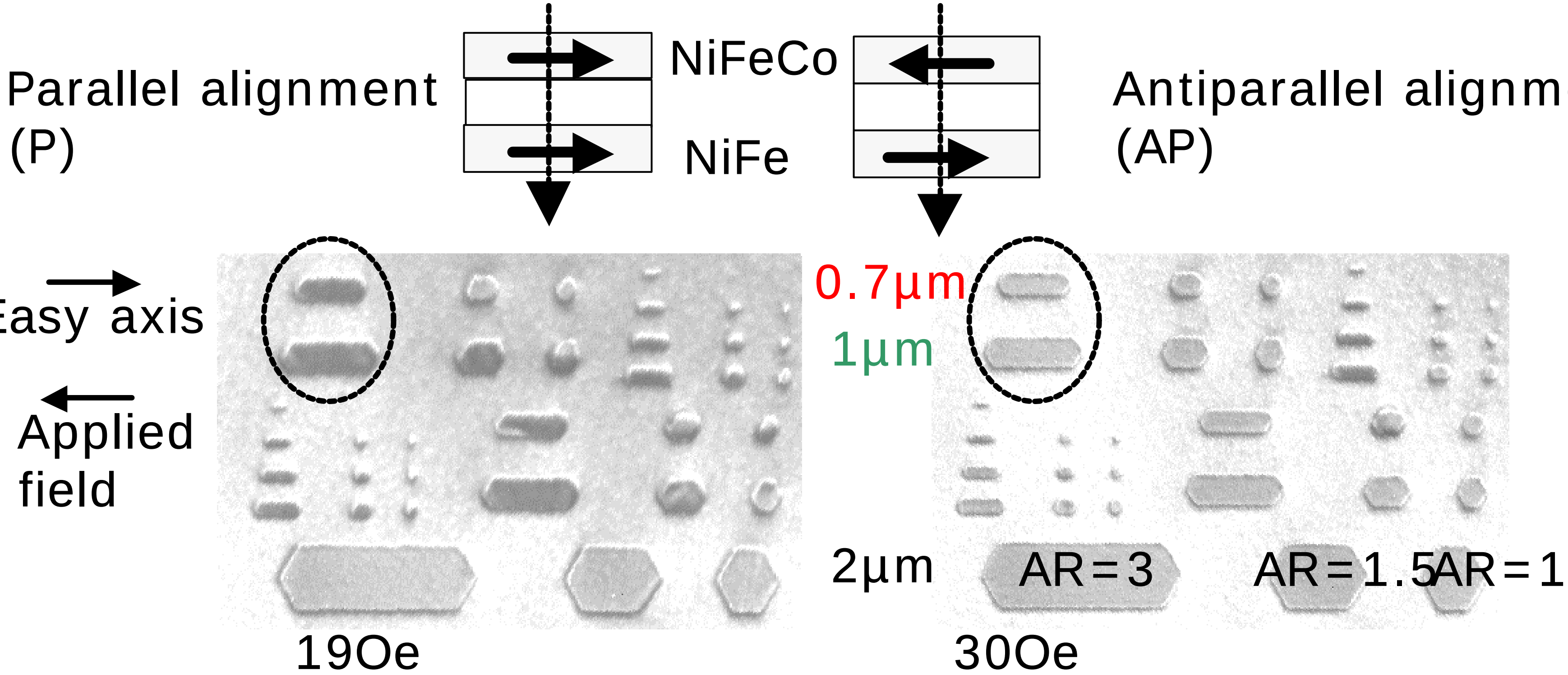

Two reversal modes are observed :

- domain nucleation and propagation (for 2µm wide elements)
- single domain reversal (for 0.7µm and 1µm wide elements)

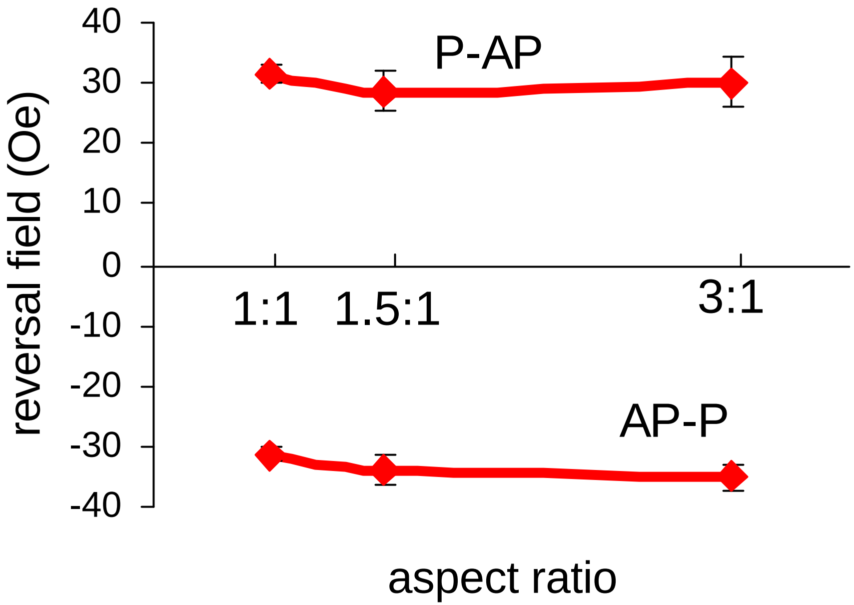

Asymmetry of the reversal

AP–P reversal : the reversal field increases as the aspect ratio increases

P–AP reversal : no strong variation in reversal field as a function of aspect ratio

B.Warot et al., J. Appl. Phys., 2003 **93** 7287-7289

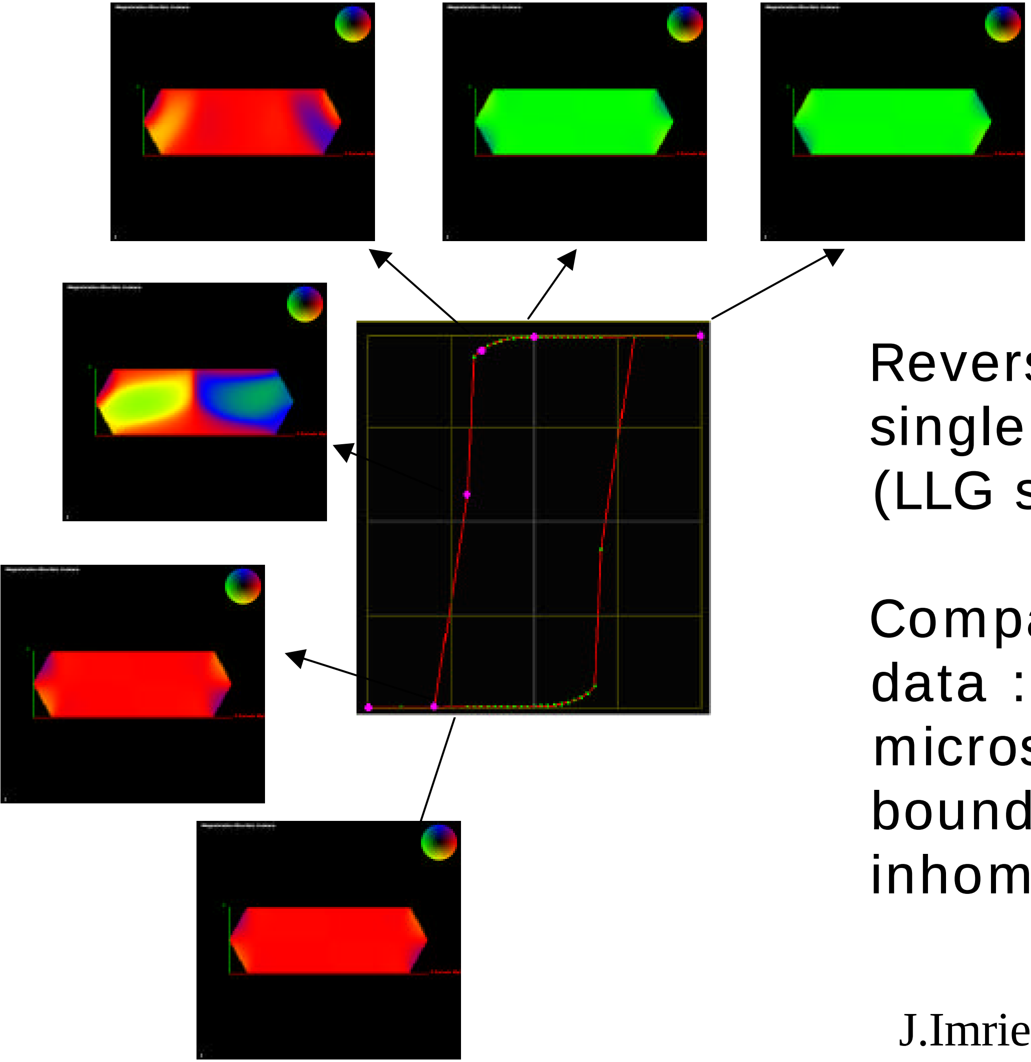

Reversal simulation of NiFeCo single layers
(LLG software)

Comparaison with experimental data : discrepancy explained by microstructural defects (grain boundaries, composition inhomogeneities...)

J.Imrie, Part II, Oxford (2003)

A current passes through a spin valve element during simultaneous application of a magnetic field

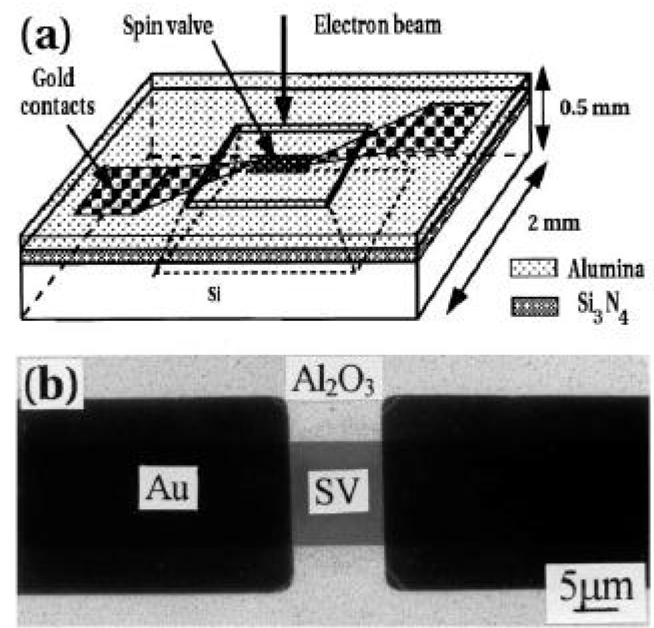

Fig. 1. (a) Scheme of the device developed for in situ LTEM experiments. (b) TEM image of a 10 µm × 10 µm SV element with the Au contacts at each end of the element, allowing the magnetoresistance to be measured for various current values in both directions.

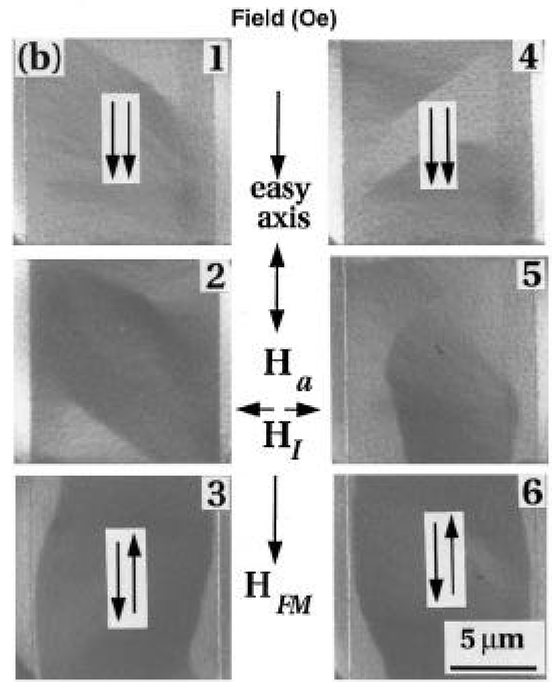

Fig. 3. (a) Plot of the GMR curves for a current value of 6 mA corresponding to the (a i) and (a ii) configurations of Fig. 2. Numbers refer to the Foucault images shown in 3b. (b) Sequence of Foucault images showing the P to AP transitions for both current directions. H_a, H_I and H_{FM} are the applied field, the field induced by the current and the field induced by the magnetostatic coupling between the FM layers, respectively.

Portier et al., Appl. Phys. Lett., 1997 **71** 2042
Portier et al., J. Mag. Mag. Mat., 1998 **187** 145

To get quantitative information out of Lorentz images

- the differential phase contrast method (DPC)
- the non interferometric phase retrieval method

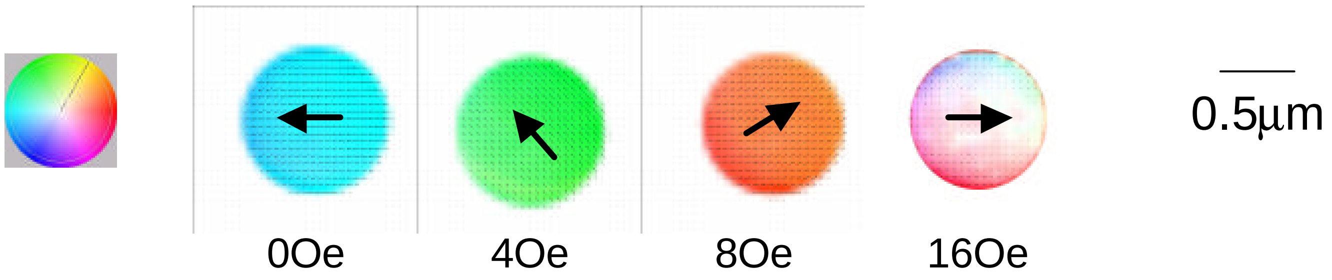

Measure of the deflection angle in a STEM by noting the differences between the current falling on opposite segments of a quadrant deflector

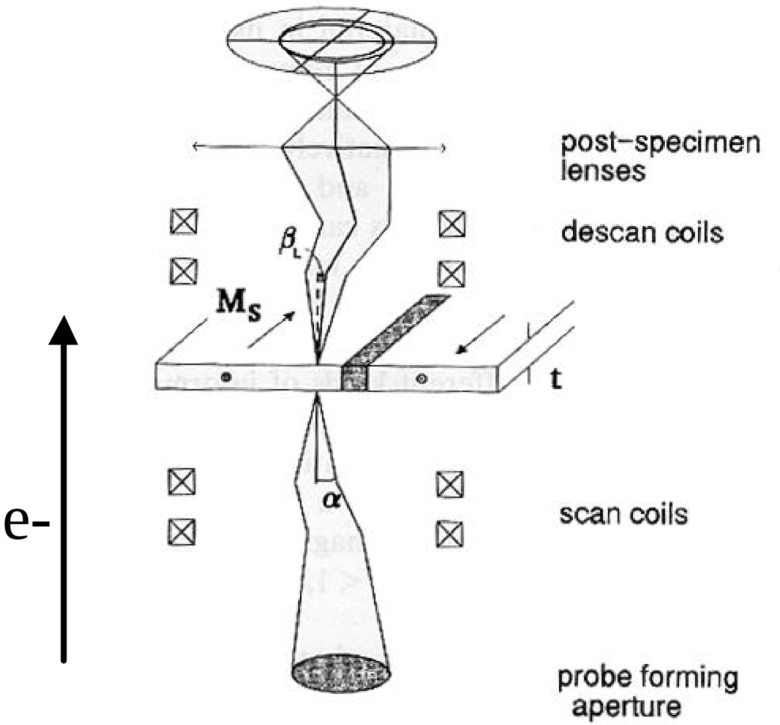

Fig. 1. Schematic of contrast generation from a magnetic specimen in DPC microscopy.

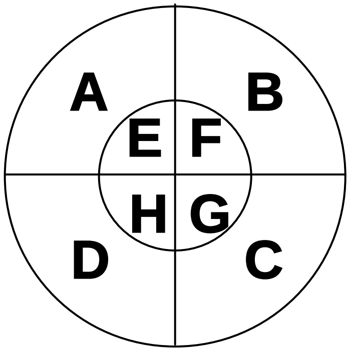

Magnetic signal : A-C, D-B
Structural signal : E-G, F-H

Chapman et al. Ultramicroscopy 1978 **3** 20
Ultramicroscopy 1992 **47** 33

Examples DPC

JOURNAL OF APPLIED PHYSICS VOLUME 95, NUMBER 1 1 JANUARY 2004

Observation of magnetic structures in Fe granular films by differential phase contrast scanning transmission electron microscopy

Takumi Sannomiya, Yumiko Haga, Yoshio Nakamura,[a] and Osamu Nittono[b]
Department of Metallurgy and Ceramics Science, Tokyo Institute of Technology, 2-12-1 Ookayama, Meguro-ku, Tokyo, 152-8550, Japan

Yoshio Takahashi
Research and Development Group, Hitachi, Ltd., 1-280 Higashi-Koigakubo, Kokubunji, Tokyo 185-8601, Japan

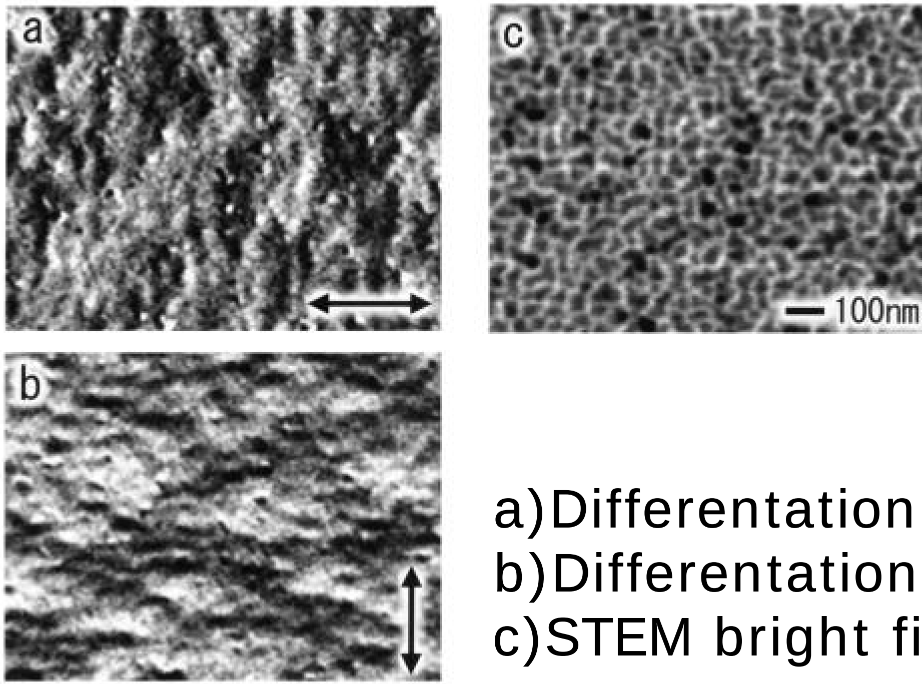

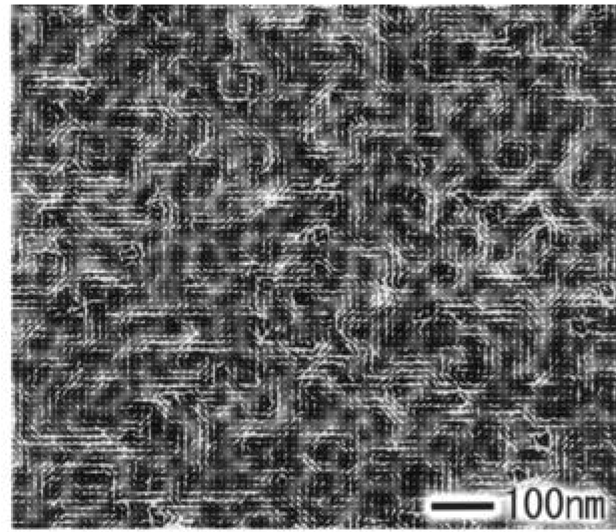

FIG. 4. Vector map of magnetization of sample I. The STEM bright-fi
image is superimposed on the vector map.

a) Differentation along the x axis
b) Differentation along the y axis
c) STEM bright field image

Lorentz microscopy

DPC in a TEM : Summed Image Differential Phase Contrast

Daykin et al., Ultramicroscopy 1995 **58** 365

A.K.Petford-Long et al., IEEE Trans. On Mag. 1999 **35** 788

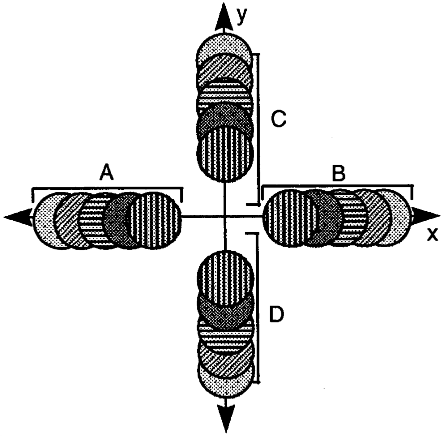

Schematic illustrating the SIDPC technique for obtaining quantitative magnetisation maps using Lorentz microscopy

B_{sum}-A_{sum} = y component

C_{sum}-D_{sum} = x component

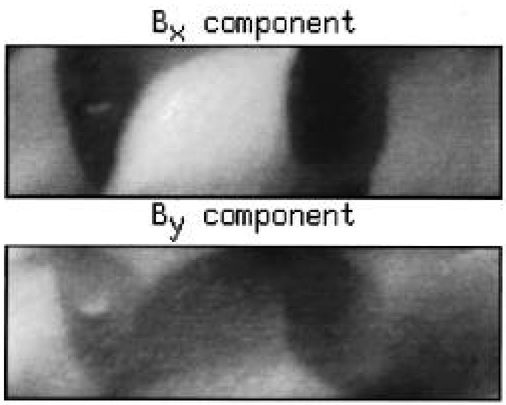

FIG. 1. SIDPC images showing the x and y components of the -plane magnetization in the 10 μm × 30 μm SV element in an pplied field of −10.26 Oe. The applied field as well as the x axis e parallel to the long axis of the element. The y axis is vertical.

Portier et al., Phys. Rev. B 1998 **58** R591

Ta/NiFe/Cu/Co/NiFe/MnNi/Ta
(5/8/3/2/6/25/5 nm)

Aharonov–Bohm phase shift : Relation between the phase of the electron wave to a trajectory integral of the magnetic and electrostatic potentials along the electron path

Phase?

Mathematic formalism to extract the phase out of Lorentz images the transport-of-intensity equation (TIE)

$$\nabla \cdot [I(r_\perp,0)\, \nabla\, \phi(r_\perp)] = -\frac{2\pi}{\lambda} \left.\frac{\partial I(r_\perp,z)}{\partial z}\right|_{z=0}$$

Intensity of the in-focus image

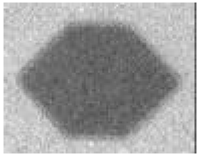

Calculated from a derivative of the image intensity along the optic axis *z* (from out-of-focus images, in Fresnel mode)

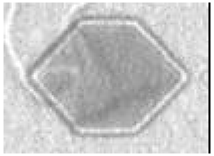

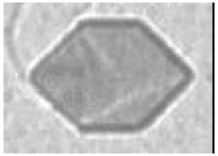

Magnetic?

If the electrostatic contribution is neglected:

$$\nabla f(r_\perp) = -\frac{e}{\hbar}(B_\perp \times n_z)t$$

$$\phi_e = \frac{2\pi}{\lambda}\frac{E_0 + E}{E(2E_0 + E)}V_{ip}t \equiv \sigma(E)V_{ip}t$$

Only the electrostatic component is energy dependent

↓

Images recorded at various electron energy

Only some magnetic materials have suitable properties (domain wall thickness, value of B) to be studied with this method

Kohn et al., Phys. Rev. B 2005 **72** 0144444

Induction maps in Co islands (7µm wide)

H=0

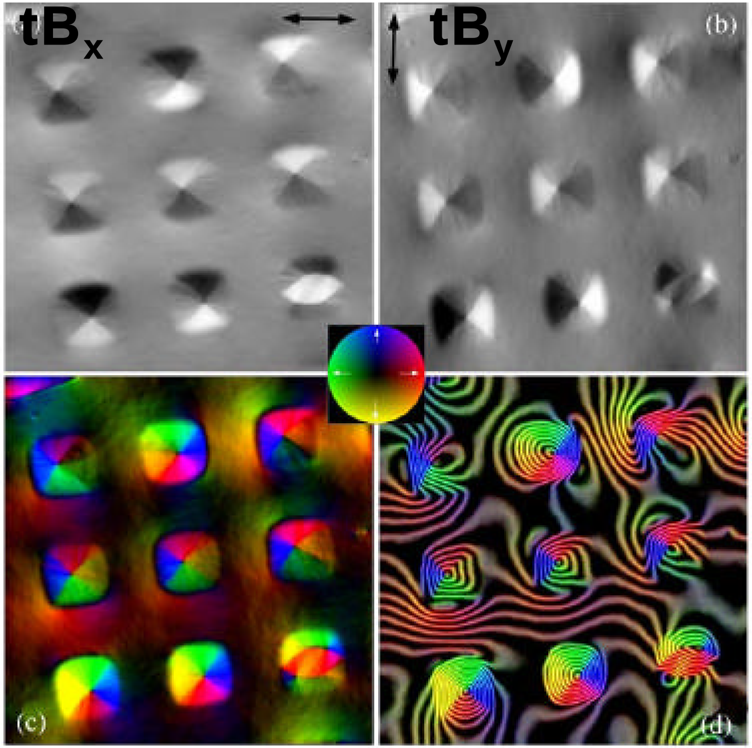

tB(r) Phase contours
(electrostatic contribution neglected)

H=28Oe

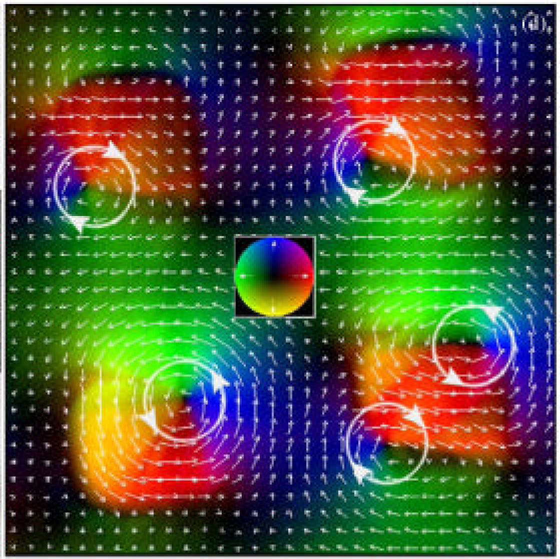

Volkov et al., Ultramicroscopy 2004 **98** 271–281

Groups

University of Glasgow, UK
http://www.ssp.gla.ac.uk/ResSum/SSPSummary.htm

University of Oxford, UK
http://www-magnetics.materials.ox.ac.uk/

University of Cambridge, UK
http://www-hrem.msm.cam.ac.uk/research/index.shtml

Arizona state university, USA
http://www.asu.edu/clas/csss/chrem/main.html

National Center for Electron Microscopy, Berkeley, USA
http://ncem.lbl.gov/

Carnegie Mellon University, Pittsburgh, USA
http://neon.mems.cmu.edu/

Brookhaven national laboratory, New York, USA
http://www.bnl.gov/tem/

Introduction on electron microscopes

SEMPA

SPLEEM

Lorentz microscopy

Electron holography

Theoretical principle

Experimental set-up

Examples

$$\psi_0 = \exp(\mathrm{i}\boldsymbol{K}.\boldsymbol{r})$$

$$\psi_S = A_S(\boldsymbol{r})\exp(\mathrm{i}\boldsymbol{K}.\boldsymbol{r} + \varphi_S(\boldsymbol{r}))$$

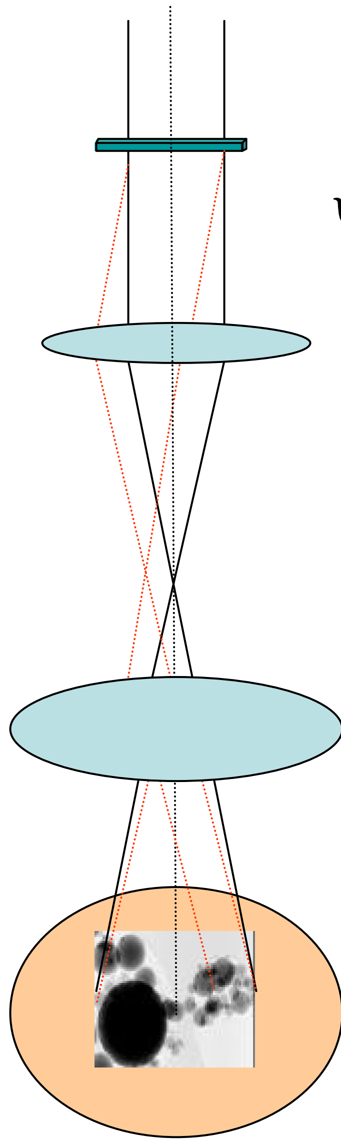

$$\mathbf{I(x,y)} \propto |\Psi_s \Psi_s^*| \propto A_s^2(\boldsymbol{r})$$

$\varphi_S(\mathbf{r})$ is lost

Theoretical principle

$$\psi_0 = \exp(i\mathbf{K.r})$$

Electromagnetic field

electrostatic potential : V

magnetic vector potential : **A**

$$\psi = \exp(iK.r + \varphi(r))$$

$$\varphi(r)??$$

$$\Delta\varphi = \frac{e}{\hbar}\oint(V.dt\ \mathbf{-\ ?\ .}ds)$$

Ehrenberg & Siday (1949)

Aharonov & Bohm (1959)

$$\Delta\varphi(x,y) = C_E\int V(x,y,z)dz - \frac{e}{\hbar}\iint B_n(x,y)dxdz$$

What is lost?

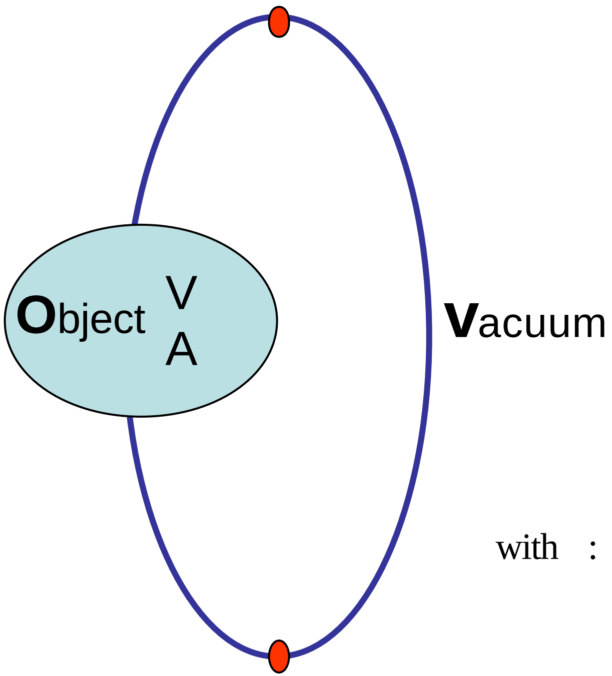

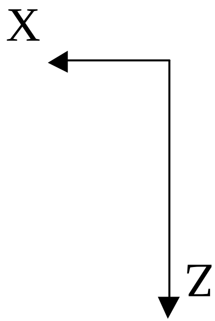

with : $C_E = \left(\frac{2p}{?}\right)\left(\frac{E+E_0}{E(E+2E_0)}\right)$

E : kinetic energy of the e^-

E_0 : rest energy of the e^-

h = Planck C^{te}

l = e^- wave length

B_n = magnetic induction perpendicular to the surface

Electron Holography

Theoretical principle

Phase contributions

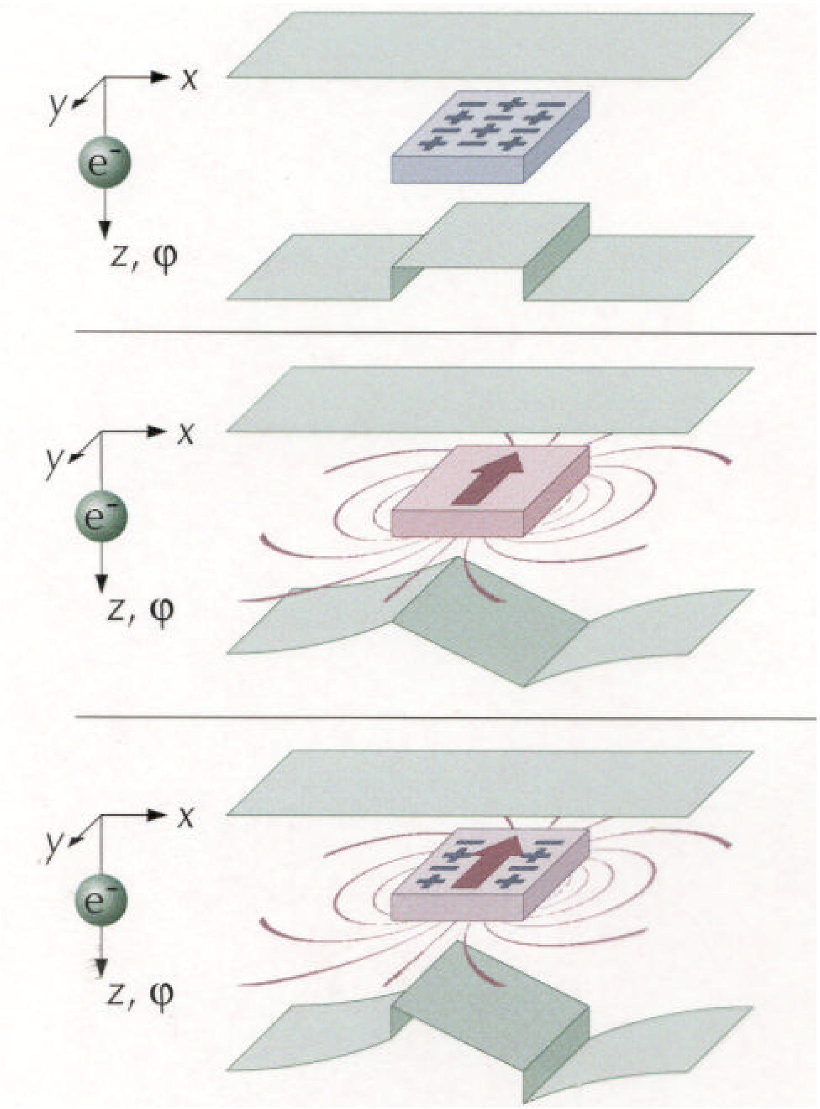

Phase shift due to the electrostatic potential

$$\boxed{j_{elect}(\mathrm{x}) = \mathrm{C_E} \int V(x,z)\,dz}$$

Phase shift due to the magnetic induction

$$\boxed{j_{mag}(\mathrm{x}) = -\frac{e}{\hbar} \iint B_{\mathrm{n}}(\mathrm{x},\mathrm{z})\,\mathrm{dxdz}}$$

Total phase shift

$$j_{Tot}(\mathrm{x}) = j_{elect}(\mathrm{x}) + j_{mag}(\mathrm{x})$$

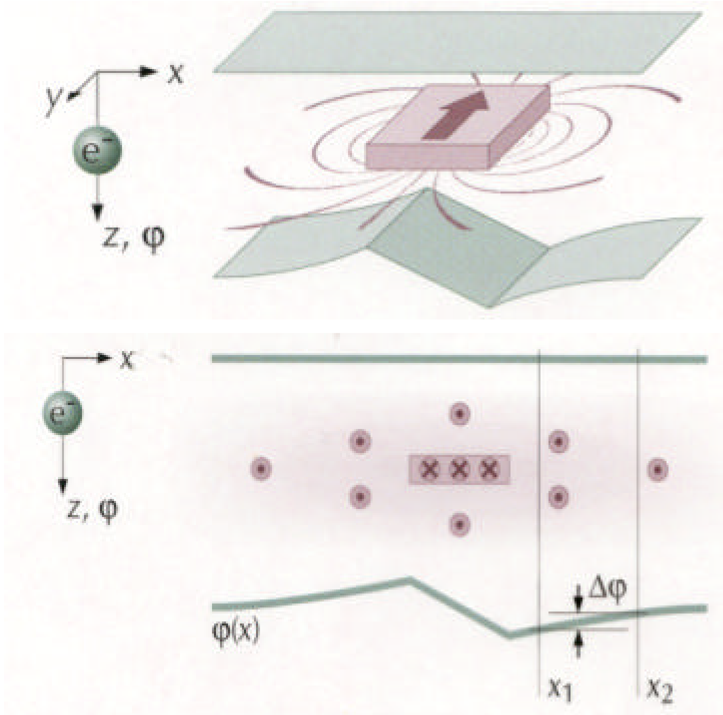

$$\Delta j = j\,(x_2, y) - j\,(x_1, y) = -\frac{e}{\hbar} \int_{x=x_2}^{x_1} \int B_n(x, y, z)\,dxdz$$

$$\boxed{\frac{\partial j\,(x)}{\partial x} = \frac{e}{\hbar} B_n(x).t}$$

The phase gradient is proportional to the in-plane induction component B_n and the equiphase lines give the direction of B

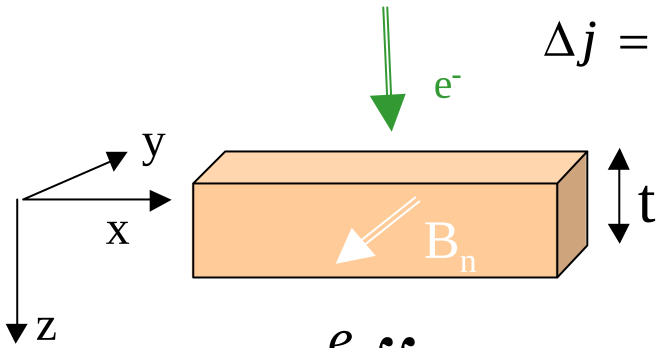

$$\Delta j = -\frac{e}{\hbar}\iint B_{n}(x,y)\,dS$$

$$\Delta j = -\frac{e}{\hbar}\iint B_{n(y)}\,dx\,dz$$

$$\frac{\partial \Delta j}{\partial x} = -\frac{e}{\hbar} B_{n(y)}\, .t$$

$$B_n = -\frac{\hbar}{e.t}\cdot\frac{\partial \Delta\varphi}{\partial x}$$

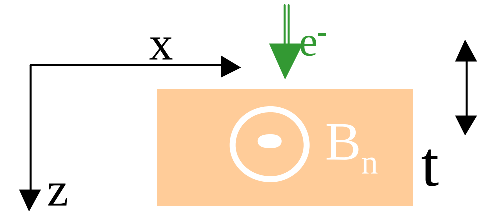

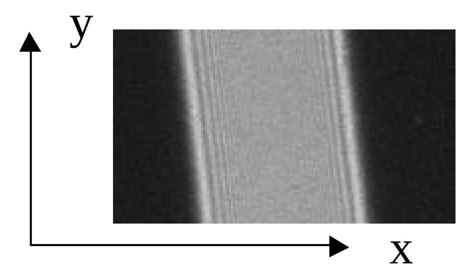

If B only varies in the (x,y) plane :B_x, B_y

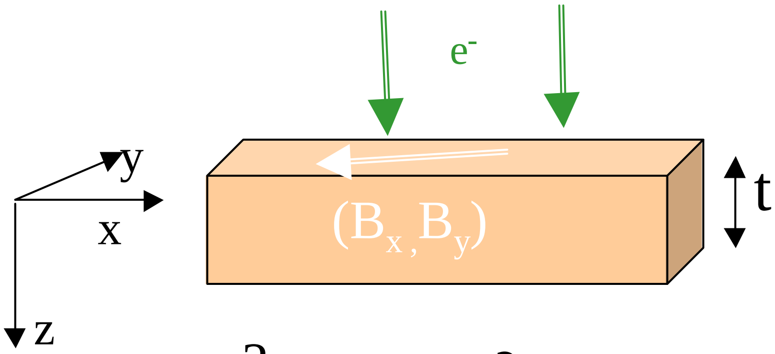

$$\frac{\partial^2 \Delta\varphi}{\partial x \partial y} = -\frac{et}{\hbar}\frac{\partial B_y(x,y)}{\partial y}$$

$$B_x = -\int \frac{\partial B_y}{\partial y} dx = \frac{\hbar}{et}\frac{\partial^2 \Delta j}{\partial x \partial y} dx$$

$$\boxed{DivB = 0 \Rightarrow \frac{\partial B_x}{\partial x} = -\frac{\partial B_y}{\partial y}}$$

$$B_x = \frac{\hbar}{et}\frac{\partial \Delta\varphi}{\partial y}$$

$$B_y = \frac{\hbar}{et}\frac{\partial \Delta\varphi}{\partial x}$$

Theoretical principle

Experimental set-up

Examples

How to get rid of the magnetic field due to the objective lens?

How to measure the phase shift?

How to separate the electrostatic and magnetic contributions?

Problem : objective lens magnetic field : 2T

How to get rid of this field?

- Turn of the objective lens -> no magnification
- **Lorentz lens**

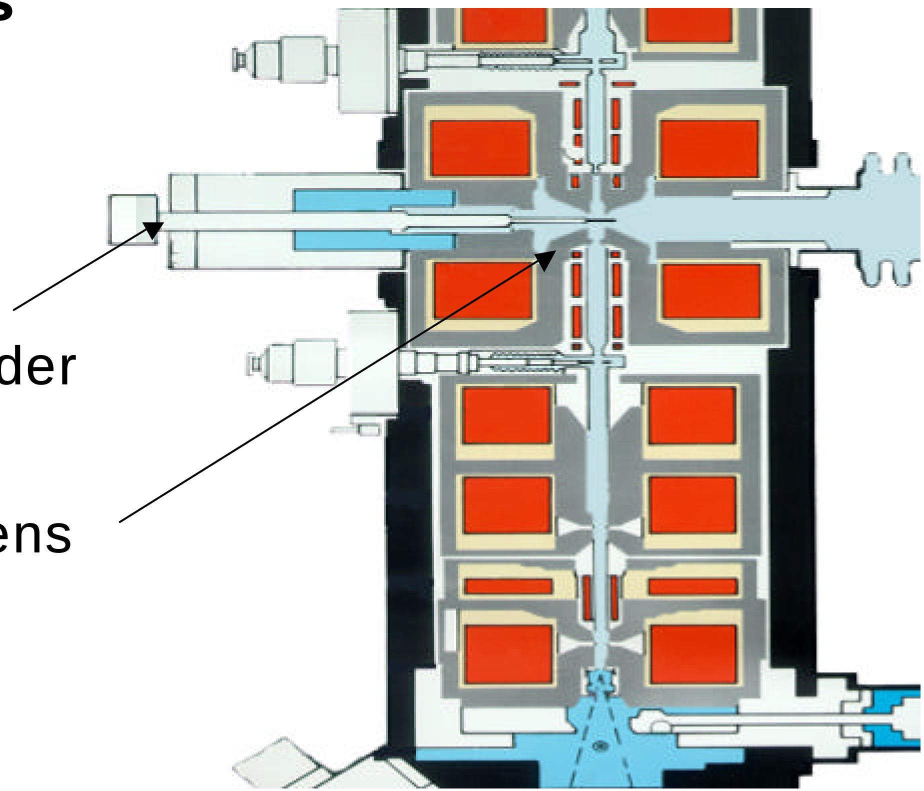

Holography method : making the interference between a reference electron beam Υ_0 and a second one Υ_s, of same wave length but presenting a phase shift, φ_s

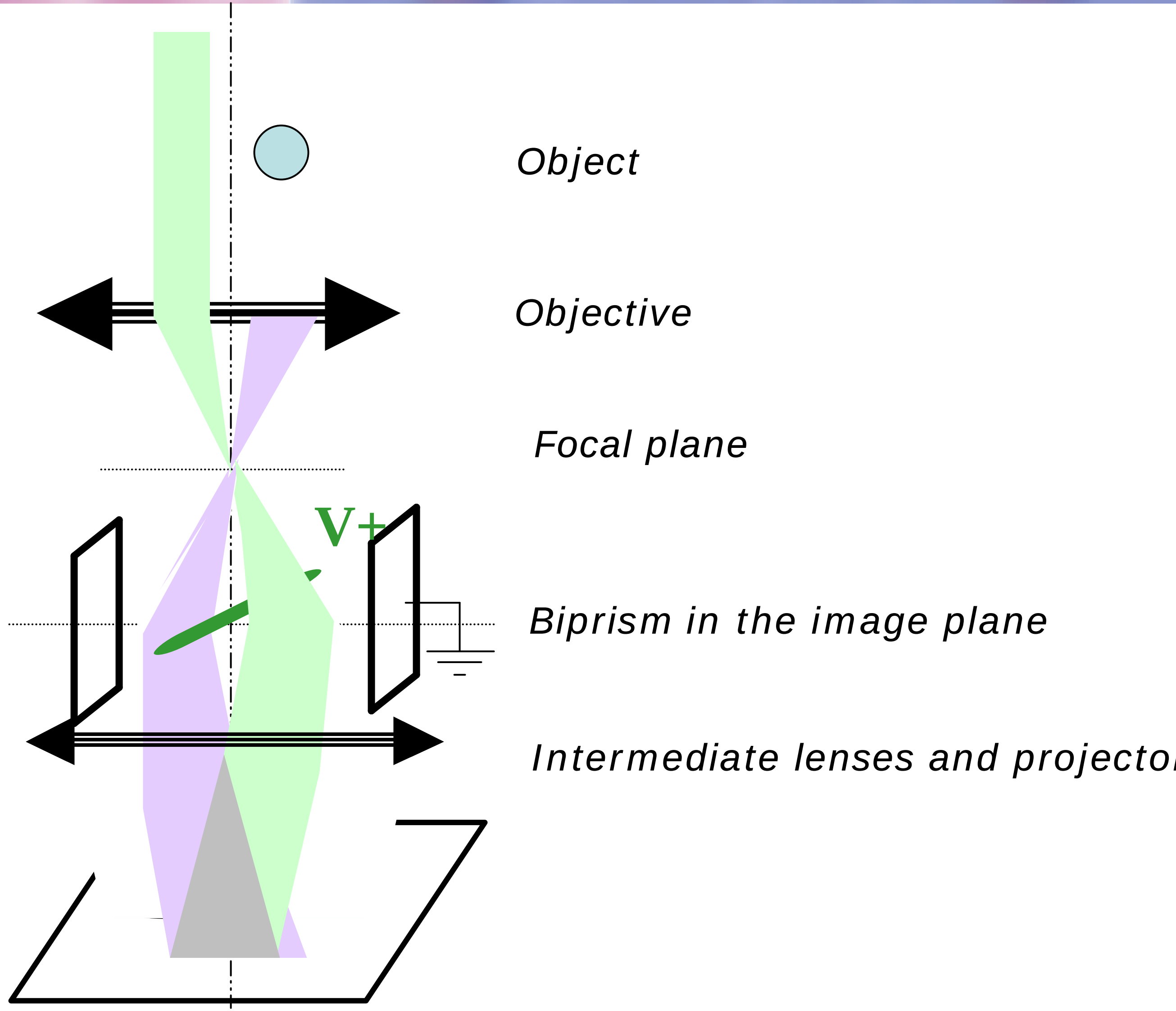

Sactem FEI – FEG Cs corrected + biprism + Tridiem (Gatan)

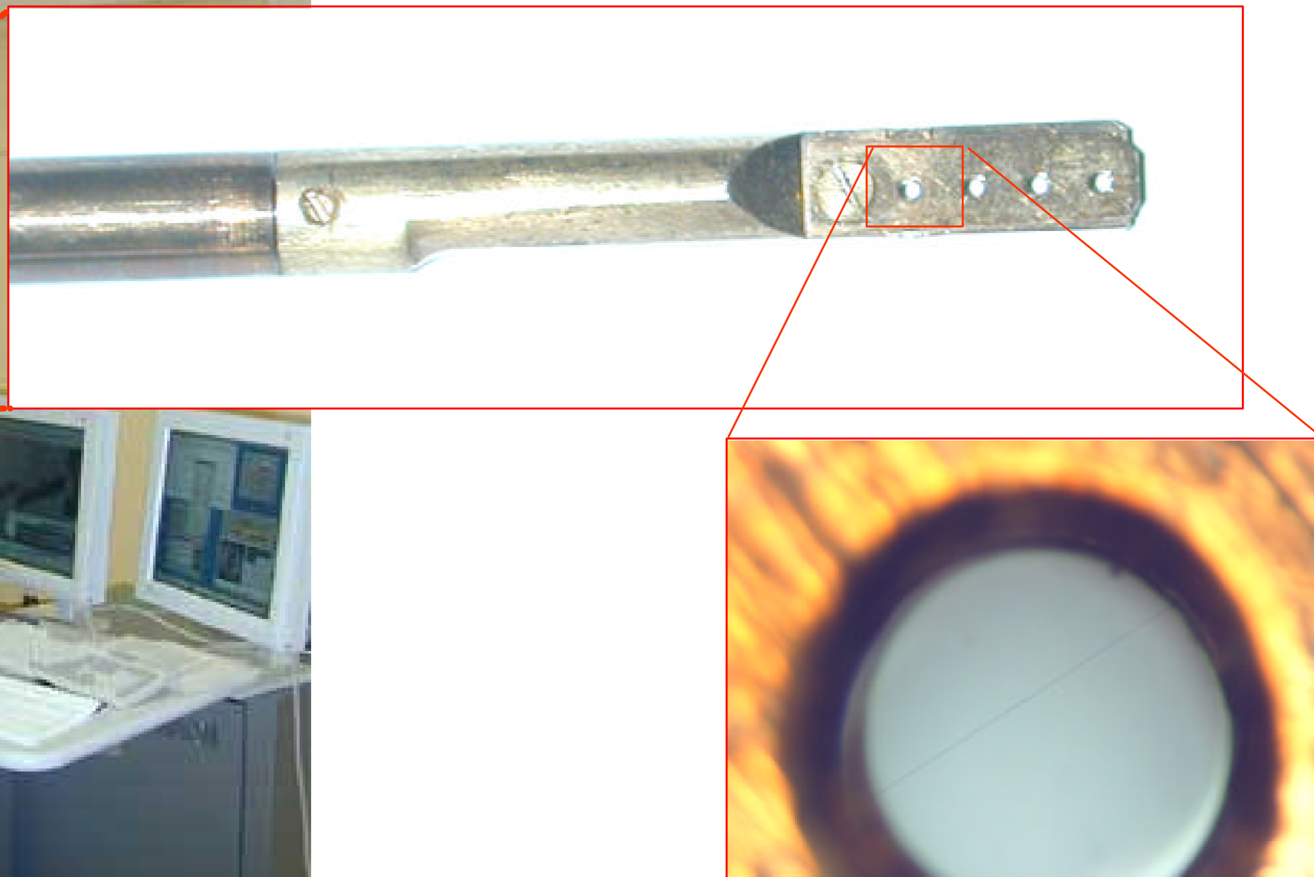

Experimental set-up

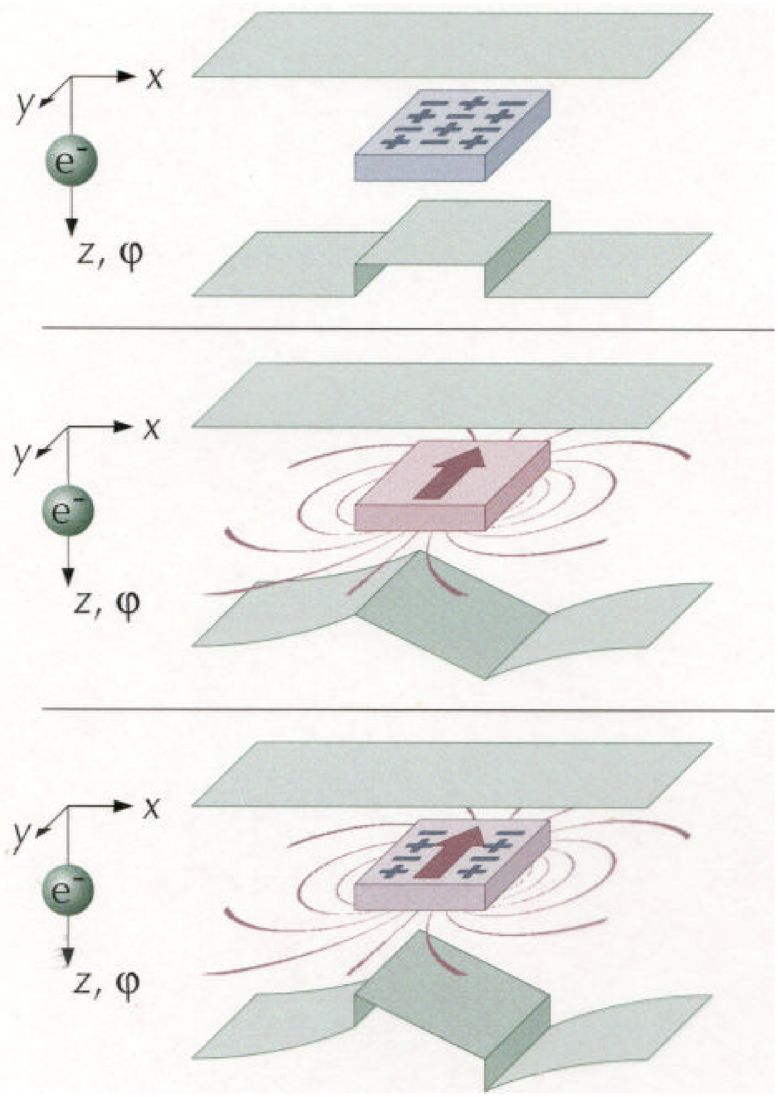

Elec. and magn. contributions

Phase shift due to the electrostatic potential

$$\boxed{j_{elect}(\mathrm{x}) = \mathrm{C_E} \int V(x,z)\,dz}$$

Phase shift due to the magnetic induction

$$\boxed{j_{mag}(\mathrm{x}) = -\frac{e}{\hbar} \iint B_{\mathrm{n}}(\mathrm{x},\mathrm{z})\,\mathrm{dxdz}}$$

Total phase shift

$$j_{Tot}(\mathrm{x}) = j_{elect}(\mathrm{x}) + j_{mag}(\mathrm{x})$$

$$\varphi(x) = C_E \int V(x,z)dz - \frac{e}{\hbar}\iint B_n(x,z)dxdz$$

1 / Taking two holograms (4 with the reference holo) with the TEM sample switched upside down

=> the sign of the « B » contribution changes not the electrostatic one.

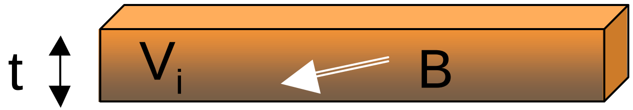

$$\Delta\varphi_1 = C_E V_i.t - \frac{e}{\hbar}\iint B_n ds$$

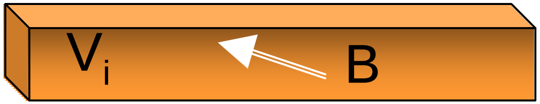

$$\Delta\varphi_2 = C_E V_i.t + \frac{e}{\hbar}\iint B_n ds$$

$$\boxed{\Delta\varphi_2 - \Delta\varphi_1 = 2\frac{e}{\hbar}\iint B_n ds}$$

$$\boxed{\Delta\varphi_2 + \Delta\varphi_1 = 2C_E V_i t}$$

<u>Problem</u> : finding back the same area after returning the sample

$$\varphi(x) = C_E \int V(x,z)dz - \frac{e}{\hbar}\iint B_n(x,z)dxdz$$

2/ Taking two holograms changing the TEM accelerating high voltag

$$C_E = \left(\frac{2p}{?}\right)\left(\frac{E+E_0}{E(E+2E_0)}\right)$$

$$\Delta\varphi_1 = C_{E_1} V_i.t - \frac{e}{\hbar}\iint B_n ds$$
$$\Delta\varphi_2 = C_{E_2} V_i.t - \frac{e}{\hbar}\iint B_n ds$$

$$V_i t = \frac{\Delta\varphi_2 - \Delta\varphi_1}{(C_{E_2} - C_{E_1})}$$

Problem : keeping the same acquisition conditions when changing the high voltage

$$\varphi(x) = C_E \int V(x,z)\,dz - \frac{e}{\hbar}\iint B_n(x,z)\,dx\,dz$$

3 / Switching the magnetization of the sample with the objective lens field

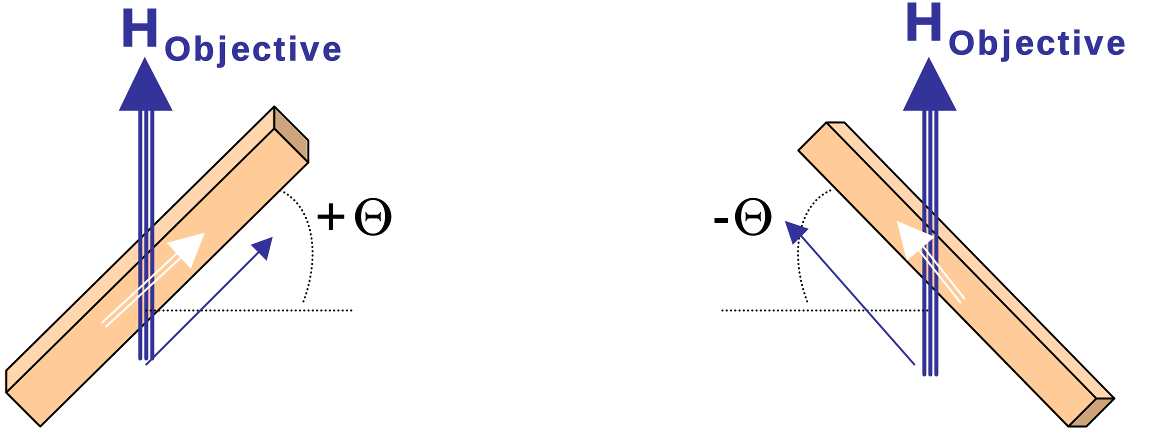

Back to Θ = 0 – objective off

$$\varphi_1 = C_E V_i.t - \frac{e}{\hbar}.t.\int B_n(x).dx \qquad \varphi_2 = C_E V_i.t + \frac{e}{\hbar}.t.\int B_n(x).dx$$

$$\frac{e}{\hbar}.t.\int B_n(x).dx = \frac{\varphi_2 - \varphi_1}{2} \qquad C_E V_i t = \frac{\varphi_2 + \varphi_1}{2}$$

Magnetic contribution **Mean inner potentiel** (MIP)

Measurement of the phase shift

$$\psi_o = \exp(i\boldsymbol{K}.\boldsymbol{r}) \qquad \psi_s = A_s(\boldsymbol{r})\exp(i\boldsymbol{K}.\boldsymbol{r} + \varphi_s(\boldsymbol{r}))$$

$$I_{Holo} = \tfrac{1}{2}\Psi_o \Psi_s^* | + \text{background} = 1 + A_s^2(x,y)$$
$$+ 2A_s(x,y)\cos[2\pi R_0.x + \varphi_s(x,y)]$$
$$+ I_{inelast}(x,y)$$

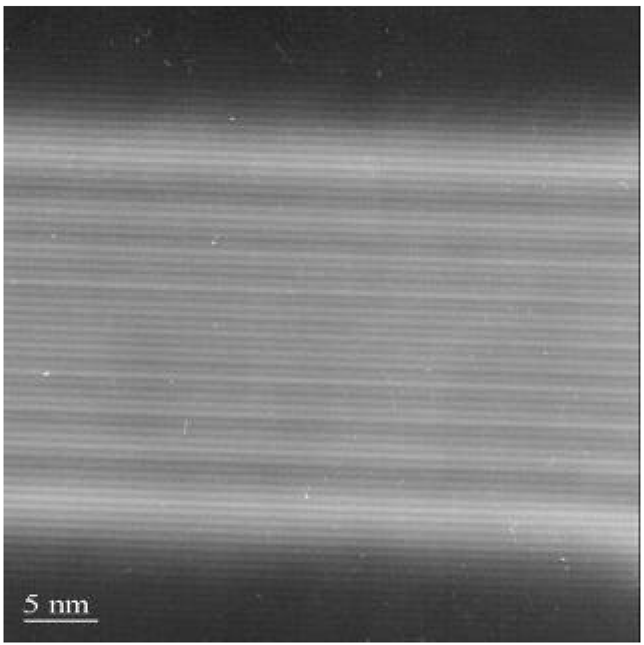

Interference fringes of period : $\Lambda = 2\pi/R_o$

R_0 depends on
- the incident beam wavelength
- the biprism polarisation
- the beam convergence

How to extract $\varphi(r)$?

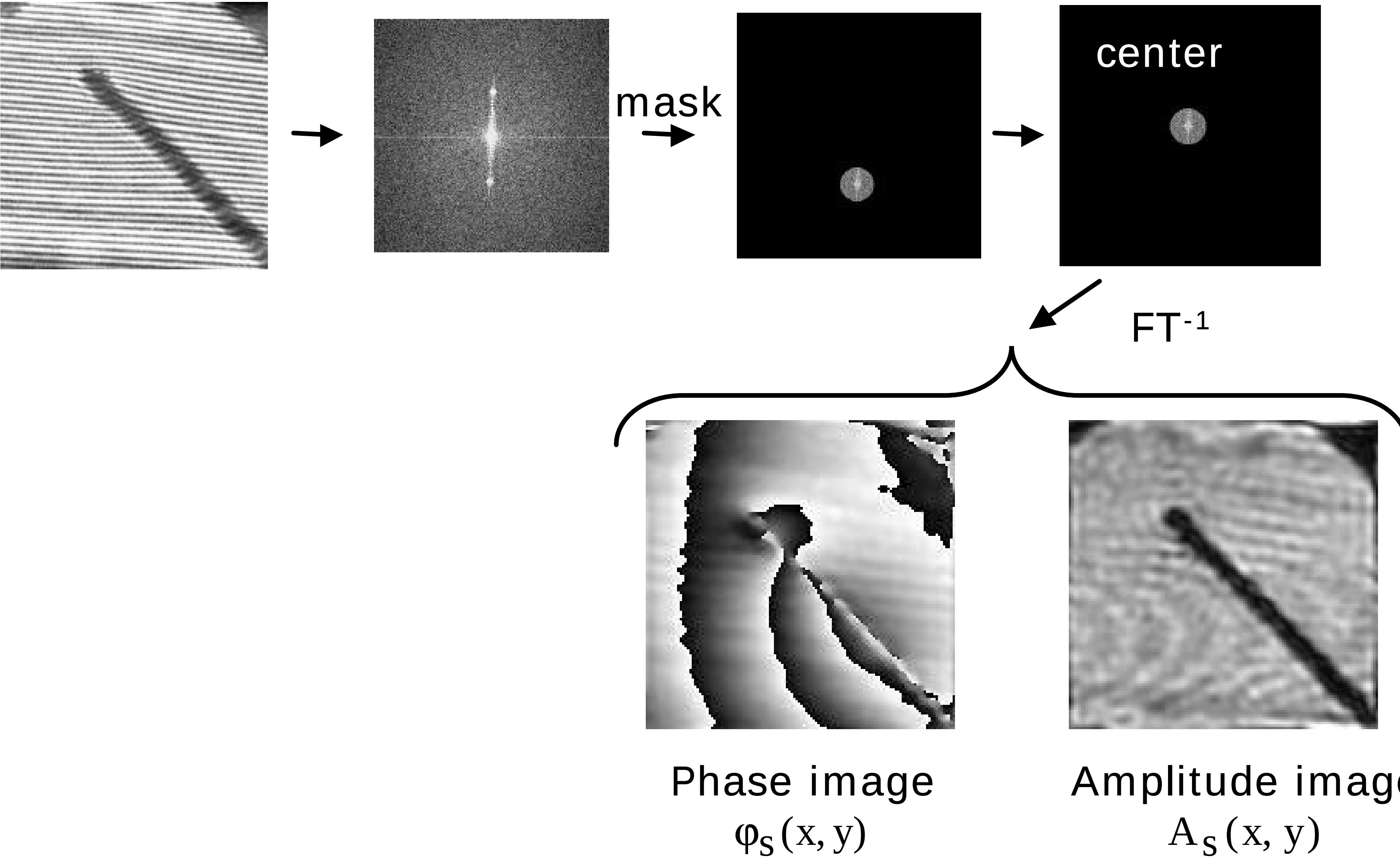
mask
center
FT-1
Phase image
φS(x, y)
Amplitude image
AS(x, y)

Experimental set-up

Measurement of the phase shift

Hologram with the object

Reference hologram (vacuum)

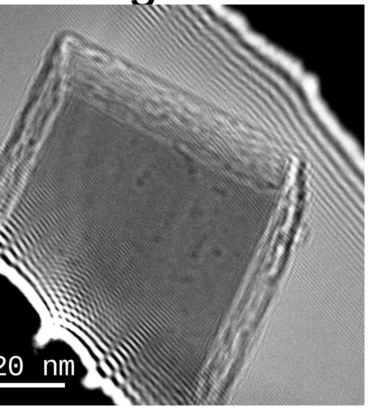

FT

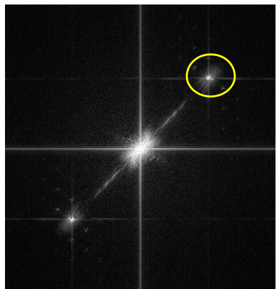

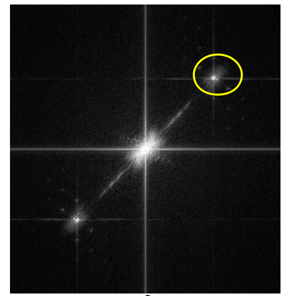

FT

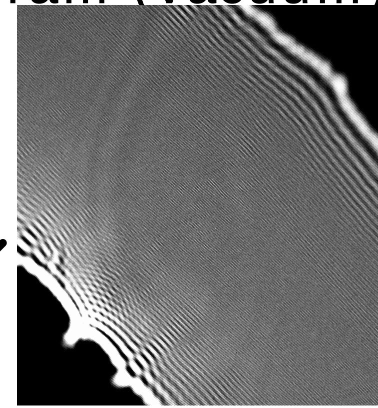

FT^{-1}

FT^{-1}

$$I_S = A_S e^{i\varphi_S} \qquad I_R = A_R e^{i\varphi_R}$$

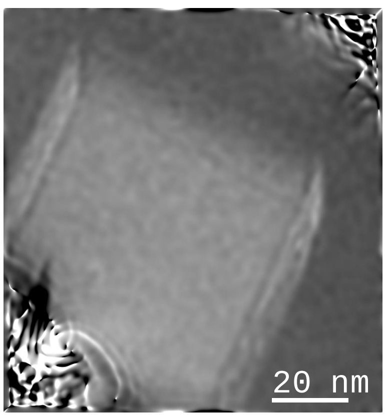

$$\frac{I_S}{I_R} = \frac{A_S}{A_R} e^{i(\varphi_S - \varphi_R)}$$

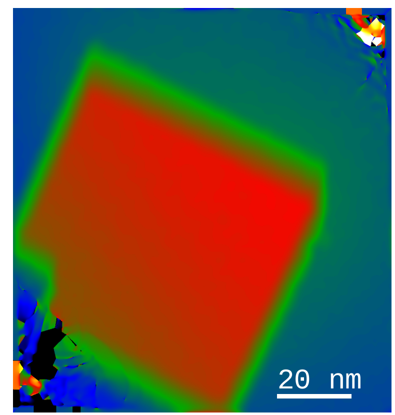

$$\frac{A_S}{A_R} = A_N$$

Phase shift due to the object $\varphi_S - \varphi_R = \Delta\varphi$

Electron Holography

Samples

Transparent to the electron beam

Mainly particles deposited on carbon grids

Deposition on transparent membranes

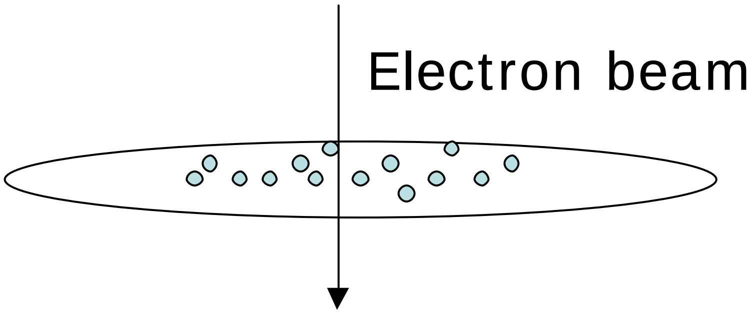

Resolution

5nm

Large energy coherence of the electron beam

	FEG	LaB_6
J (A/m^2)	10^{10}	10^{6}
Brightness ($A/m^2/sr$)	10^{13}	5.10^{10}
ΔE (eV)	0.3	1.5

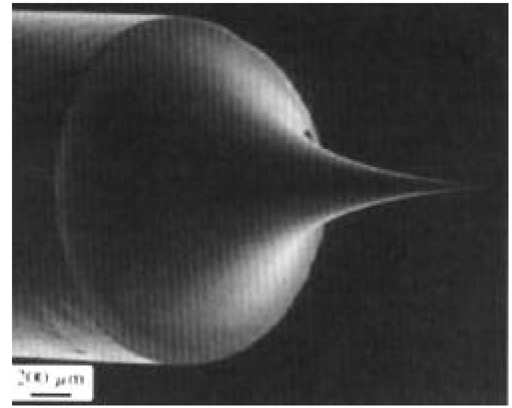

- Elliptic illumination (large condenser astigmatism)

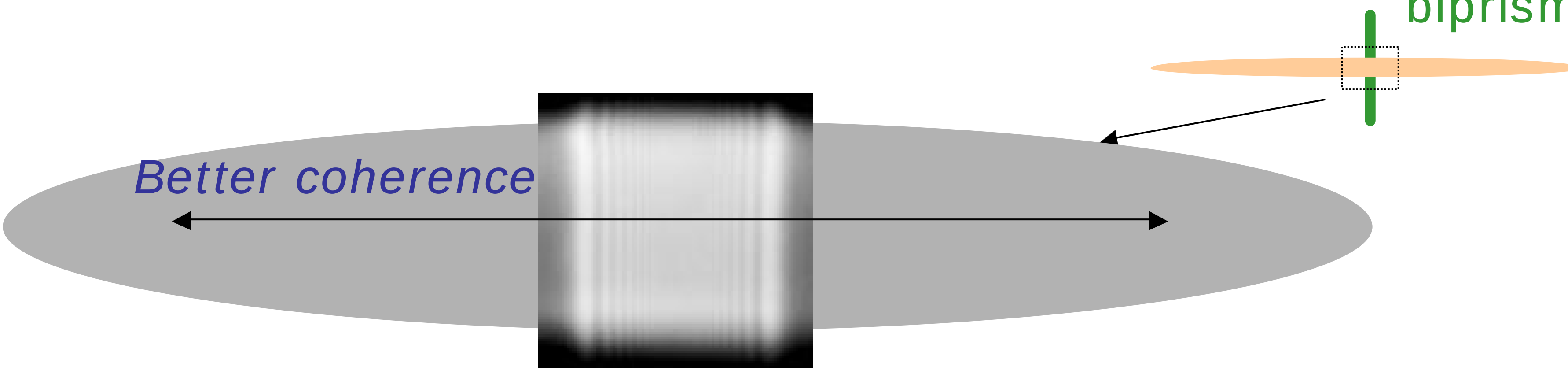

- Reducing dynamical effects by being far from a zone axis
- Optimising fringe contrast $\frac{I_{max}-I_{min}}{I_{max}+I_{min}}>15\%$
- Setting the biprism polarisation to get optimum fringe period to detect the phase shift

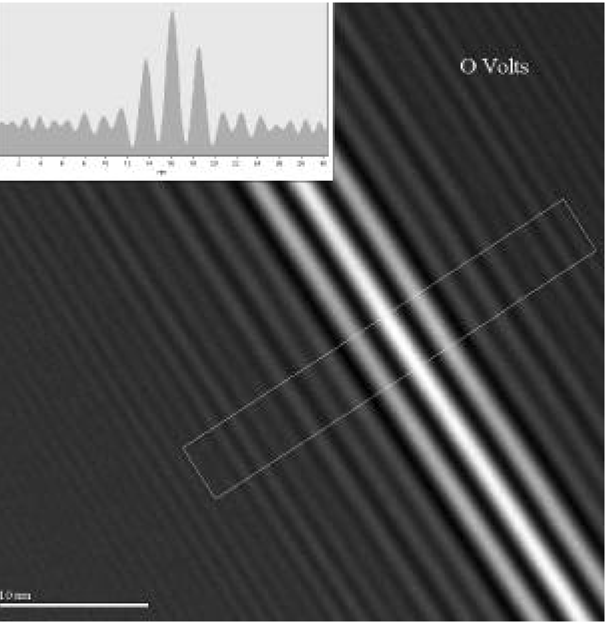

V = 0 Volts

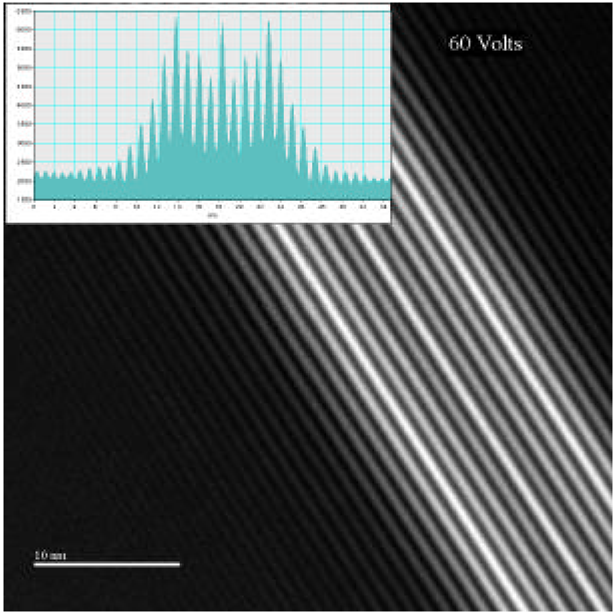

V = 60 Volts

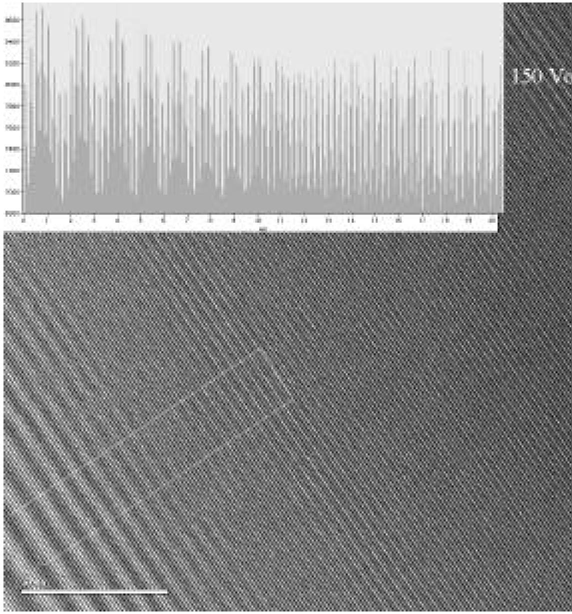

V = 150 Volts

Theoretical principle

Experimental set-up

Examples

Observation of the magnetisation and the ferromagnetic domains in baryum ferrite particles

T. Hirayama, A. Tonomura et al. Appl. Phys. Lett. 1993 **63** 418

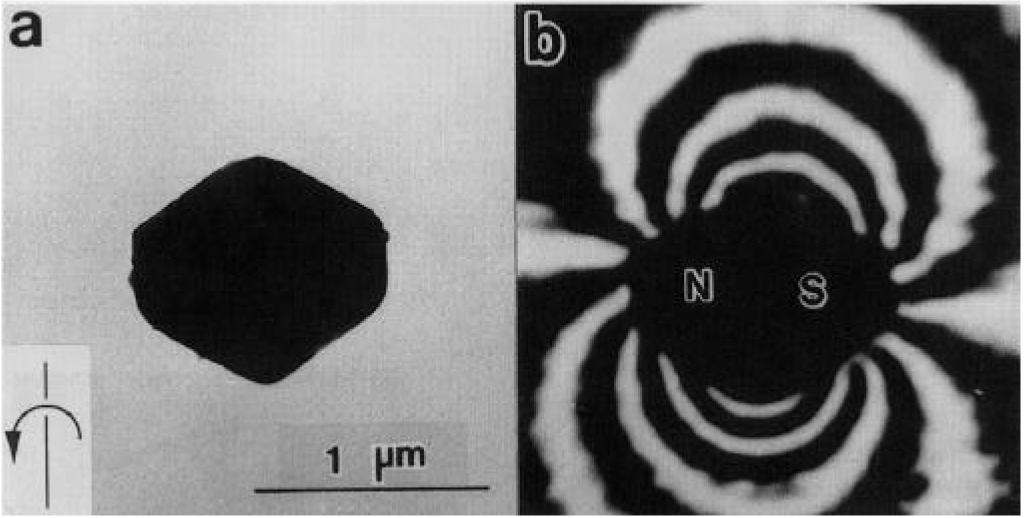

TEM micrograph of a particle

Phase image of the stray field

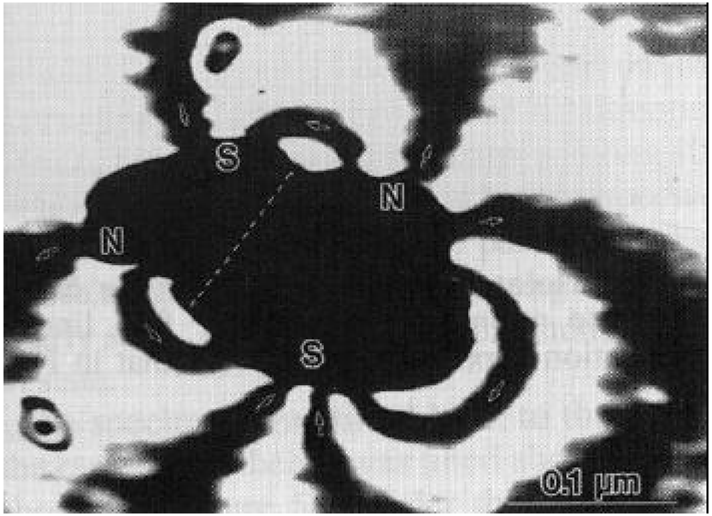

Image showing magnetic domains

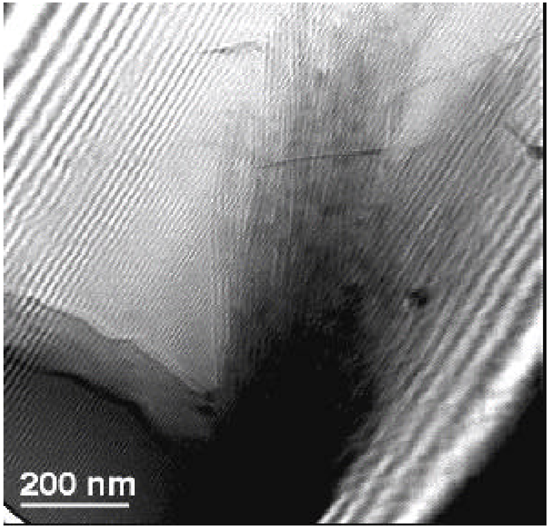

Magnetic contribution magnified 128 times

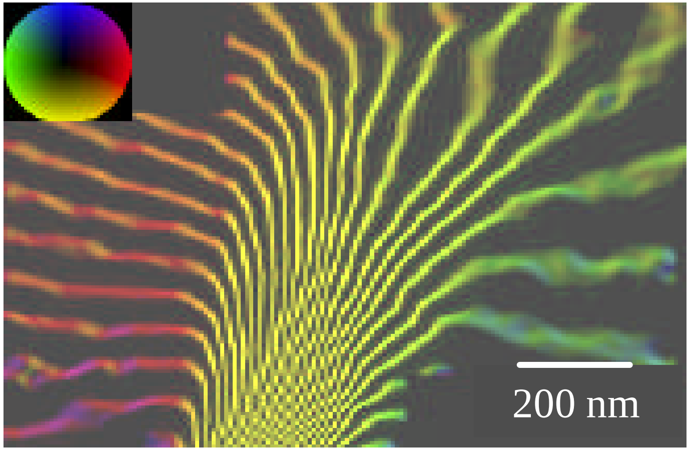

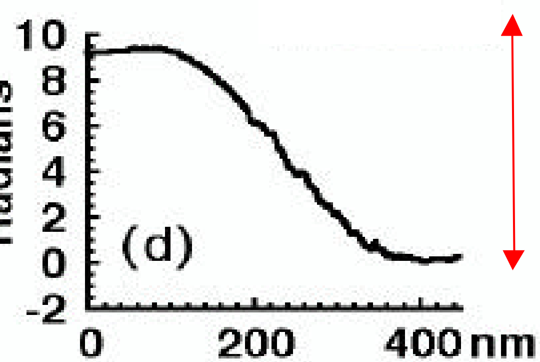

$\Delta\phi$ = 9.0 ±0.2rad

Magnetic contribution

Magnetic contribution of 280 nanowires uniformly magnetized with a saturation magnetisation of B = 1.7 T

E. Snoeck, R. E. Dunin-Borkowski, et al. Appl. Phys. Lett. **82**, p 88 (2003).

Isolated Co nanowire

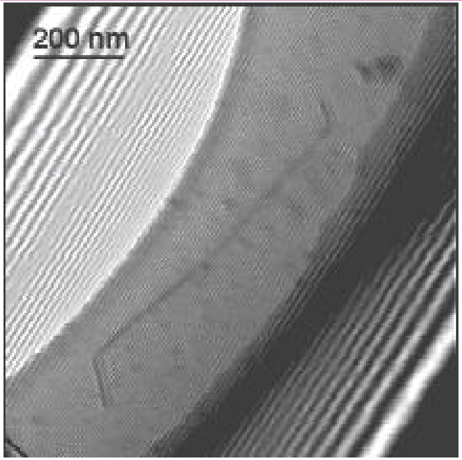

hologram

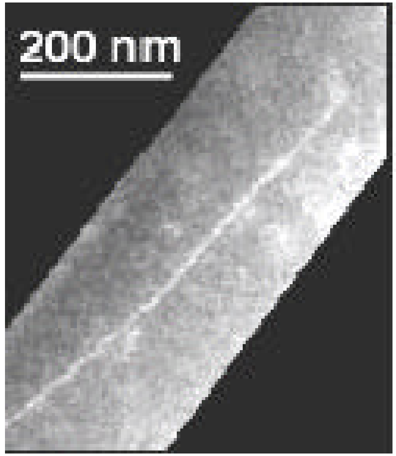

MIP cont.

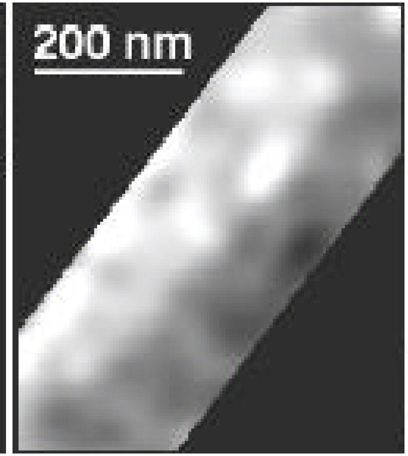

Mag. cont.

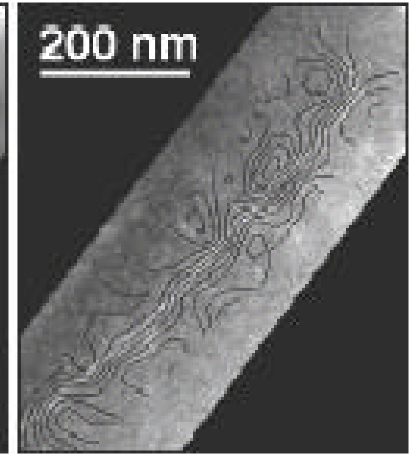

0.005 rad contour

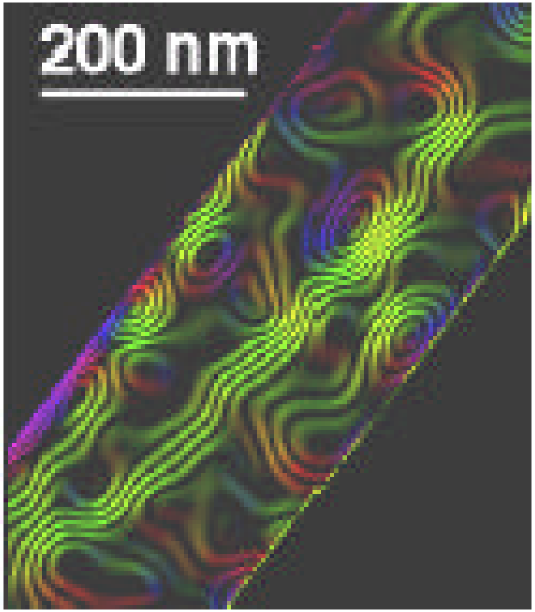

Cosine of 256 times the magnetic contribution

$$\Delta\varphi = C_E V_i.t - \frac{e}{\hbar}\iint B_n ds$$

$$\Delta\phi_{MIP} = C_E V_i.t$$

$$\Delta\phi_{Mag} = -\frac{e}{\hbar}\iint B_n ds$$

- $V_{i\text{ - cobalt}} = 26$ V
- $B = \mu_0 Ms = 1.7$ Tesla

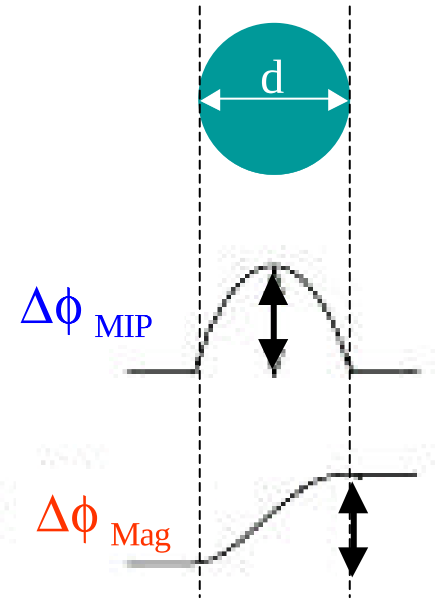

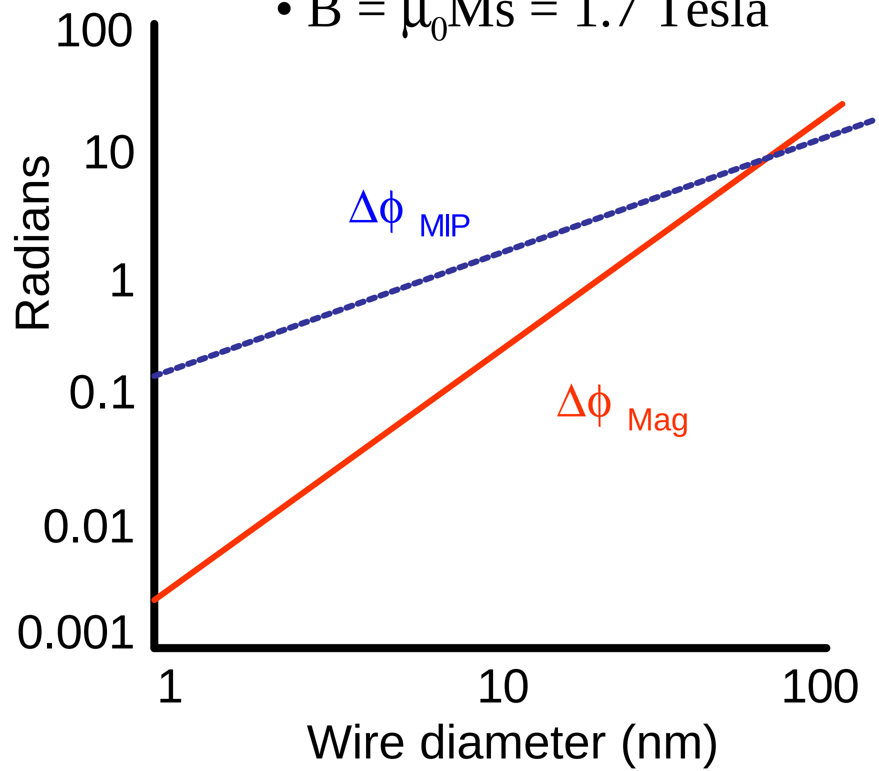

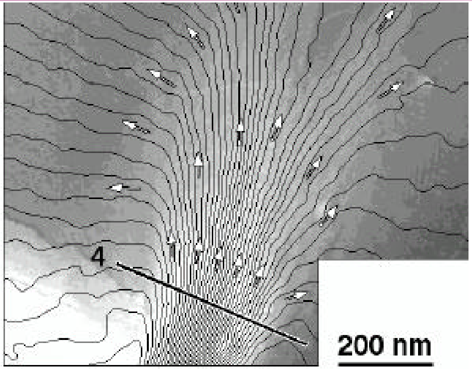

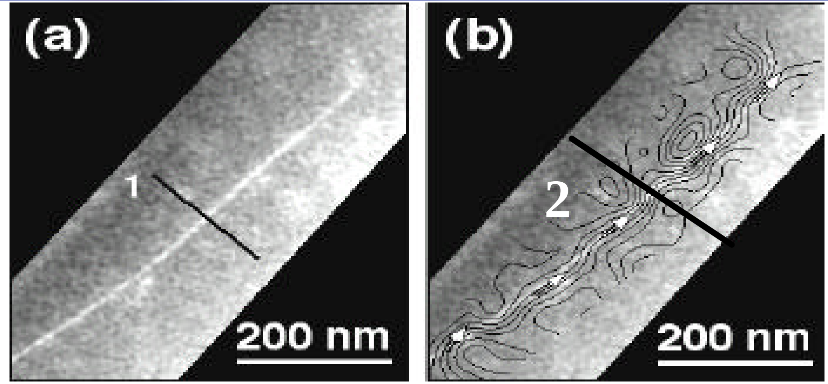

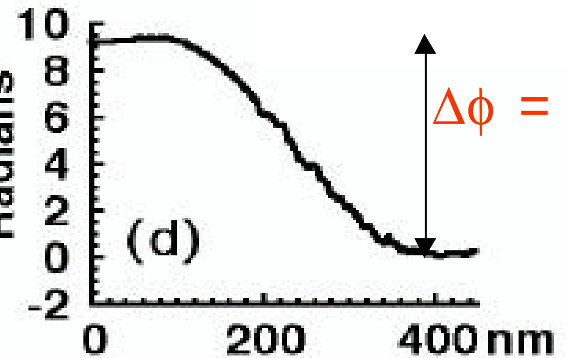

$\Delta\phi$ = 9.0 rad (± 0.2)

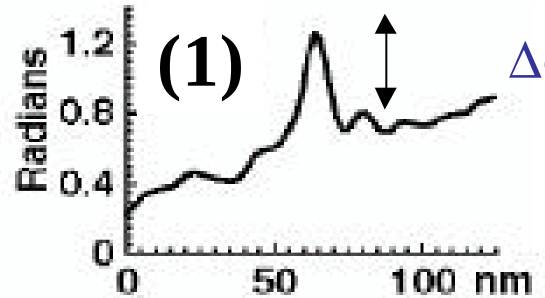

$\Delta\phi_{MIP}$ = 0.65 rad (± 0.005)

MIP

Magnetic contribution of 280 wires uniformly magnetized with B = 1.7 T

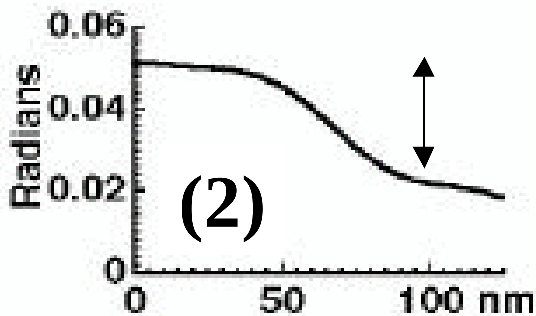

$\Delta\phi_{Mag}$ = 0.03 rad (± 0.005)

Magnetic contribution

100% ±0.19 of the Co nanowire is fully magnetized

Examples

Co nanoparticle ring

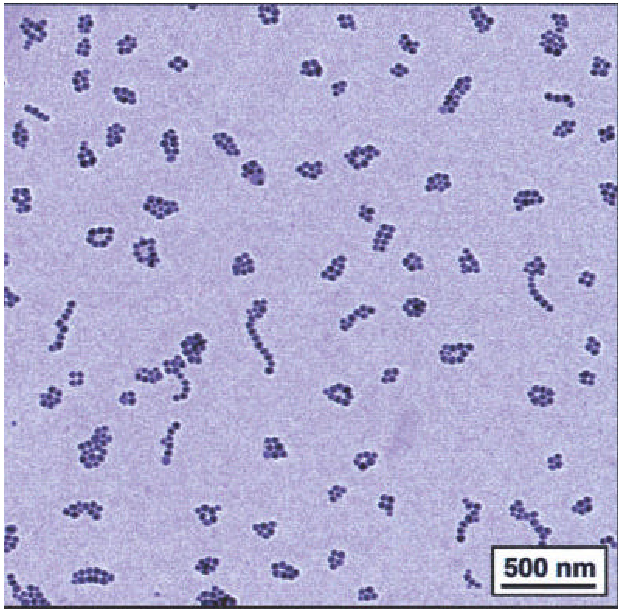

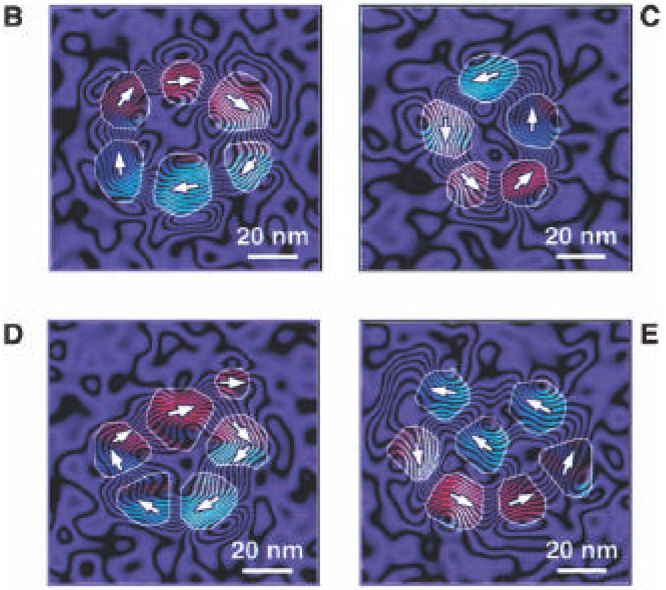

Image of self-assembled Co nanoparticle rings and chains deposited onto an amorphous carbon film.
Co diameter ~ 20-30 nm

Magnetic phase contours (0.049 radian spacing), formed from the magnetic contribution to the measured phase shift, in four different nanoparticle rings.

R E Dunin-Borkowski et al., Microsc. Res. Techn. 2004 **64** 390-402

Electron Holography

lanar array of Titanomagnetite natural system (magnetite rich locks separated by non-magnetic materials)

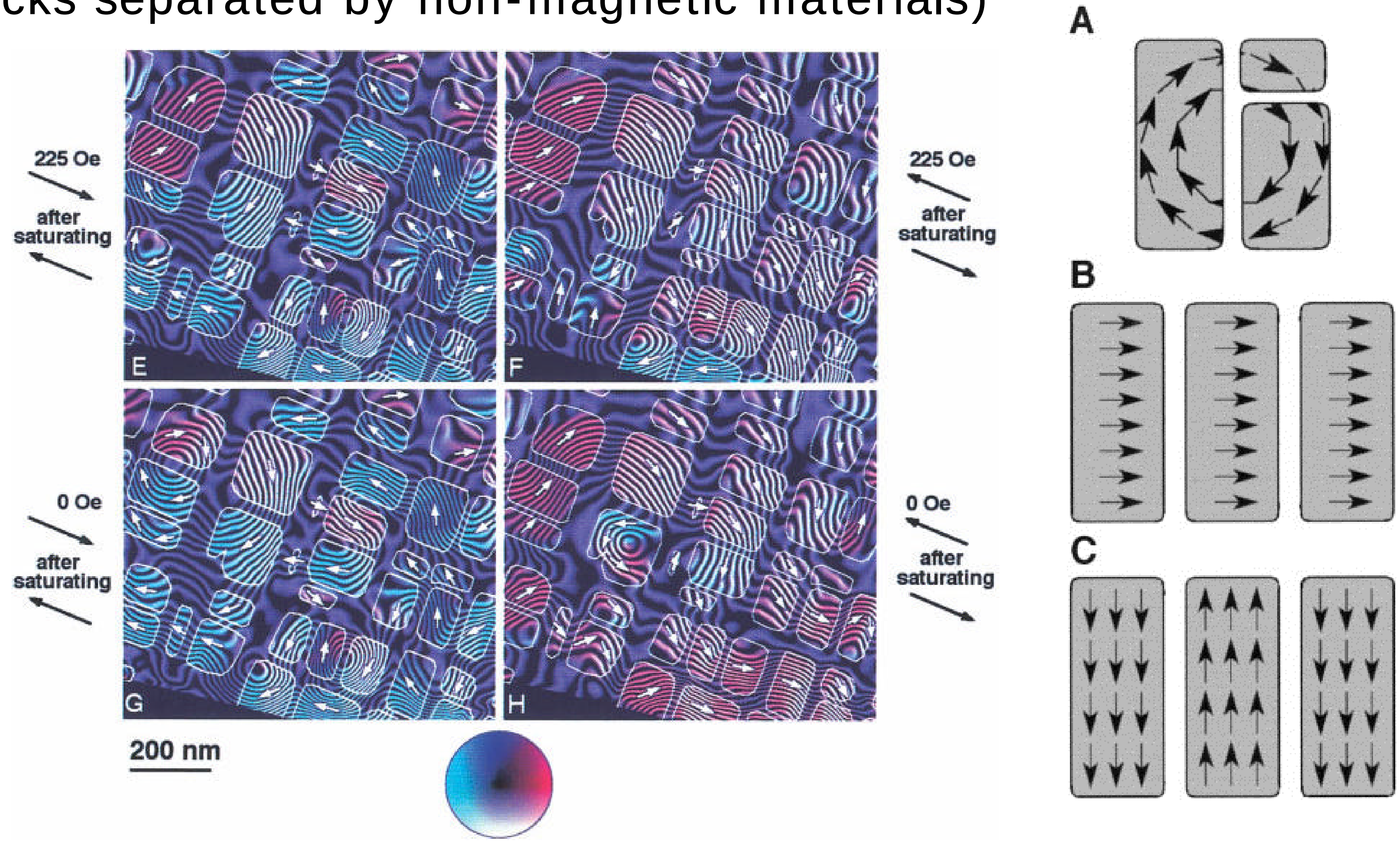

R E Dunin-Borkowski et al., Microsc. Res. Techn. 2004 **64** 390-402

C nanotubes filled with Fe

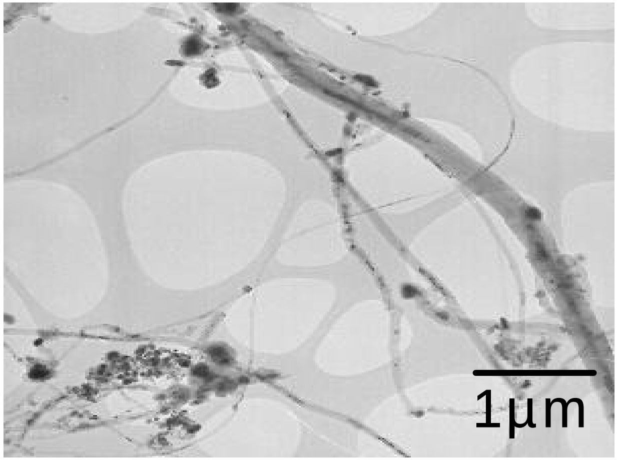

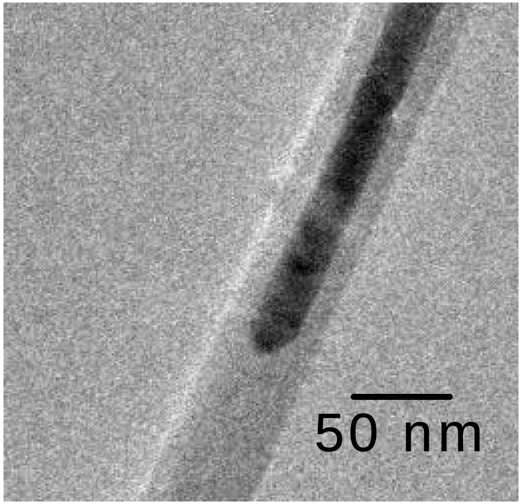

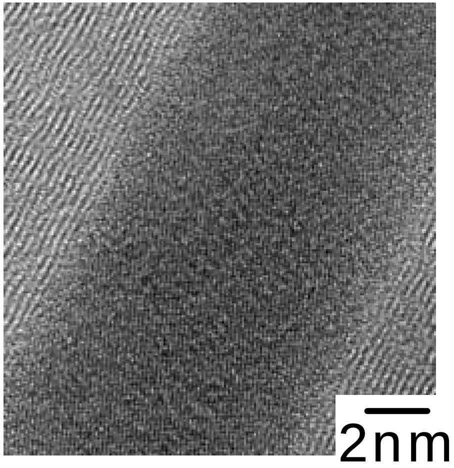

Groups

CEMES, Toulouse, France
http://www.cemes.fr/

University of Cambridge, UK
http://www-hrem.msm.cam.ac.uk/research/index.shtml

Institute of Structure Physics (ISP), Dresden University, Germany
http://www.physik.tu-dresden.de/isp/member/wl/TBG/start/lichteS.htm

University of Arizona, USA
http://www.asu.edu/clas/csss/chrem/main.html

EPFL, Lausanne, Switzerland
http://cime.epfl.ch/

Hitachi, Japan
http://www.hqrd.hitachi.co.jp/global/fellow_tonomura.cfm